PARAMETRIC SENSITIVITIES OF 3G UTRA CELLULAR SYSTEM

A thesis submitted in partial fulfillment of the requirements

for the degree of Master of Philosophy

in the Department of Electronic and Information Engineering

at The Hong Kong Polytechnic University

By

Yueh, Raymond Hok Man

December 1999

ACKNOWLEDGMENTS

The author wishes to express his sincere appreciation to Professor Asrar U. H. Sheikh for his invaluable advice, helpful guidance, and constant encouragement during the course of study. He would like to express his thanks to Dr. Morris M. Z. Wang, who took over the supervision work from Professor Sheikh, for his useful advice and assistance. Gratitude is expressed to Panson S. Tantikovit for his assistance and helpful discussions. It is the author's pleasure to acknowledge all of his friends, fellow colleagues, and staff of the Department of Electronic and Information Engineering, The Hong Kong Polytechnic University, for their support.

ABSTRACT

Technologies of the third generation (3G) mobile radio system are expected to be standardized by the end of year 1999. Support of multimedia services and multirate data transmission are some of the many attractive features of the 3G systems. Universal Terrestrial Radio Access (UTRA) system, which is based on wideband CDMA, is considered to be a leading candidate for standardization.

In this thesis, the parametric sensitivities of 3G UTRA cellular system are investigated. The essence of a Rake receiver in mobile radio channel is discussed with simulation results. The number of fingers in the Rake receiver is one of the parameters investigated. Situations when the number of fingers is matched (and unmatched) to the number of signal paths in the channel are investigated. The performance gain obtained by the use of path searching algorithm in an unmatched Rake receiver is shown and compared with theoretical analysis. Sensitivities of the UTRA system performance to the parameters interleaving depth and Doppler frequency are studied. Antenna diversity used as another means to combat fast fading in order to improve the system performance is also discussed. Performance results are given for two kinds of diversity technique, which are bit error based antenna diversity and post-detection antenna diversity. Power control is essential in CDMA systems and the situations when imperfect power control happens on the desired user and on other user are investigated with simulation results.

TABLE OF CONTENTS

LIST OF ABBREVIATIONS

AWGN	additive white Gaussian noise
AMPS	Advanced Mobile Phone Service
ARIB	Association of Radio Industries and Businesses
BPSK	binary phase shift keying
BER	bit error rate
BCH	Bose-Chaudhuri-Hocquenghem
CDMA	code division multiple access
dB	decibel
DPSK	differential phase shift keying
DQPSK	differential QPSK
DECT	Digital European Cordless Telecommunication
DTX	discontinuous transmission
EGC	equal gain combining
ETSI	European Telecommunications Standards Institute
ESC	extended structured codes
FEC	forward error correction
FL	forward link
FDD	frequency division duplex
FDMA	frequency division multiple access
GMSK	Gaussian minimum shift keying
GCL	generalized chirp-like

GHz	giga-Hertz
GPS	global positioning system
GSM	Global System for Mobile communication
Hz	Hertz
HPA	high power amplifier
IS-54	Interim Standard-54
IS-95	Interim Standard-95
IMT-2000	International Mobile Telecommunications-2000
ITU	International Telecommunication Union
IPI	interpath interference
ISI	intersymbol interference
kbits/sec	kilo-bits per second
ksymbols/sec	kilo-symbols per second
LOS	line-of-sight
LAN	local area network
MRC	maximal ratio combining
Mchips/sec	mega-chips per second
μsec	micro-second
Mbits/sec	mega-bits per second
MHz	mega-Hertz
MPDP	multipath power delay profile
MAI	multiple access interference
nsec	nano-second

NMT	Nordic Mobile Telephone
NA-TDMA	North America TDMA
OVSF	orthogonal variable spreading factor
PDC	Personal Digital Cellular
pdf	probability density function
PN	pseudo-noise
PSTN	public switched telephone network
QoS	quality of services
QPSK	quaternary phase shift keying
rad/sec	radian per second
RS	Reed-Solomon
RL	reverse link
rms	root-mean-square
RRC	root-raised cosine
SC	selection combining
SFG	shift register generator
SMS	short message service
E_b/N_0	signal energy per information bit-to-background noise power spectrum density ratio
SIR	signal-to-interference ratio
SNR	signal-to-noise ratio
SF	spreading factor
3G	third generation

TD-CDMA	time division CDMA
TDMA	time division multiple access
TACS	Total Access Communication System
TPC	transmitter power control
UTRA	Universal Terrestrial Radio Access
W-CDMA	wideband CDMA
WSSUS	wide sense stationary uncorrelated scattering

LIST OF SYMBOLS

a_k	amplitude of k-th signal path
$R_c(t)$	autocorrelation
B_c	channel coherence bandwidth
f_d	Doppler frequency
f_m	maximum Doppler frequency
γ_b	input SNR to combiner
γ_c	SNR per signal path
h_c	channel impulse response
λ	wavelength of carrier frequency
L	total number of fingers in Rake receiver
M	total number of signal paths in channel
$s(t)$	transmitted signal
$r(t)$	received signal
$r_l(t)$	lowpass equivalent received signal
θ	angle of arrival
τ_{max}	maximum delay spread
τ_{rms}	rms delay spread
τ_k	time delay of k-th signal path
T_s	symbol duration
v	speed of mobile unit

LIST OF FIGURES

LIST OF TABLES

Chapter 1

INTRODUCTION

1.1 Overview

In 1864, James Maxwell introduced the electromagnetic wave theory, which is the basis for radio wave propagation. The successful transmitting and receiving radio waves over short distances is shown by Heinrich Hertz in 1887. Eight years later in 1895, Guglielmo Marconi developed the first wireless telegraph system that transmits a radio signal over a distance of a few miles. In the mean time, Alexander Graham Bell's invention of the telephone led to the first transmission of speech over a wire-connected telephone network in 1876. And the first wireless communication of speech was in practice in 1906.

Figure 1.1 shows a general communication system block diagram. The source block represents the message sender from one side while the user block is the one whom the sender is communicating with. Although the two parties are usually far apart in geographical distance, they can keep in touch by the transmission of data through the channel as depicted in the diagram. Information exchange becomes easier and more convenient with the communication system. The wire-connected telephone network, which is

known as public switched telephone network (PSTN), can be described by Figure 1.1 with the exception that a telephone is both a transmitter and a receiver device. This is to say that a telephone is a transceiver that can both transmit and receive data and therefore establish a two-way communication. Telephones are connected to the local exchange network that is analogous with the channel in a communication system and this channel is wire-connected. Telephones are commonly and widely used nowadays and many households have installed more than one telephone. However, the fixed telephone network system could no longer satisfy users' needs because of the mobility of cars and people. And this led to the deployment of wireless communications systems.

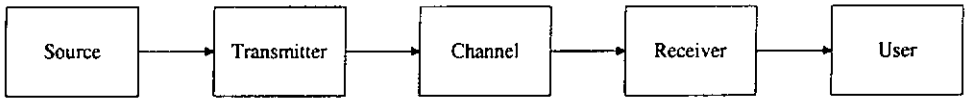

Figure 1.1 Communication system block diagram

The deployment of cordless telephone systems such as CT2 in United Kingdom and Digital European Cordless Telecommunication (DECT) in several European countries provides the means of mobile data communications. CT2 is also known as Telepoint and it allows a CT2 phone to connect to Telepoint base stations that are connected to the wire-connected telephone network. The coverage area of a Telepoint base station is small, which is about 200 metres of distance. Since no handoff capability is available

for this cordless phone system, when the user is moving outside of a zone into a new one, the call has to be terminated and a new call has to be reinitiated. This terminate-and-reinitiate process is inconvenient especially to users with wide and high mobility. Moreover, the CT2 phones can only initiate but not receive calls and the limited number of base stations gives the inconvenience to users. The DECT standard is more sophisticated than CT2 standard in terms of system structures and features. While CT2 uses FDMA as the radio interface, the TDMA signal structure in DECT provides power savings by virtue of discontinuous transmission (DTX). In addition, the handoff capability provided by DECT makes the terminate-and-reinitiate process no longer a necessity even when a user moves outside of a base station's coverage area. DECT allows users to both initiate and receive calls, which gives more convenience and flexibility to users.

Advanced Mobile Phone Service (AMPS), Total Access Communication System (TACS), and Nordic Mobile Telephone (NMT) system are examples of the first generation mobile radio system. Data transmission rate is designed to be low because the only data communication between users is voice. However, the deployment of these systems still gave users the convenience of information exchange within a local area. The demand for wireless communication usage has been increasing steadily because the mobility of personal hand-held telephone gives the convenience and provides an instant means to exchange information. In addition, the needs of harmonization of system standards lead to the development of the second

generation mobile radio system. The first digital cellular radio communication system, a European standard system, Global System for Mobile Communication (GSM) was developed in 1992. On the other hand, a time division multiple access (TDMA) system, Interim Standard-54 (IS-54) and a code division multiple access (CDMA) system, Interim Standard-95 (IS-95), became available in the United States in 1993 and in 1995, respectively. The introduction of digital technology gives many advantages including lower cost of manufacturing and power consumption for the mobile unit. Other improvements over the first generation analog systems are the capability of transmitting data in higher rate and as well in a more secure way. For example, in GSM, the maximum user data rate is 28.8 kbits/sec. Besides higher data transfer rate, the second generation Phase B mobile radio communication systems provide new services such as call waiting, call diverting, call conferencing, caller number display, short message service (SMS), and many others. Electronic commerce on cellular telephones is also available and getting popular. For example, in Hong Kong, stock trades can be performed by a cellular telephone. In addition, bank account information can be retrieved by a cellular telephone. Other useful information such as weather forecasts, lottery results, stock quotes, and traffic reports can be obtained from the cellular telephone as well. However, the interest in mobile communications does not end with this. The growing application of multimedia communications in the 1990s and in the forthcoming 21st century in wireless communications implies the requirements of transmission of real-time video images and high speed

information over the mobile radio channel. The increased data rate requires wider system bandwidth and as well more powerful error correction codes. This leads to the development of the third generation (3G) system.

The International Telecommunication Union (ITU) is currently in the process of standardizing the 3G mobile radio communications systems capable of providing multimedia services over mobile radio channels. The International Mobile Telecommunications-2000 (IMT-2000) systems will provide variable rate services ranging from 144 kbits/sec for applications in a wide area that changes rapidly, 384 kbits/sec for high-speed data, and 2 Mbits/sec for image applications in local slowly changing environments [1]. The CDMA is considered to be a promising air interface for cellular radio systems. CDMA scheme, which is based on spread spectrum technology, has been used by the United States Military since World War II. Its anti-jamming ability and low-probability of detection are advantageous especially to today's electronic commerce exploited on wireless radio communications. Not only because of the security issue, but also the radio capacity is another reason of applying CDMA in mobile cellular systems. Lee presented a general description of CDMA in [2] and it is shown that four times more radio capacity can be achieved by CDMA than by TDMA. Soft handoff can be applied on CDMA since every cell uses the same frequency band (i.e., frequency reuse factor of 1). In addition, guard time between time slots as used in TDMA is not necessary in CDMA. Therefore overhead is smaller and spectrum efficiency is higher.

In [3], a CDMA-based 3G mobile radio system is described. Attractive features such as high spectrum efficiency, soft handoff, cell-site diversity, and flexible frequency management make CDMA a promising candidate for the 3G system. Variable rate transmission is one of the features of 3G mobile radio system and this can be realized by using orthogonal variable spreading factors (OVSF). For a lower bit rate data, a spreading sequence with higher spreading factor is used and therefore a lower transmit power is allowed. Besides OVSF, multi-code can also be adopted for variable rate transmissions. In multi-code transmissions, higher rate data is split in parallel into multiple channels for spreading with same spreading factors. Since the 3G system supports mixed cell operation, it is possible that a user moves from a micro cell to a pico cell. And the soft handoff operation that CDMA supports is no longer feasible since different RF channels are assigned to different layered cells. Therefore a process called inter-frequency handoff is required in the 3G systems.

Quality of services (QoS) is one of the measurements to describe the performance of a system. For wireless communications, channel plays an important role on the system reliability. On the other hand, QoS is promising for data transmission through computer networks even without powerful error correction mechanism because the networks are wire-connected. Local area network (LAN) is an example of high speed data transmissions between small area networks such as in a university or in a company. Data transmissions via wire-connected networks are commonly and widely used nowadays. However, the wireless channels receive so much attractions even though it is hard to

achieve reliable performance for data transmission through the wireless channel. Mobile radio channel is an unreliable transmission medium where undesirable effects such as fading, near-far problem, and shadowing can severely degrade the system performance. A large amount of researches is ongoing to investigate how to mitigate those effects to achieve reliable performance under the time-varying mobile channel. While the mobile channel changes with time and behaves differently under different environments, it becomes more difficult to investigate the situations. It is possible that a mobile radio channel in an urban area is completely different from the one in a rural area. Therefore in order to achieve reliable performance, the behavior of a mobile radio channel has to be investigated thoroughly. After the behavior of a radio channel is known, suitable receiver can be designed to combat the impairments. Therefore three main things can be done to achieve a more reliable system: (i) obtain the statistical behaviors of a mobile radio channel under different environments; (ii) design an optimum receiver; and (iii) employ some techniques to achieve a more reliable performance. In the next section, aspects of mobile radio system are discussed.

1.2 Aspects of Mobile Radio System

As mentioned in the previous section, in order to have a more reliable communication system, three main things can be done. The first is to obtain the statistical behaviors of a mobile channel for different environments. This information is readily available from many literature [4]-[7] and it provides

good source of reference to design an optimum receiver to cope with the impairments caused by the mobile channel. For example, Price and Green [8] investigated the multipath reception that is caused by obstructions and scatterers such as buildings and cars in the environments. It is well known that the reliability of a mobile channel is severely degraded in a multipath channel environment. A Rake receiver that resolves and combines multipath signals was proposed in 1958 and the prototype system was proved to have superior performance than a classical correlator receiver under multipath channel environment. By utilizing the correlation detection techniques, a Rake receiver decorrelates received multipath signal and combines the resolved, time-delayed signal from the fingers. The resultant composite signal gives better performance for decision.

The channel behavior and Rake receiver are discussed above. Now we can discuss some of the techniques to achieve a more reliable system performance. Different methods can be used to combine the multipath signals resolved by the Rake receiver. They are: selection combining (SC), where only the finger with the strongest power is selected for combining; equal gain combining (EGC), where all fingers are equally weighted for combining; and maximal ratio combining (MRC), where the fingers are amplitude-weighted prior combining. It is shown that the MRC method gives the best performance [9].

Besides different kinds of combining methods, there are two kinds of detection methods– coherent and non-coherent. For a multipath channel where

delays between paths are not known, a differential phase shift keying (DPSK) receiver can be used [10]. The DPSK receiver is known as a non-coherent receiver since phase-coherent techniques are avoided in this kind of receiver. Non-coherent detection receiver is preferable than coherent receiver in terms of hardware complexity but it is inferior to coherent detection by 3 dB [11, p. 684]. The optimal receiver with known delays implies the necessity of implementing the phase detection mechanism. This not only complicates the hardware design but also hard to achieve reliable results because of rapidly changing path phases with fast moving mobile unit. Therefore it is a tradeoff between hardware complexity and performance improvement. Performance results for different kind of receivers are readily available in literature [12]-[20]. In [12], the performance of a two branch SC receiver under correlated Rayleigh fading channels is analyzed with a closed form solution of the BER probability. In [13], the performance of a MRC Rake receiver under correlated fading channels is analyzed. In [14], the BER performance of a MRC Rake receiver under correlated Nakagami fading channels is evaluated. In [15], SC and EGC Rake receivers are analyzed with approximate expressions of BER probability. In [16], closed form solutions of the BER performance of an EGC Rakè receiver in Nakagami fading channels are derived. In [17], closed form solution of the BER probability of a MRC Rake receiver in Rayleigh fading channels is evaluated. In [18], the exact BER probability of a Rake receiver in a Rayleigh fading channel is given. In [19],

the performances of SC and MRC Rake receivers are compared. In [20], the exact BER probabilities of MRC and SC Rake receivers are given.

The performance of a Rake receiver is usually presented in scenario where the number of fingers in it is matched to the number of signal paths in the channel. However, it is unrealistic, especially for wideband systems where the number of resolvable paths is usually high, to have a matched Rake receiver. Therefore a Rake receiver with number of fingers not matched to the number of signal paths is investigated [21]. In addition, the unmatched Rake receiver case with path searching algorithm implemented is investigated [9][19][21]-[26]. In [9], the performances of matched and unmatched Rake receivers with path searching algorithm are compared. In [19] and [22]-[24], expressions of BER probability for an unmatched Rake receiver that combines the first few strongest paths are derived and compared with the MRC and SC Rake receivers. In [21], the performance improvement obtained by the use of path searching in an unmatched Rake receiver is analyzed. In [25] and [26], performance of an unmatched Rake receiver with path searching algorithm in Rayleigh fading channels is evaluated. The results presented in most of these literature are in scenarios of single user and they are not presented in the sense of parametric sensitivities of the system. That is, in these literature, only the theoretical BER performance and comparisons are given. But the performance improvements under different circumstances are ignored. For example, the performance gain for the use of path searching algorithm varies on the number of fingers used in the Rake receiver is not investigated. This is an important

topic since performance improvement depends greatly on different settings of the system parameters. Therefore in this thesis, the parametric sensitivities of the 3G system are investigated by means of simulation experiments and the results are compared with the theoretical ones.

1.3 Outline

The outline of this thesis is as follows. The mobile radio channel is discussed in Chapter 2 of this thesis. In particular, multipath fading phenomenon in a mobile radio channel is described in detail. A mathematical model is given to describe the multipath channel in different environments. Four types of multipath channel are classified depending on the channel parameters– delay spread and Doppler spread. The system performance mainly depends on the characteristics of the multipath channel that is described by these channel parameters. The behavior of a channel under different environments is also investigated. In addition, techniques such as forward error correction and diversity to make the multipath fading channels more reliable (i.e., to improve error rates) are presented.

Generations of mobile radio systems are described in Chapter 3. For the first generation systems such as Advanced Mobile Phone Service, Total Access Communication System, and Nordic Mobile Telephone system, voice is the main service supported. New features such as improved system capacity and higher data rate transmissions are found in the second generation systems such as Interim Standard-95, Personal Digital Cellular, and Global System for

Mobile Communication. High speed video images transfer in multimedia applications are exploited in the 3G systems. Data rate as high as 2 Mbits/sec are supported in these systems. W-CDMA is the most promising candidate for the 3G system because of many advantages provided by W-CDMA technology. Also in Chapter 3, the air interface and multirate transmission for W-CDMA system are discussed. In particular, the discussion of FDD and TDD modes of operation in Universal Terrestrial Radio Access (UTRA) system is provided. Different aspects of the UTRA system such as channel coding, spreading, modulation, power control, and inter-frequency handoff can all be found in Chapter 3. Finally in that chapter, the operation of UTRA system over practical wireless channel is discussed. In particular, the parameters used to investigate the performance of the UTRA system are given and explained in detail.

In Chapter 4, system model used in the computer simulations is discussed followed by the description of multirate transmission realized by the orthogonal variable spreading factor scheme. System and simulation parameters are presented and different aspects of the system model are provided. Two levels of spreading and, in particular, the generation of tree-structured code are presented. The multipath fading channel modeled by Jakes' model and Rake receiver implemented with path searching algorithm are discussed. Different diversity techniques used in the simulation experiments are explained in that chapter as well. In addition, some miscellaneous issues

regarding the designing process of the system model are provided and illustrated with diagrams.

Simulation results are given in Chapter 5. Different scenarios such as Rake receiver with number of fingers matched to the number of signal paths in the channel, Rake receiver with number of fingers less than the number of signal paths in the channel are investigated. In addition, performance improvement obtained by the use of path searching algorithm under unmatched Rake receiver case is investigated and compared with the theoretical results. System performances with different interleaving depths under different Doppler frequencies are discussed followed by the performance of two types of antenna diversity. Imperfect power control is also considered in that chapter. Finally, conclusions are drawn in Chapter 6.

Chapter 2

MOBILE RADIO CHANNEL

2.1 Introduction

In any communication system, the channel plays an important role in reliability. In wireless communication, the mobile radio channel is impaired by fading, shadowing, interference, frequency selectivity and of course noise. Because of buildings, hills, and moving objects such as cars in the environment, a transmitted impulse arrives at the receiver as a series of delayed replicas of the impulse. This phenomenon commonly happens in a mobile radio channel is known as multipath fading and it is discussed in Section 2.2. In addition, a mathematical model describing the multipath channel in different scenarios is presented in that section. The system performance depends on the characteristics of the multipath channel, which is described by channel parameters such as delay spread and Doppler spread. Four types of multipath channel can be classified depending on these channel parameters and they are all described in Section 2.3. Techniques such as forward error correction and diversity to improve the system performance in the presence of a multipath

fading environment are provided in Section 2.4. Finally, this chapter is summarized in Section 2.5.

2.2 Multipath Fading

In a mobile radio channel, because of scatterers such as buildings, hills, and other obstacles, a single transmitted impulse arrives at the receiver as a series of delayed impulses modified in amplitude. This phenomenon can be described as multipath reception shown in Figure 2.1. Since the scatterers are at random locations in the environment, the multipath signals arrive at the receiver with different time delays. Moreover, the amplitudes of these paths are modified according to different path losses due to characteristics of the obstacles. As depicted in Figure 2.1, a symbol is transmitted from the base station antenna at time t, after a time delay τ_0, path 0 arrives at the receiver. Similarly, paths 1 and 2 arrive at the receiver after delays of τ_1 and τ_2, respectively. Two cases can be considered for this multipath situation. First, both the receiver and the scatterers are standing still. Secondly, the receiver and/or the scatterers are in motion. Obviously, the most usual case is when both the receiver and the scatterers are in motion.

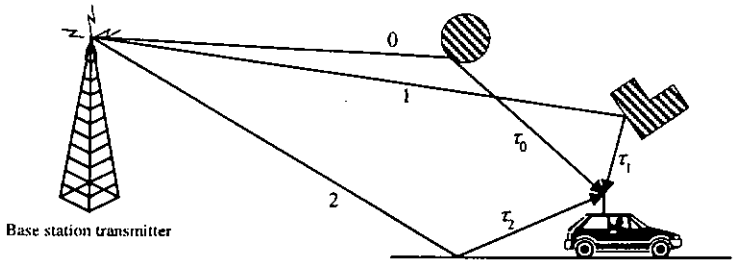

Figure 2.1 Multipath phenomenon

To investigate the different cases in detail, first let us define the signal being transmitted through the multipath channel as

$$s(t) = \mathrm{Re}[s_l(t)e^{j\omega_c t}], \tag{2.1}$$

where ω_c is the carrier frequency in rad/sec.

And the received bandpass multipath signal is

$$r(t) = \sum_{k=0}^{M-1} a_k(t)s(t-\tau_k(t)), \tag{2.2}$$

where M is the total number of signal paths with amplitudes a_k and delays τ_k.

Substitute (2.1) into (2.2) gets

$$r(t) = \mathrm{Re}\left[\sum_{k=0}^{M-1} a_k(t)s_l(t-\tau_k(t))e^{j\omega_c(t-\tau_k(t))}\right]$$

$$= \mathrm{Re}\left\{\left[\sum_{k=0}^{M-1} a_k(t)s_l(t-\tau_k(t))e^{-j\omega_c\tau_k(t)}\right]e^{j\omega_c t}\right\}. \tag{2.3}$$

And the lowpass equivalent received signal is

$$r_l(t) = \sum_{k=0}^{M-1} a_k(t)s_l(t-\tau_k(t))e^{-j\omega_c\tau_k(t)}. \tag{2.4}$$

For the transmission of an unmodulated carrier at frequency ω_c, $s_l(t) = 1$ for all t. Therefore (2.4) becomes

$$r_l(t) = \sum_{k=0}^{M-1} a_k(t)e^{-j\omega_c\tau_k(t)}$$

$$= \sum_{k=0}^{M-1} a_k(t)e^{-j\phi_k(t)}, \tag{2.5}$$

where $\phi_k(t) = \omega_c \tau_k(t)$.

After the lowpass equivalent received signal is defined, we can now investigate the different cases. For the first case where both the receiver and the scatterers are standing still, the time variant channel becomes static and (2.5) becomes

$$r_l(t) = \sum_{k=0}^{M-1} a_k e^{-j\phi_k} . \tag{2.6}$$

In other words, the channel gains and phase shifts of the multipath signals remain constant with time. It should be noted that in this situation, no fading occurs since the received signal envelopes remain unchanged. However, this situation rarely happens because the scatterers such as cars and pedestrians surrounding the receiver (or transmitter) are unlikely standing still at all times. The second situation where the receiver and/or the scatterers are in motion is considered next. The example of one moving scatterer (while the receiver is standing still) is depicted in Figure 2.2. Since the scatterer is in motion, the delay time that is observed at time t_0 is different from the one that is observed at time t_1. And this can be described by (2.5) where both the amplitudes and phases change with time. Signal in separate path fades independently since the multipath channel is considered to be time variant in this situation. This fading phenomenon is a result of time variations in $\phi_k(t)$ associated with the vectors $a_k e^{-j\phi_k}$. Since the scatterers are in random locations, the amplitudes and phases received from one reflected path are different from other paths. Besides of that, the composite received signal also exhibits fading behavior because at

some times, the vectors $a_k e^{-j\phi_k}$ add constructively, which results in large composite received signal. At other times, the vectors $a_k e^{-j\phi_k}$ add destructively, which result in small composite received signal. As a result, the composite received signal varies with amplitude and thus fades with time.

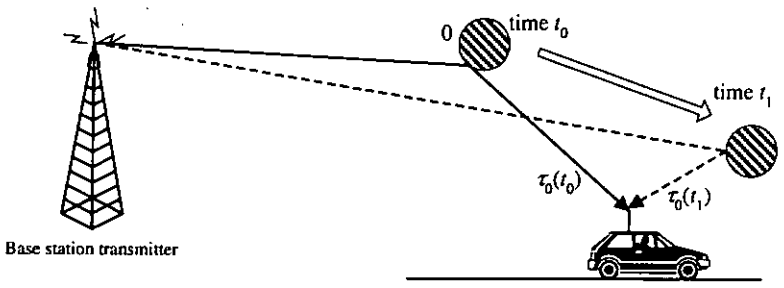

Figure 2.2 Multipath phenomenon with moving scatterer

Because of the relative motion of the two ends of the link, an additional frequency (i.e., Doppler frequency) is contributed and (2.5) becomes

$$r_l(t) = \sum_{k=0}^{M-1} a_k(t) e^{-[j(\phi_k(t)+\beta vt\cos\theta_k)]}, \tag{2.7}$$

where $\beta = 2\pi/\lambda$,

λ = wavelength of carrier frequency,

v = speed of receiver,

θ = angle of arrival,

and (2.7) can be written as

$$r_l(t) = \sum_{k=0}^{M-1} a_k(t) e^{-[j(\phi_k(t)+2\pi f_m\cos\theta_k t)]}$$

$$= \sum_{k=0}^{M-1} a_k(t) e^{-[j(\varphi_k(t)+2\pi f_{d_k} t)]} . \qquad (2.8)$$

The Doppler effect can accrue if either the receiver or the scatterers (or both) is in motion. And the situation when the receiver is in motion is depicted in Figure 2.3. The additional Doppler frequency is described as $f_{d_k} = f_m \cos\theta_k$, where $f_m \equiv v/\lambda$ is the maximum Doppler frequency. It should be noted that the Doppler frequency, f_d, can be negative or positive, in the range $-f_m \le f_d \le +f_m$.

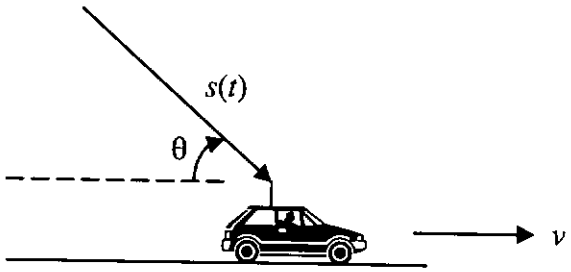

Figure 2.3 Doppler effect due to the motion of receiver

Several models can be used to describe the statistical characteristics of the fading phenomenon. The Rayleigh distribution is frequently used to model the short term amplitude fading of a mobile radio channel. The amplitude (i.e., a_k) at any instant time t is Rayleigh distributed in a Rayleigh fading channel. Figure 2.4 shows the Rayleigh fading signal envelope and it depicts the amplitude variation of the signal as the mobile unit is moving. As shown in the figure, minima (or maxima) occur every ½ - ¾ of the wavelength, λ, of the

carrier transmission frequency (f_m = 100 Hz). Other distribution functions that are used to model the fading amplitude are Nakagami-*m* and Rice distributions. When a strong line-of-sight (LOS) path exists, the multipath fading is usually modeled as Rician; otherwise, it is usually modeled as Rayleigh.

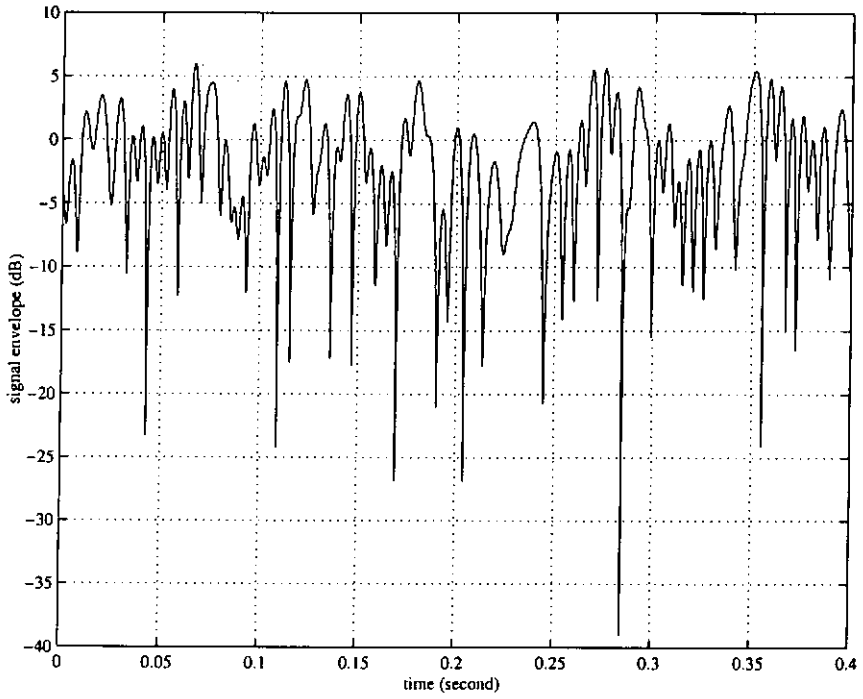

Figure 2.4 Rayleigh fading envelope

2.3 Channel Measurements

In the previous section, multipath reception and fading of signals due to the presence of environmental features and relative motion of the two ends of the link were discussed respectively. For mobile radio communications, the channel impulse response completely characterizes the channel and could

determine how a system will perform on this kind of channel. And the channel impulse response of a multipath propagation environment first suggested by [27] is defined as

$$h_c(\tau;t)=\sum_{k=0}^{M-1}a_k(t)\delta(\tau-\tau_k(t))e^{-j\phi_k(t)}, \tag{2.9}$$

where M is the total number of signal paths with amplitudes a_k and delays τ_k with phases ϕ_k. Both a_k, τ_k, and ϕ_k are time varying variables and ϕ_k is uniformly distributed from 0 to 2π.

Figure 2.5 shows a typical channel impulse response. The simplest way to describe the time dispersion of a multipath channel is the measurement of the time difference between the first arrival path and the last arrival path, which is referred to as excess delay spread [28, p. 55], τ_{max}, or impulse response length. In general, the impulse response length of a channel is infinite. However, the maximum length is usually measured 30 dB down from the highest level of the impulse. Still, this quantity cannot well describe the characteristics of a channel because as shown in Figure 2.6, channels having different multipath power delay profiles (MPDP's) can have the same excess delay spread. The uniform and exponential MPDP's shown in Figure 2.6 (a) and (b), respectively, both have the same excess delay spread of τ_5-τ_0, but their different MPDP's will have different impacts on the performance of a system. Therefore root-mean-square (rms) delay spread is used as a better parameter to describe the delay spread of a multipath channel.

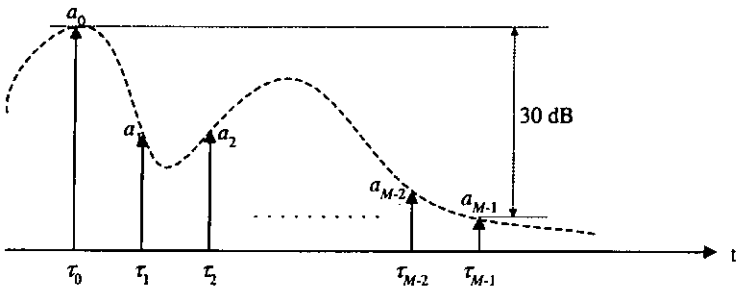

Figure 2.5 Typical channel impulse response

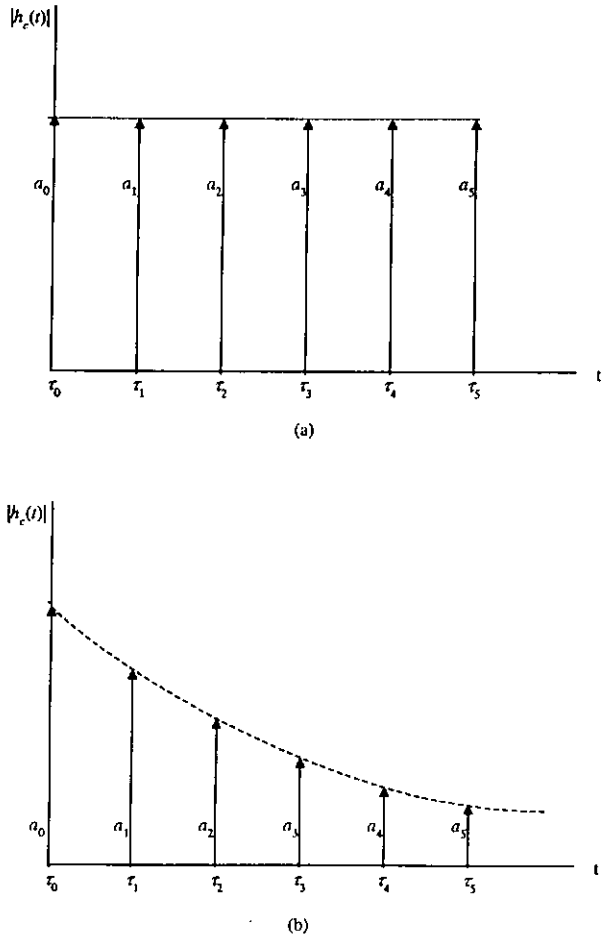

Figure 2.6 (a) Uniform and (b) exponential MPDP's

The rms delay spread, which is the second central moment of the channel impulse response, is defined as

$$\tau_{rms} = \sqrt{\langle \tau^2 \rangle - (\langle \tau \rangle)^2}\,, \tag{2.10}$$

where

$$\langle \tau^n \rangle = \frac{\sum_{k=0}^{M-1} a_k^2 \tau_k^n}{\sum_{k=0}^{M-1} a_k^2}. \tag{2.11}$$

It should be noted that in (2.11), the amplitudes a_k are treated as time invariant variables.

We have a general idea of the time dispersion of the channel and how the system performs on that particular channel with the rms delay spread. The channel is completely characterized by both the knowledge of the shape of the MPDP and the rms delay spread.

In practice, the channel impulse response can be measured by means of a channel sounder, which is a transmitter that emits impulses at regular intervals and the receiver measures the responses. Figure 2.7 shows different channel impulse responses under different environments [29, p. 109]. As shown in the figure, for a typical rural area, the impulse response length is short (about 0.5 μsec) and the impulses are close to each other. On the other hand, in a typical urban area, the impulse response length is about 5 μsec and the impulses are loosely separated. For hilly terrain, impulse response length is as long as 20 μsec. Multipath measurements at the 2 GHz bandwidth are

reported in [4] for rural and urban terrain. The rms delay spreads in downtown Toronto were measured as 3 μsec and 7 μsec in urban and suburban/rural terrain, respectively, in [5]. Heavily built up area such as New York City in the United States has delay spread as large as 3.5 μsec [6]. At 910 MHz, the average rms delay spreads for outdoor urban terrain and indoor environment are from 0.26 to 0.72 μsec and 50 nsec, respectively, as reported in [7].

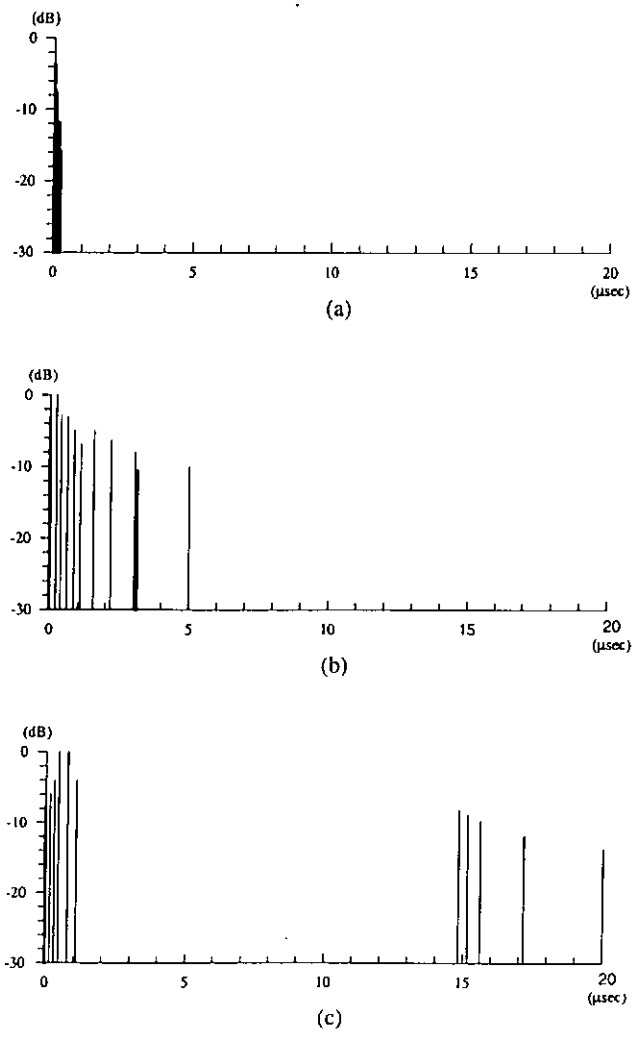

Figure 2.7 MPDP under different environments (a) typical rural area (b) typical urban area (c) typical hilly terrain

In relation to the delay spread of a channel, another useful quantity is the channel coherence bandwidth, B_c. B_c is the range of frequencies over which two signals are highly correlated and it is defined as

$$B_c = \frac{1}{2\pi\tau_{rms}}. \tag{2.12}$$

It should be noted that in some literature, the coherence bandwidth is defined as [30]

$$B_c = \frac{1}{8\tau_{rms}}, \tag{2.13}$$

and [11]

$$B_c = \frac{1}{2\pi\tau_{\max}}. \tag{2.14}$$

If the bandwidth of the transmitted signal is smaller than B_c, all frequencies within the signal bandwidth fade in the same manner. That is, the signal is subjected to frequency non-selective fading and the multipath signals fade independently but they are correlated. On the other hand, if the bandwidth of the transmitted signal is greater than B_c, the channel is said to be frequency selective. While the channel delay spread relates to time dispersion of the channel, the Doppler spread relates to frequency dispersion of the channel. Similar to the inverse proportion relationship between the delay spread and coherence bandwidth, Doppler spread is also inversely proportional to the coherence time of a channel.

A signal will undergo time selective fading if the duration of the symbol is larger than the channel coherence time. Since the maximum Doppler frequency f_m is proportional to the speed of the receiver, Doppler spread is small when the receiver is moving slowly. That is, the upper limit of the speed of mobile unit is the rule of thumb to time selective fading.

As a summary, fading channels can be classified into four types: (i) frequency selective and time selective fading channel, (ii) frequency selective and time non-selective fading channel, (iii) frequency non-selective and time selective fading channel, and (iv) frequency non-selective and time non-selective fading channel. The delay spread (coherence bandwidth) and Doppler spread (coherence time) define the channel type. When the transmission bandwidth of the signal is greater than the coherence bandwidth, time dispersion is significant and frequency selective fading occurs. When the duration of the symbol is larger than the coherence time of the channel, frequency dispersion is significant and time selective fading occurs. Figure 2.8 summarizes these four kinds of channel.

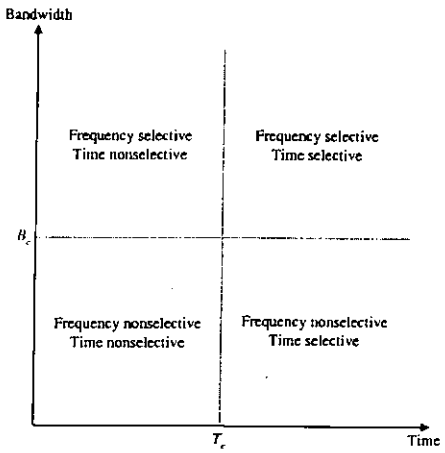

Figure 2.8 Four types of multipath fading channel

A mobile radio channel can be distinguished as narrowband or wideband depending on the signal transmission bandwidth and rms delay spread of the channel. In a narrowband system, frequency selectivity is unlikely if the signal transmission bandwidth is much smaller than the channel coherence bandwidth. Since the channel coherence bandwidth is inversely proportional to the rms delay spread of the channel as shown in (2.12), it can be said that

$$T_s > 2\pi\tau_{rms}, \tag{2.15}$$

where T_s is the symbol period. When T_s is greater than the rms delay spread of the channel, intersymbol interference (ISI) does not occur in narrowband systems. Moreover, since the data rate for narrowband systems is low, the duration of the symbol period is usually greater than the coherence time of the channel. Therefore time selective fading is likely to occur in narrowband systems. On the other hand, frequency selective fading is likely to occur in a wideband channel since the transmitted signal bandwidth is usually larger than the coherence bandwidth. Again, the following relationship is apparent from (2.12):

$$T_s < 2\pi\tau_{rms}. \tag{2.16}$$

In wideband systems, the rms delay spread is a rule of thumb to set the upper limit to ISI-free transmission rate.

Power received that is modeled by the power distance relationship is of significant importance in narrowband systems. On the other hand, a frequency

selective multipath fading channel model can well characterize a wideband channel since frequency selective fading usually occurs in wideband systems. Different from a narrowband system, where the system performance depends greatly on the power received, the major cause of performance degradation in wideband systems is fading. Many techniques can be employed to make a system under multipath fading environments more reliable and they are discussed in the following section.

2.4 System Improvement Techniques

Wireless data communication is unreliable because of the presence of several channel impairments such as fading. To mitigate the undesired effects caused by the multipath fading channel, several error control techniques are possible. Forward error correction is one of the most commonly used techniques to improve the system performance. In addition, in the presence of multipath reception, path diversity provides gain on the system performance. Several system improvement techniques are discussed in the following sections.

2.4.1 Forward Error Correction

2.4.1.1 Block Codes

Block codes are a class of parity check codes. In block coding, data bits are partitioned into blocks of length k, and the channel encoder outputs a longer block of n mapped codewords. And this is called a (n, k) block coder. Many

kinds of block codes have been developed. Hamming codes [31] are the codes with single error correction capability. For binary Hamming codes, $(n, k) = (2^m\text{-}1, 2^m\text{-}1\text{-}m)$, where $m = n\text{-}k$ is the number of parity symbols. Bose-Chaudhuri-Hocquenghem (BCH) cyclic codes are efficient block codes since they achieve higher error-correction capability, and can be implemented at high speed data transmissions. The block length of BCH codes is $n = 2^m\text{-}1$ for $m \geq 3$ and BCH codes can correct multiple errors. While the BCH codes are binary codes, another class of non-binary BCH codes known as Reed-Solomon (RS) codes is created by using m bits per codeword. The block length of RS codes is $2^m\text{-}1$ and the number of errors an RS code can correct is $(n\text{-}k)/2$. The above mentioned linear block codes are memoryless codes, which means the decoding process of the current bit needs not have the knowledge of the previous bits. Codes with memory can be used to obtain higher system performance and convolutional codes are one of the codes with memory.

2.4.1.2 Convolutional Codes

A (n, k, K) convolutional encoder as shown in Figure 2.9 consists of kK finite-state shift registers. The constraint length that controls the redundancy of the message bits is represented as K and k is a number of M-ary bits (i.e., $M = 2^k$). For binary input bits, $k = 1$; for 4-ary input bits, $k = 2$. n is the number of coded bits for k input bits. Therefore a (n, k, K) convolutional encoder has a code rate $R = k/n$. Figure 2.10 shows a (3, 1, 3) convolutional encoder. Since

the input bits are binary, $k = 1$ and the generator polynomial $g(X)$ can be expressed as

$$g(X) = \sum_{i=1}^{K} a_i X^{i-1}, \tag{2.17}$$

where $a_i = 0, 1$. A 0 represents that there is no connection between the shift register and the modulo-2 adder while a 1 represents the shift register is connected to the modulo-2 adder.

Therefore the convolutional encoder shown in Figure 2.10 has generator polynomials $g_1 = (1, 0, 0)$, $g_2 = (1, 0, 1)$, and $g_3 = (1, 1, 1)$.

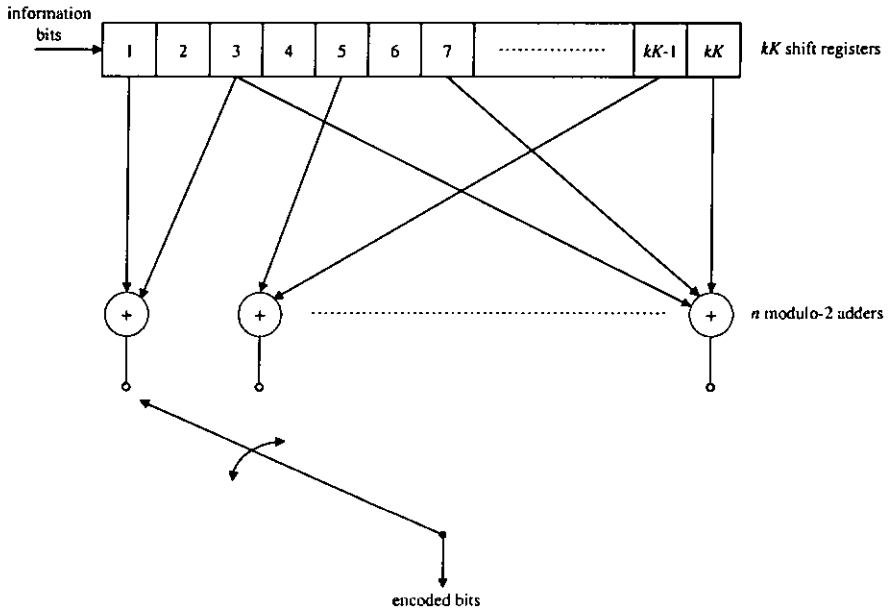

Figure 2.9 Convolutional encoder

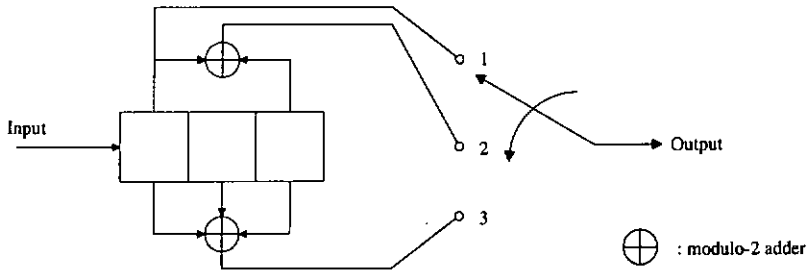

Figure 2.10 (3, 1, 3) convolutional encoder

Besides using polynomial functions to characterize the convolutional encoder, a tree diagram can also be used to describe the convolutional code. For example, the convolutional encoder shown in Figure 2.10 has a tree diagram as shown in Figure 2.11. The coded output sequence for message input bit 101 is 111001100 as indicated by the heavy trace in the figure.

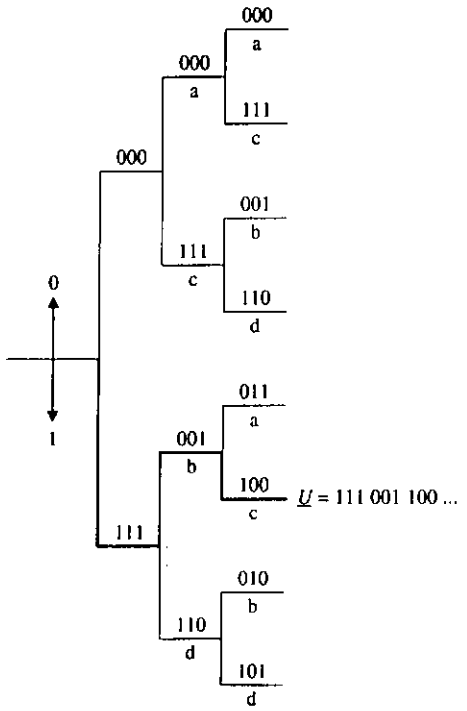

Figure 2.11 Tree diagram for (3, 1, 3) convolutional code

It can be seen from the diagram that as more input bits are coming into the encoder, the tree diagram expands its size. In this case, the tree diagram becomes unmanageable and difficult to use. Trellis diagram is another way to represent the convolutional encoder, which is more manageable. It is observed that the diagram repeats itself thereafter between time t_3 and t_4. As shown in Figure 2.12, dotted line represents an input bit of 1 while solid line represents an input bit of 0. Similarly, for the message bits 10100, the coded bits at the output of the encoder are 111001100001011.

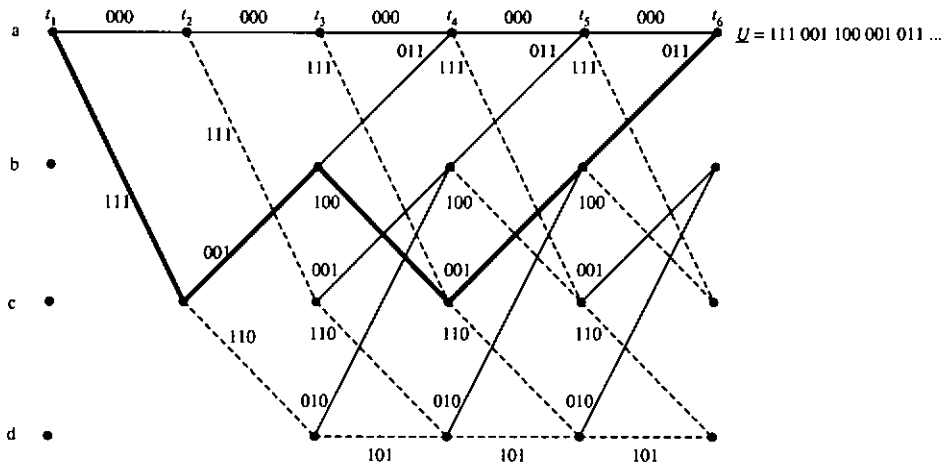

Figure 2.12 Trellis diagram for (3, 1, 3) convolutional code

Better system performance can be obtained with higher constraint length. Commonly used convolutional coders nowadays have a constraint length of 7 to 9. The Universal Terrestrial Radio Access (UTRA) system proposed in [32] uses convolutional coder with constraint length of 9. However, more computation power is required because more states have to be

gone through in the Trellis code tree for decoding. Thus, there is a tradeoff between hardware complexity and system improvement. Many convolutional decoding methods are available such as Fano's sequential decoding [33], the stack algorithm, and feedback decoding. However, Viterbi algorithm is the one commonly used [34]. Two kinds of decoding methods are utilized in Viterbi algorithm, which are soft-decision and hard-decision methods. The soft-decision method is a maximum likelihood decoding algorithm for additive white Gaussian noise (AWGN) channel [35] and the advantage of it varies with the channel characteristics. But, in general, it is 2-3 dB superior to the hard-decision method [36].

2.4.2 Path Diversity

For a single path fading channel, signal goes into deep fade at a rate proportional to the mobile receiver speed. However, for a multipath fading channel, it is less probable for the final composite signal to be in deep fade. It is because the probability of signals on all paths to go into deep fade simultaneously is low. Therefore multipath propagation can be used to an advantage in increasing the system performance provided their phases are properly aligned. To show this, consider the case for two signal paths. If the first path is arrived zero degree out of phase (i.e., $\phi_0 = 0$) while the second path is arrived 180 degrees out of phase (i.e., $\phi_1 = \pi$), then the vector sum of the two multipath signals has a destructive sum (i.e., $|a_0 - a_1|$), which gives a degradation on the performance. On the other hand, if the two signals are

arrived with the same phase (i.e., $\phi_0 = \phi_1$), there is a constructive sum (i.e., a_0+a_1), which gives an improvement on the performance. The phases of the multipath signals therefore have significant impact on the system performance. For that reason, the phases of the multipath signals should be properly aligned prior to combining.

The Rake receiver proposed by Price and Green [8] is designed to cope with the undesired effects caused by a multipath channel. A Rake receiver, which can resolve multipath signal into paths, consists of a bank of time delayed correlators termed as fingers. Assuming that the signal on each finger is frequency non-selective and fades slowly, the amplitudes and phases are therefore constant over one symbol period. And (2.4) can be written as

$$r_l(t) = \sum_{k=0}^{M-1} a_k e^{-j\phi_k} s_l(t-\tau_k). \tag{2.18}$$

For spread spectrum systems, a spreading code is multiplied with the signal prior to transmission over the channel and (2.18) becomes

$$r_l(t) = \sum_{k=0}^{M-1} a_k e^{-j\phi_k} s_l(t-\tau_k)c(t-\tau_k), \tag{2.19}$$

where $c(t)$ is the spreading sequence.

Each finger correlates the received signal with a time delayed spreading sequence:

$$y_n(t) = \int_0^{T_s} r_l(t)c(t-\tau_n)dt, \qquad n = 0, 1, ..., L$$

$$= \sum_{k=0}^{M-1} a_k e^{-j\phi_k} \int_0^{T_s} s_l(t-\tau_k)c(t-\tau_k)c(t-\tau_n)dt\,, \qquad (2.20)$$

where T_s is the symbol period and L is the number of fingers in the Rake receiver. We only consider the case where the number of fingers is same as the number of signal paths. That is, $L = M$. If interpath interference (IPI) is not considered, that means

$$\int_0^{T_s} c(t-\tau_k)c(t-\tau_n)dt = 0, \qquad for\ k \neq n\,, \qquad (2.21)$$

and

$$\int_0^{T_s} c(t-\tau_k)c(t-\tau_n)dt = 1, \qquad for\ k = n\,, \qquad (2.22)$$

only one path is filter out at the k-th finger:

$$y_k(t) = a_k e^{-j\phi_k} s_l(t)\,. \qquad (2.23)$$

Finally at the correlator outputs, all the filtered out paths are combined to give a signal with improved power for bit decision:

$$y(t) = \sum_{k=0}^{M-1} w_k e^{j\phi_k'} y_k(t)$$

$$= \sum_{k=0}^{M-1} (w_k e^{j\phi_k'})(a_k e^{-j\phi_k} s_l(t))\,, \qquad (2.24)$$

where w_k and ϕ_k' are the channel estimates. If coherent detection is considered, (2.24) becomes

$$y(t) = \sum_{k=0}^{M-1} (w_k e^{j\phi_k})(a_k e^{-j\phi_k} s_l(t))$$

$$= \sum_{k=0}^{M-1} w_k a_k s_l(t). \tag{2.25}$$

However, coherent detection requires the prior knowledge of the phases of the received multipath components. This channel coefficient can be obtained by using channel estimation but is difficult especially in a rapidly changing channel. And differential detection avoids the needs of estimating the phase information. Instead, the received signal at an instant is compared to the phase of the received signal at the previous instant of time. Since differential detection does not require phase estimation, it is often considered as non-coherent detection method. However, it is expected to be 3 dB inferior to the coherent detection method.

After all multipath components are resolved by the Rake receiver, they can be combined by different methods such as selection diversity (SD), equal gain combining (EGC), and maximal ratio combining (MRC). In SD, only the strongest component (i.e., the finger that has the highest power) is selected for bit decision:

$$a_N = \max\{a_k\}, \tag{2.26}$$

$$w_k = \begin{cases} 1, & if\ k = N \\ 0, & if\ k \neq N \end{cases}, \tag{2.27}$$

and (2.25) then becomes

$$y(t) = a_N s_l(t). \tag{2.28}$$

In EGC, all the paths are weighted equally and combined. Thus (2.25) becomes

$$y(t) = w\sum_{k=0}^{M-1} a_k s_l(t), \qquad w = w_0 = w_1 = \ldots = w_{M-1}. \tag{2.29}$$

On the other hand, each path is weighted according to the amplitude of that signal path in MRC method. Therefore a stronger signal has a larger weight than a weaker signal as described by

$$y(t) = \sum_{k=0}^{M-1} a_k \cdot a_k s_l(t)$$

$$= \sum_{k=0}^{M-1} a_k^2 s_l(t). \tag{2.30}$$

MRC is the optimal combining method among the other two in the presence of Gaussian noise only. But it requires the information of the signal path amplitude (so does in SC). Path diversity (or called Rake diversity) gives significant system improvement in a multipath channel environment. As a result of the improved signal-to-noise ratio (SNR) at the output of the receiver, lower transmit power for the user will deliver the same performance. As a consequence the multiple access interference (MAI) is decreased and the capacity of the system is then increased. In theory, given that an optimum Rake receiver is implemented in the system, the more the resolvable signal paths are, the better the performance is. However, this has not considered the situation

where some of the paths are not significant for detection and instead act as noise contribute to the combiner. In addition, IPI is another issue to be considered since the correlation between spreading sequences is not zero as assumed in the analysis done in this section and in other publications (e.g., in [11], p. 800). IPI is described in more detail in Section 5.2 of Chapter 5.

The path resolution time is inversely proportional to the chip rate of the system. In other words, the path resolution in wideband systems is higher than those in narrowband systems. This can be shown with the Interim Standard-95 (IS-95) narrowband system as an example. In IS-95, a 4-finger Rake receiver is implemented in this 1.25 MHz narrowband system. However, this 4-finger Rake receiver is of little use in operation environments where delay spread is smaller than 0.8 μsec. Because in this case, it is impossible for the Rake receiver to resolve more than one path and there is no path diversity gain. In the case of wideband systems, more paths can be resolved and a greater diversity gain is obtained.

2.5 Summary

In this chapter, the mobile radio channel of a wireless communications network is described. A multipath channel is characterized by impulse response. Different environments result in different impulse response lengths and different rms delay spreads. The difference between excess delay spread and rms delay spread is also discussed in this chapter. Four types of multipath fading channels are addressed and channels can be classified as narrowband or

wideband depending on the data transmission rate and channel coherence bandwidth. Transmission impairment such as multipath fading degrades the system performance severely and coding techniques such as block codes and convolutional codes used to cope with these impairments are discussed in this chapter. Path diversity employed by Rake receiver with different combining methods is essential in wideband systems and is thoroughly presented in this chapter.

Chapter 3

THIRD GENERATION MOBILE SYSTEM

3.1 Introduction

Telephony services standards such as Advanced Mobile Phone Service (AMPS), Total Access Communication System (TACS), and Nordic Mobile Telephone (NMT) system deployed in the early 1980's are known as the first generation mobile radio systems. Those analog systems used frequency modulation and frequency division multiple access (FDMA) method. Voice was the sole service provided. However, low data transmission speed at 2.4 kbits/s within the voice band could also be used. This voice-only transmission and low data rate applications could not meet the increasing needs of the users. Furthermore, due to relatively low spectral efficiency, the network became congested very quickly. The second generation systems installed in the early 1990's provided solutions to some of the drawbacks of first generation systems. Interim Standard-95 (IS-95) system in the United States, Personal Digital Cellular (PDC) system in Japan, and Global System for Mobile Communication (GSM) in Europe are capable of providing voice and data information at a rate between 2.4 kbits/s to 28.8 kbits/s. In IS-95, code division

multiple access (CDMA) and quaternary phase shift keying (QPSK)/binary phase shift keying (BPSK) modulation are used. In GSM, time division multiple access (TDMA) method and Gaussian minimum shift keying (GMSK) modulation are used. PDC uses the multiple access method similar to North America TDMA (NA-TDMA) of Interim Standard-54 (IS-54) and with $\pi/4$-differential QPSK (DQPSK) modulation. In terms of system capacity, security, and quality, the second generation digital systems have advantages over the first generation systems. However, the demand for wireless communication continued to accelerate and the quality of service provided by the second generation systems failed the demand. The rapid growth in the application of multimedia communications necessitated transmission of data carrying real-time video images and high speed information over the wireless channel. However, the current second generation systems cannot support such services. In parallel to this, the second generation systems also started to get congested. For example, it has become difficult to get a connection on PDC, and in the case of grant of connection, it is difficult to complete the call. The pressure on the International Telecommunication Union (ITU) to start work on the new generation system has been heavy. In March 1997, ITU-R invited proposals for radio transmission technology for International Mobile Telecommunications-2000 (IMT-2000). Eleven proposals were received by the deadline in June 1998. These proposals have been evaluated and it is expected that a family of third generation (3G) systems will be standardized by the end of year 1999. The main features that the 3G systems will support are:

- **High quality of service (QoS)**

The voice quality provided by the 3G systems is expected to have comparable quality to the services provided by the wire-line telephones. For data transmission rate as high as 2 Mbits/sec, the expected bit error rates (BER's) are as low as 10^{-3} and 10^{-8} for delay constrained and delay unconstrained services, respectively.

- **Multi and high rate data services**

The support of multi data rate transmission is well suited for different kinds of services provided by the 3G systems from low data rate voice to high data rate multimedia applications. Data rate as high as 2 Mbits/sec is a requirement for real-time video images and high speed data transmissions.

- **Mixed cell environments operations**

The 3G systems are expected to operate in different cell environments. For rural outdoor operating environment, where data rate is low (to a maximum of 144 kbits/sec) and speed of mobile unit is high (vehicle type of services), macro-cell is used. For urban to suburban operating environments, where data rate is as high as 384 kbits/sec (pedestrian type of services), micro- and macro-cells are used. For indoor operating environment, where data rate is as high as 2 Mbits/sec and speed of mobile unit is low (indoor type of services), micro- and pico- cells are used. The mixed cell environments operations give the flexibility of providing various types of data rate services. In addition, the 3G systems are required to be able to work with the second generation systems

that are operating in the macro-cell environment to ensure backward compatibility.

- **Family of global standards**

IMT-2000 initially wanted one unified universal standard to fulfill the idea of "one cellular phone around the world". But because of different considerations, it became impossible and it is likely that the United States will adopt the standard cdma2000 while the Europe and Japan will adopt the standard Universal Terrestrial Radio Access (UTRA).

And the requirements for the 3G mobile communication systems are:

- **Flexible to be upgraded**

One of the requirements for the 3G systems is flexibility. The goal of the 3G systems is to provide users worldwide coverage by roaming between different networks using a single mobile unit. The capability of roaming allows the 3G mobile unit to work with GSM system, which is commonly used in Europe and Asia, or with CDMA system, which is commonly used in North America. In UTRA specifications, the 3G mobile unit will be able to work in two modes, which are frequency division duplex (FDD) and time division duplex (TDD) modes. No major hardware change is required for these two modes to work on a single mobile unit. In the base station side of view, new cells can be developed without complicated frequency assignments. Therefore the upgrade of new cells is flexible.

- **Efficient utilization of spectrum**

Because of the limited spectrum left in the 2 GHz frequency band, frequency assignment for 3G systems, which will be operated in the 2 GHz band, is a prime consideration. On the other hand, the 3G systems should efficiently utilize the spectrum. For example, the use of discontinuous transmission (DTX) improves spectrum utilization. Capacity of the system is therefore increased and the probability of system congestion is low.

- **Power efficient**

Power efficiency is an important issue for the mobile unit because users demand mobile unit in smaller size and the battery with longer standby time. When the 3G systems are designed to be power efficient by virtue of techniques such as diversity, path searching, and DTX, the mobile unit has less power consumption and results in longer battery standby time.

- **Support wide range of services**

Different from the first and second generation mobile systems, where only voice and low rate data services are supported, the 3G systems support wide range of services including high quality voice, real-time video images, and high rate data services. The support of multi-services is a necessity because of the rapid growth of multimedia applications over wireless channels.

There are several promising candidates for the IMT-2000 systems. In this thesis, the UTRA system [37] is discussed in particularly detail. The wideband CDMA (W-CDMA) air interface that is suggested in the UTRA proposal is discussed in the next section.

3.2 Air Interfaces

Two major air interfaces suggested in the proposals submitted to ITU-R are TDMA and W-CDMA. Proposals from the European Telecommunications Standards Institute (ETSI) SMG2 and Japan Association of Radio Industries and Businesses (ARIB) are based on W-CDMA as the air interface for the FDD mode of UTRA system [38][39]. It is likely that T1P1-ATIS of USA (NA: W-CDMA), ARIB of Japan (W-CDMA), and European ETSI SMG2 (UTRA: W-CDMA) will harmonize their activities. In Korea, W-CDMA is also being used as the air interface for its CDMA I and CDMA II systems. In addition, W-CDMA technology is studied as the air interface for USA TIA TR45.5 (cdma2000) [38]. Therefore W-CDMA is a major part of most of the proposals. Before the UTRA system is discussed in detail, some features of W-CDMA air interface are summarized in the following.

- **Efficient utilization of spectrum**

Different technologies to improve spectrum utilization can be applied to CDMA. Those include DTX, where signal is transmitted at a lower power when there is no voice activity detected. This has the advantage that the link and the call are maintained while interference to other users is kept at a minimum level. In addition, different data rate services are multiplexed to achieve efficient utilization of spectrum for the system. In multi-code transmission, data streams are split into data channels and the data channels from different users can be multiplexed to transmit over the channel. Similarly, in single-code transmission, higher rate data is spread with lower spreading

factor while lower rate data is spread with higher spreading factor and they are multiplexed prior transmitting over the channel.

- **Flexible frequency management**

In CDMA, each cell or base station uses a cell specific long pseudo-noise (PN) code. Because of the near-orthogonal properties of the PN code, frequency can be reused in each cell while the inter-cell interference is kept at minimum level. And since the same radio band is reused in every cell, frequency planning is not a necessity in a CDMA system anymore. On the contrary, in TDMA systems, frequency re-assignment becomes necessary because some frequencies are to be assigned to the new cell. Because of the difficulty in re-assigning frequencies due to the irregular geographic topologies, the imperfect frequency assignment planning can result in lower the spectrum utilization efficiency. CDMA systems do not pose these difficulties. A new cell can be identified by assigning it a new PN code. Therefore system upgrade and frequency management is very simple and flexible.

- **Increased system capacity**

Because of the higher chip rate in the 3G systems, improved path resolution in W-CDMA results in greater number of resolvable paths. Therefore transmit power can be decreased because of increased path diversity gain. In consequence, interference to other users also decreases. This results in increase in the CDMA system capacity.

- **Interference limited**

There is a hard limit to the number of users that can be supported by a TDMA system. On the contrary, the limit on the number of users supported by CDMA systems is soft because any additional user lowers the QoS of all other users, but none of the user will be blocked. Numerous researches have been done with an aim to find methods to maximize the number of simultaneous users that a CDMA system can support for given performance requirements under different operating environments [40]-[43]. In [40], the maximum number of simultaneous users supportable by an asynchronous CDMA system using differential phase shift keying (DPSK) detection method under different scenarios is investigated. In [41], the use of Rake receiver to increase the capacity of a CDMA system is discussed. As shown in [42], coherent detection offers a 50% increase in cell capacity than non-coherent detection and further increase can be obtained by using Rake combining. In [43], maximum number of simultaneous users that is supportable while maintaining a certain level of QoS is analyzed.

- **Soft handoff**

When a mobile unit travels, the signal level received at the base station and at the mobile unit changes due to fading. When the signal level drops below a certain operating threshold value, it becomes necessary to switch to another base station in order to maintain continuity of the call and its quality. The process of switching from the current base station to a new one is called handoff. Two kinds of handoff are employed in cellular systems– hard handoff

and soft handoff. In a hard handoff, the current link with the serving base station needs to be broken before a link to a new base station is formed. It is called "break-before-make". In soft handoff, also called "make-before-break", the connection with the target base station is made before the link between the current base station and the mobile unit is broken. Soft handoff is a powerful technique to improve the transmission performance at the cell boundary as described in [3][44]. Another method called inter-frequency handoff [1][3][45] is capable of performing seamless handoff with base stations having different bandwidth allocations. This is especially useful for dual FDD and TDD mode operations in 3G systems. Inter-frequency handoff is discussed in more detail in Section 3.8.

Of course, none of a system is prefect and CDMA systems also have their own disadvantages. Near-far effect is one of the problems that a CDMA system has to deal with. Since all CDMA users share the same bandwidth, power assignment is of prime consideration, otherwise interference between users becomes intolerable. In the reverse link, the power received from the mobile user that is nearer to the base station is higher than the one that is far away if both users transmit the same power. This puts the near side users to an advantage user because of the higher received power but it could have disadvantageous effect on the far side user. The power control process can correct this problem by making sure that the received powers at the base station from all users are equal. Without power control, a CDMA system capacity cannot reach an optimum level [46]. Therefore power control is

essential in CDMA systems and this topic is thoroughly researched [47]-[49]. In [47], the performance degradation caused by imperfect power control is analyzed. In [48], the relationship between power control process and capacity of a cellular CDMA system is investigated. In [49], power control for a multirate wireless multimedia communication system is discussed. There are two types of power control– open loop and closed loop. Open loop power control is a purely mobile controlled operation and it is used to compensate for power fluctuations due to slowly varying and log-normal shadowing fading. Closed loop power control is a process which involves both the mobile unit and the base station. In closed loop power control, the received signal-to-interference ratio (SIR) is measured at the base station (for reverse link transmission) in every transmitter power control (TPC) cycle. When the measured value is higher than the preset SIR value, the transmitter power is lowered; otherwise it is raised.

As mentioned earlier, one of the main features of the 3G mobile radio system is the support of multirate transmission for multimedia applications. In the next section, multirate transmission schemes used in UTRA systems are described.

3.3 Multirate Transmission

Different from the second generation mobile radio systems, which are designed mainly for voice services and low rate data transmission, 3G mobile radio systems are designed to support multi-services and variable rate data

transmission. Low and high rate data can be multiplexed together to achieve better bandwidth efficiency. Bandwidth on demand, where the user can opt for different rate services during a single transmission, will also be supported. In UTRA system, variable rate data transmission is realized by assigning multiple codes to users [50], or by using single code with different spreading factors according to the data rate [51]. In multi-code transmission, data rate that is higher than the basic data rate, R_b, is split serial-to-parallel. For example, a rate R_s data signal is split into K different fixed rate data streams and each data stream is then having a rate of $R_s/K = R_b$, which is the basic rate. This basic rate is fixed and therefore the number of split data streams, K, varies according to data rate R_s. The higher the data rate, the more number of split data streams. K different spreading codes with the same chip rate are used to spread the K different data streams. If the chip period of the spreading codes is defined as T_c, the spreading factor of each data stream is $1/(T_cR_b)$, which is fixed regardless of the information data rate. Using orthogonal variable spreading factor (OVSF) codes is another way to realize multirate transmission [52]. Different from the multi-code transmission scheme, the OVSF scheme results in different spreading factors depending on the data rate. For a rate R_s data, the spreading factor is $1/(T_cR_s)$; and a rate $2R_s$ data will have a spreading factor of $1/(2T_cR_s)$, which is half of that of the rate R_s data. In other words, the higher the data rate, the lower the spreading factor. It should be noted that in all cases the resultant transmission bandwidth is the same. That is, the chip rate of the system is fixed. When comparing the multi-code scheme [53] with single code

scheme, the BER performance is similar in both schemes [54][55]. But in terms of hardware complexity, OVSF scheme has advantages over the multi-code scheme. Only a single Rake receiver is needed in the receiver for a system employing OVSF scheme that supports variable rates. This is important especially in the forward link because of the requirement for small-sized and power efficient mobile units. On the other hand, since the spreading factor is inversely proportional to the user data rate in OVSF scheme, the disadvantage of using this scheme is when the user data rate is high, the resulting spreading factor is low and the system losses its CDMA characteristics. A system with low spreading factor is investigated in [56], where the effects of interpath interference (IPI) on a low spreading factor system are analyzed. In [58], a multi-code system is shown to have greater capacity than a system that utilizes the OVSF scheme in multipath fading environments. However, the large variations in the signal amplitude of a multi-code system [54][57] require the implementation of high power amplifiers (HPA's) in the transmitter in order to obtain sufficient transmitting power. And the nonlinear distortion introduced by the HPA's [59] severely degrades the system performance.

3.4 FDD Mode and TDD Mode

Both the FDD and TDD modes are supported in the proposed UTRA system. The frequency allocation for the 3G system in Europe is shown in Figure 3.1. In W-CDMA FDD mode, different frequency bands are assigned for forward and reverse links respectively. On the contrary, in time division CDMA

(TD-CDMA) TDD mode, same frequency band is used for both forward and reverse links. As shown in Figure 3.1, 35 MHz of unpaired spectrum is assigned for TDD mode and paired spectrums of 60 MHz (total of 120 MHz) are assigned for FDD mode in Europe. The usage of both FDD and TDD increases the flexibility and allows for efficient frequency allocation according to the conditions of different regions of the world. TDD is particularly useful where paired spectrum is not assigned in that specific area. TDD mode system is usually employed in hot spots or regions where capacity requirement is high or data traffic rate is asymmetric and it gives the advantages of efficient spectrum utilization in asymmetric data transmission [60]. For example, in multimedia services, where the forward link (FL) traffic is usually higher than the reverse link (RL) traffic, more time slots can be allocated for forward link transmission in TDD mode of operation as depicted in Figure 3.2. In Figure 3.2 (a), symmetric transmission is shown as the loads of the forward link and reverse link are identical. A frame that has a forward link capacity 3 times more than that of the reverse link is shown in Figure 3.2 (b). And this ratio can be changed accordingly to the traffic characteristics.

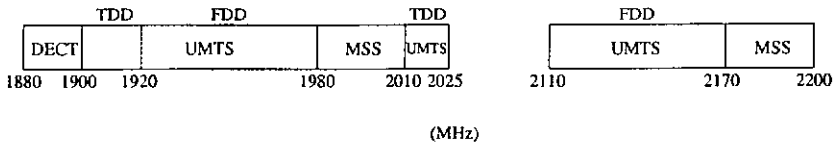

Figure 3.1 Frequency allocation for the 3G system in Europe

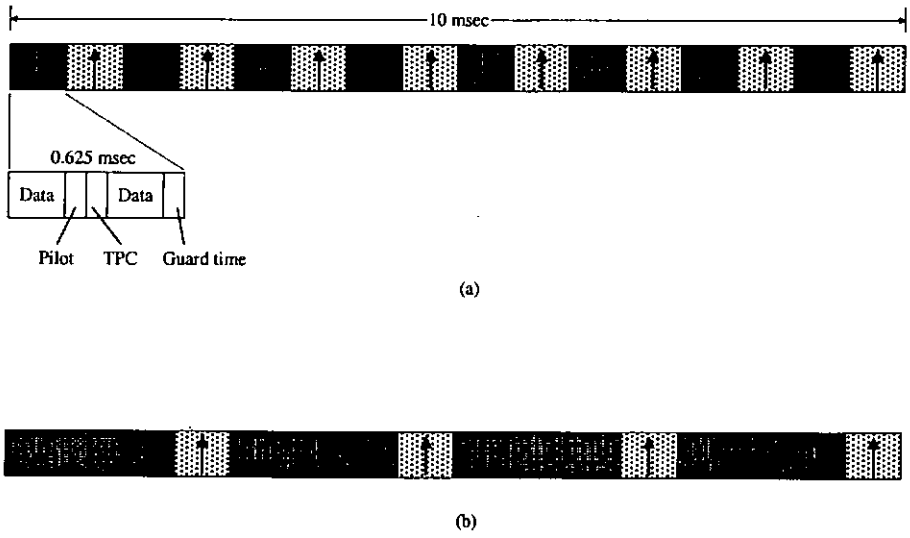

Figure 3.2 Data transmission in TDD system (a) symmetric transmission (b) asymmetric transmission FL:RL load = 3:1

Since both forward and reverse links use the same frequency band in TDD mode, the pre-Rake filter [61] implementation eliminates the need of Rake receiver in the base station [62]. This lowers the complexity of base station and is ideally suited to the deployment of many small TDD cells. On the other hand, a Rake receiver can be implemented at the base station instead of in the mobile unit because of the same channel impulse response during a short period of time [63][64]. Therefore the use of a conventional receiver in the mobile unit can still achieve the diversity gain provided by a Rake receiver. The comparison of pre-Rake and Rake systems is given in [64]. The TDD mode requires inter-cell synchronous operation since synchronization between base stations is required. However, since the synchronization accuracy is not severe, the implementation of synchronization does not necessarily rely on the

global positioning system (GPS). By combining the use of wire-line network, the GPS can be used only for the initial adjustment of the system clock. And the synchronization is maintained through the wire-line network. On the other hand, the FDD mode does not require inter-cell synchronous operation since precise synchronization between base stations is not necessary. So the deployment of base stations to indoors and outdoors is flexible and GPS is no longer needed.

3.5 Channel Coding

3.5.1 Forward Error Correction

Forward error correction (FEC) codes that are adopted in UTRA proposal include convolutional code, Reed-Solomon (RS) code, and turbo code. For standard services with BER requirements in the order of 10^{-3}, a rate 1/3 convolutional code with constraint length of 9 is used. For higher quality and higher delay tolerable services where BER requirements are in the order of 10^{-6}, the concatenation of convolutional codes and outer RS codes plus outer interleaving is used. For higher data rates, the rate 1/3 convolutional coding is replaced by rate 1/2 code. Turbo codes [65], which is a class of convolutional codes, can be used instead of the concatenated arrangement of RS and convolutional codes.

3.5.2 Interleaving

The combination usage of convolutional code and interleaving is necessary for a reliable system in fading environments. Interleaving depth is designed to be 10 msec, 20 msec, 40 msec, and 80 msec depending on the delay constraints in different kinds of services. For example, for voice services where delay is intolerable, shorter interleaving depth such as 10 msec or 20 msec should be used. On the other hand, for services such as computer data that is not sensitive to delay and high QoS is required, interleaving depth as long as 80 msec can be used.

3.6 Spreading and Modulation

Two levels of spreading are adopted in UTRA proposal. At the first level, OVSF codes are used. The OVSF codes are generated from Hadamard matrix and the way of generating them is discussed in more detail in Section 4.6.2 of Chapter 4. A cell specific long code is used at the second level of spreading. A 10 msec segment of a Gold code of length 2^{18}-1 is used in the forward link, and 737.28 sec segment of a Gold code of length 2^{41}-1 is used in the reverse link.

In the forward link, the signal is QPSK modulated with a quadrature modulator and the pulse shaping filters are root-raised cosine (RRC) with a roll-off factor of 0.22 in the frequency domain followed by BPSK spreading. That is, the data is spread by the same short code. In the reverse link, the signal is dual-channel QPSK modulated [66]. That is, the data is spread by two

different short codes. And the pulse shaping filters are the same as in the forward link.

3.7 Power Control

Power control is essential in CDMA systems since many users share the bandwidth simultaneously. In UTRA, TPC is used to mitigate the near-far problem and to increase the system capacity. The TPC method adaptively adjusts the transmitter power based upon SIR or desired signal level.

Two types of TPC in UTRA W-CDMA are used– one is SIR-based fast closed loop TPC and the other is open loop TPC. In SIR-based fast closed loop TPC, the received SIR is measured every 0.625 msec TPC cycle. When the measurement cannot be performed or the measured value is lower than the target SIR value, TPC bit is set to 1; otherwise, it is set to 0. When the received TPC bit is judged as 1 at the base station, the transmitter power is raised by 1 dB; and when it is judged as 0, the transmitter power is reduced by 1 dB. For the case where the TPC bit is not received, the transmitter power remains unchanged. Open loop TPC is a pure mobile unit controlled operation where the receiver estimates the path loss of transmission channel and the transmitter power is adjusted according to this estimation.

3.8 Inter-frequency Handoff

Because of the fading effects, the signal level received by the base station varies as the mobile unit travels. When the signal level drops below a certain threshold value, it is necessary to switch to another base station in order to ensure the continuity of the call and to maintain acceptable link quality. The process of switching from the current base station to a new target one is called handoff. Besides the usual hard handoff and soft handoff employed in many cellular systems, inter-frequency handoff is supported in UTRA. Inter-frequency handoff provides mobile unit the capability of switching to a new base station with carrier frequency different from the current one. When new micro cells is overlaid with macro cells, where these two cells are operating in different carrier frequencies, inter-frequency handoff is a requirement for seamless handoff between these cells.

3.9 Operation of UTRA System over Practical Wireless Channels

In this section, operation of UTRA system over practical wireless channels is discussed. In mobile radio communications, the reliability of a system mostly depends on the channel behavior. However, the channel characteristics are due to the signal propagation environment and are not parameters that can be adjusted or changed. Instead, a system designer can adjust parameters such as the number of fingers in the Rake receiver and interleaving depth. Therefore the impacts of varying these parameters on the system performance are investigated in this thesis. Multipath fading is one of the major impairments in

a mobile radio channel that makes wireless transmission unreliable. Several ways can be used to cope with the problems caused by multipath fading transmission. For example, in a mobile transmission environment where multipath propagation is common, a Rake receiver can be used to mitigate the problems caused by multipath fading. And the number of fingers in the Rake receiver plays an important role on the performance of the system. Therefore the sensitivities of the system performance with different number of fingers in the Rake receiver under different channel environments are investigated. A path searching technique can be implemented to improve the system performance when the number of fingers in the Rake receiver is not matched to the number of signal paths in the channel. And the parametric sensitivity of the system to path searching algorithm is investigated. Different interleaving depths have different impacts on a system and the effect of varying this parameter on the system performance is also investigated. The use of antenna diversity to improve the system performance is discussed as well. The results of the sensitivities of UTRA system performance to the parameters are given and discussed in detail in Chapter 5.

3.10 Summary

In this chapter, different aspects of the 3G mobile radio system, especially the UTRA system jointly proposed by ETSI and ARIB, are discussed. In particular, the main features and requirements of the 3G system are presented. FDD and TDD modes of the UTRA system are also discussed. Channel

coding, spreading, and modulation in UTRA system are presented with power control discussed in detail in the chapter. Different kinds of handoff including the inter-frequency that supports handoff between two cells operating in different carrier frequencies are discussed. Parameters to be investigated in the thesis are introduced in this chapter.

Chapter 4

SYSTEM MODEL AND SIMULATION EXPERIMENT DESIGNS

4.1 Introduction

The specifications and advantages of Universal Terrestrial Radio Access (UTRA) system are given in Chapter 3. In this chapter, detailed descriptions of the simulation model that is used to investigate the parametric sensitivities of the UTRA system are provided. The software packages MATLAB and SIMULINK are used in the design and simulations of the system. The performances under many scenarios are presented in terms of bit error rate (BER). To fully understand the simulation model, different aspects of the system are described in the subsequent sections. In Section 4.2, multirate transmission realized by the orthogonal variable spreading factor (OVSF) scheme is described. The different power transmission for different data rates users is explained. System and simulation parameters are also presented in that section. Channel coding used in the simulation experiments is explained in Section 4.3. Interleaving and modulation are discussed in Sections 4.4 and 4.5, respectively. Two levels of spreading and the generation of tree-structured

code are presented in Section 4.6. In Section 4.7, the multipath fading channel model is illustrated followed by the discussion of some miscellaneous issues encountered in the design process of the system model in Section 4.8. Rake receiver and diversity techniques used in the simulation experiments are explained in Sections 4.9 and 4.10, respectively. Finally, this chapter is summarized in Section 4.11.

4.2 Multirate Transmission

The simulation model used in the simulation experiments is capable of multirate transmission. Multirate transmission is realized by the OVSF scheme, which is described in Chapter 3. In all simulation experiments performed, four users share the wideband signal. Three transmit at 32 kbits/sec (designated as rate $R1$) and the remaining user transmits at 64 kbits/sec (designated as rate $R2$). In order to have the same transmitted energy per bit for all users, the rate $R2$ user transmits two times higher power than the rate $R1$ users [67] as explained below. Assume the bit energy for the rates $R1$ and $R2$ users are

$$E_{b,R1} = P_{R1} T_{b,R1}, \tag{4.1}$$

and

$$E_{b,R2} = P_{R2} T_{b,R2} = P_{R2}\left(\frac{T_{b,R1}}{2}\right), \tag{4.2}$$

respectively. In order to have the same energy per bit, $E_{b,R2} = E_{b,R1}$,

$$P_{R1}T_{b,R1} = P_{R2}\left(\frac{T_{b,R1}}{2}\right).$$

Therefore

$$P_{R2} = 2\,P_{R1}. \tag{4.3}$$

Since the spreading gain is inversely proportional to the data rate, the higher data rate user has to transmit higher power than the lower data rate users to overcome the disadvantage of lower spreading gain. This unequal power transmission for different data rate users makes the power control process even more difficult to be reached optimum [68] and many researches have been done on this issue [69][70]. In [69], a power control law for multirate CDMA systems based on quality of service (QoS) requirement is proposed. In [70], power control in multirate system based on equal bit energy rule and equal error probability rule are introduced.

Figure 4.1 depicts the block diagram of the simulation system model used in the computer simulations and the system and simulation parameters are shown in Table 4.1.

All results are obtained by 50 seconds of simulations. And the 64 kbits/sec user is the desired user. Therefore the lowest BER that is statistical confident is about 3×10^{-5}. In addition, it should be noted that in all the simulation results shown in Chapter 5, unless otherwise stated, the interleaving depth is 10 msec, Doppler frequency is 80 Hz, and the maximum delay spread is always a lot smaller than the symbol duration of the desired user (i.e., $\tau_{max} \ll T_s$).

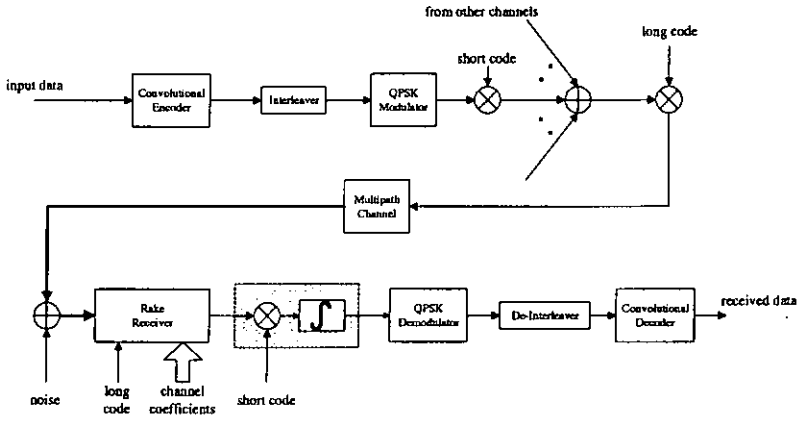

Figure 4.1 Schematic block diagram of the simulation system model

Table 4.1 System and simulation parameters

Item		**Parameter**
Chip rate (Mchips/sec)		3.072
Spreading code	Short code	Walsh-Hadamard code
	Long code	*m*-sequence PN code
Modulation	Data	QPSK
	Spreading	BPSK
Channel coding		Convolutional coding (R = 1/3, K = 3)
Channel decoding		Hard decision with traceback length = K×5
Channel		Frequency selective Rayleigh fading with uniform delay profile (maximum number of paths = 6)
Multirate		OVSF
Interleaving (msec)		10 (5, 20)
Doppler frequency (Hz)		10-80

4.3 Channel Coding

Two major kinds of channel coding available for use in telecommunications are block coding and convolutional coding as described briefly in Chapter 2. In UTRA proposal, a rate 1/3 convolutional code with constraint length of 9 is specified for standard services with BER requirements in the order of 10^{-3}. To simulate the performance of a UTRA system, the channel coding used in this thesis is a rate 1/3 convolutional code with constraint length of 3. Constraint length of 3 is adopted here because longer constraint length demands a longer simulation process, which is time-consuming and therefore undesirable. From the results for convolutional coding with constraint length of 3, the performance of a system with higher constraint length convolutional code can be predicted as given in [72]. For an additive white Gaussian noise (AWGN) channel, a degradation of 0.5 dB is expected if the constraint length is decreased by 1 as shown in [72, p.398]. On the other hand, in a fading channel situation, the gain of increasing the constraint length by 1 is 0.8 dB and 3.6 dB, for 4032 bits of interleaving depth and no interleaving, respectively, as shown in [72, pp. 399-400].

The channel decoding algorithm used is hard-decision method with traceback length of 3×5. Hard-decision is inferior by about 2-3 dB when comparing with soft-decision method [33]. Therefore by choosing the hard-decision as the channel decoding method in this thesis, the worst case results can be obtained and the actual system will always get better

performance. However, the order of complexity increases for soft decoding and therefore requires a more complex decoder.

Channel codes such as convolutional codes are optimally used in random channels (i.e., memoryless channels). They are not suitable for use in channel that exhibits fading characteristics, which is always the case in cellular radio communications. Therefore some techniques are needed after the data are channel encoded and as explained in the next section, interleaving is found to be a powerful method to mitigate the bursty errors produced by a Rayleigh fading channel when used together with convolutional codes. Interleaving is described more briefly in the next section.

4.4 Interleaving

Convolutional codes cannot efficiently correct the bursty errors that are produced by the fading channel since these codes are optimally designed for random error channels only. However, codes designed for random channel errors can still be used if there is a way to disperse the error bursts into randomly occurring errors. And this is to rearrange the channel encoded data using an interleaver so that the frequency selective fading channel can be looked as if it were a memoryless channel. This interleaving technique is also called time diversity since data symbols are time separated before transmitting through the channel. This form of diversity is powerful because it turns a memory channel into a memoryless one while there is no overhead on doing this. The only concern is the time delay caused by interleaving. For services

such as speech data and real-time video images that are sensitive to time delay, interleaving depth should be designed carefully or the delay becomes intolerable. There are two forms of interleaver, which are convolutional interleaver and block interleaver.

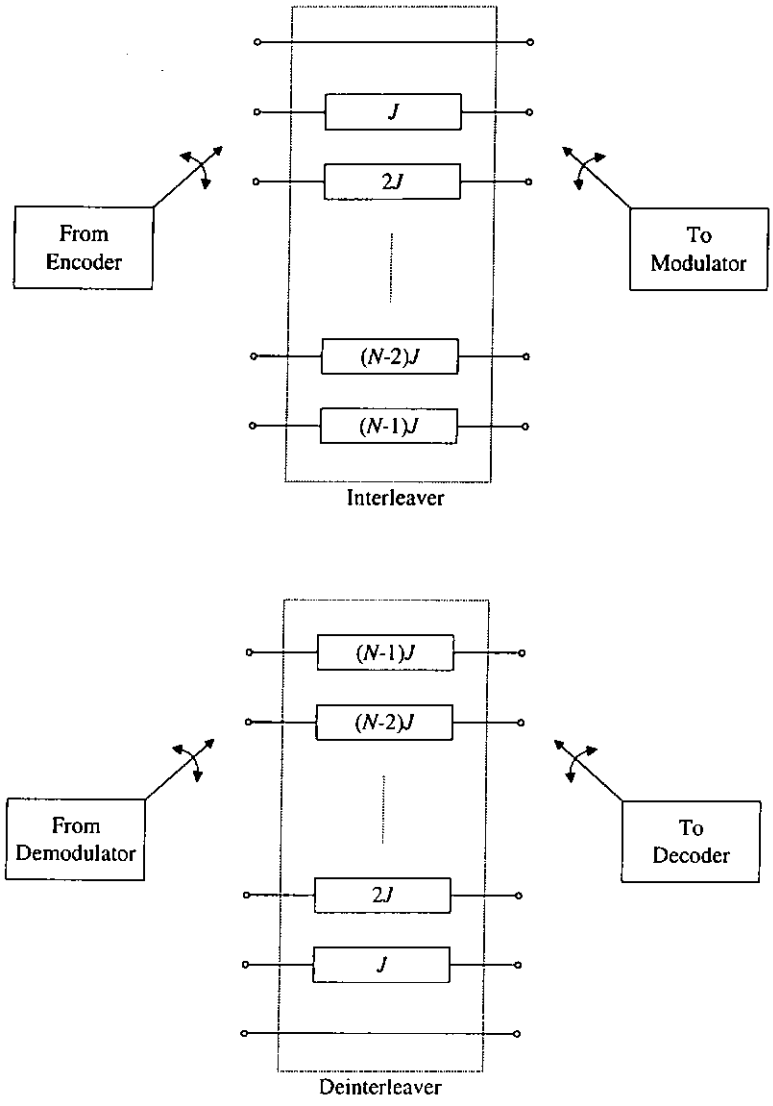

Figure 4.2 Convolutional interleaver

The structure of a convolutional interleaver proposed by Forney [73] is shown in Figure 4.2. It consists of a bank of N registers and the zeroth register has no symbol storage. With each successive register, J more symbols storage is provided. The commutator switches to a new register when new symbols are written in, while the oldest symbol is shifted out to the data modulator. The de-interleaver performs the reverse operation.

In a (M, N) block interleaver, where M and N are the number of rows and number of columns, respectively, bits that are encoded by the convolutional encoder are written in row-wise and read out column-wise to the data modulator. At the receiving end, received bits are written in column-wise and read out row-wise to the demodulator as shown in Figure 4.3. The block interleaver is designed so that when a burst occurs and is less than M contiguous errors, the errors will become independent and all separated from each other by at least N symbols as shown in Figure 4.4 (a). On the other hand, burst with bM errors ($b > 1$) becomes no more than $\lceil b \rceil$ symbol errors and each output burst at the de-interleaver is separated from other bursts by no less than $(N - \lfloor b \rfloor)$ symbols as shown in Figure 4.4 (b), where $\lceil x \rceil$ means the smallest integer greater than x and $\lfloor x \rfloor$ means the largest integer smaller than x. In addition, a periodic sequence of single errors spaced by M symbols will become a single burst of errors of length N at the de-interleaver output as shown in Figure 4.4 (c). Performance gains of different sizes of block interleaver are tabulated in [72, p. 400]. In general, the required interleaving

depth depends on the fade duration of the signal. If the vehicle speed is low, longer interleaving depth is required to mitigate the longer fade duration.

The above mentioned interleavers have different interleaving delays because of their different structures. While a block interleaver introduces a $2MN$ delay, a convolutional interleaver introduces a $NJ(N - 1)$ delay. In terms of complexity, block interleaver is less complex than a convolutional interleaver, and the former is considered in this thesis.

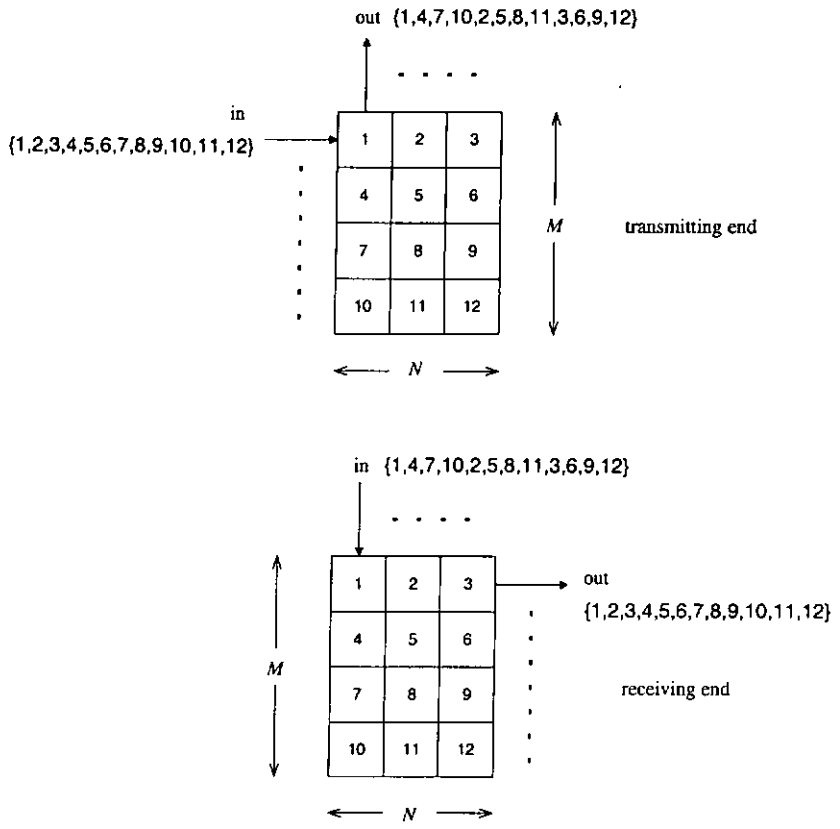

Figure 4.3 Block interleaver ($M = 4$, $N = 3$)

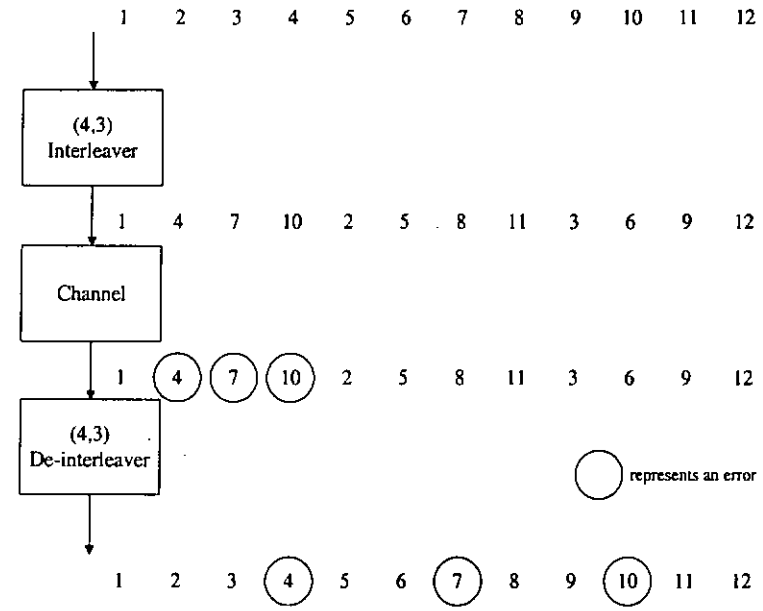
1 2 3 4 5 6 7 8 9 10 11 12
(4,3)
Interleaver
1 4 7 10 2 5 8 11 3 6 9 12
Channel
1 4 7 10 2 5 8 11 3 6 9 12
(4,3)
De-interleaver
represents an error
1 2 3 4 5 6 7 8 9 10 11 12

(a)

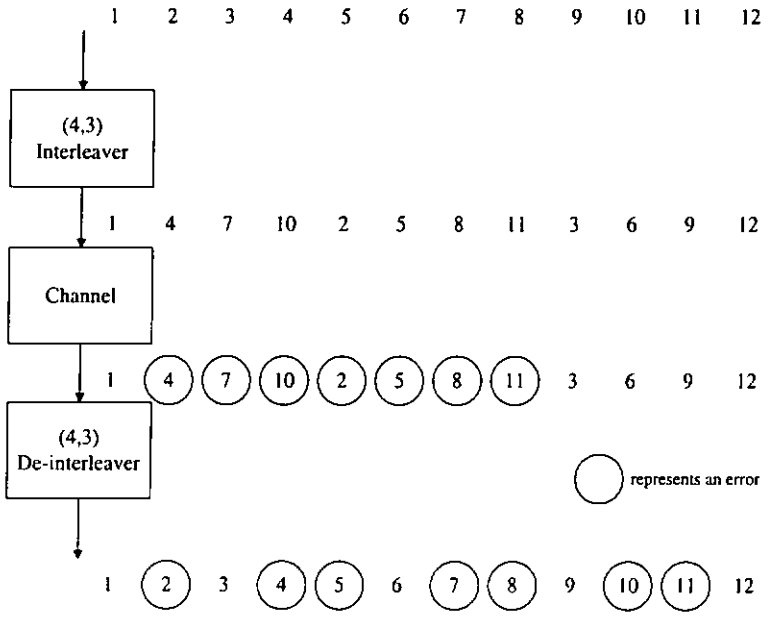
1 2 3 4 5 6 7 8 9 10 11 12
(4,3)
Interleaver
1 4 7 10 2 5 8 11 3 6 9 12
Channel
1 4 7 10 2 5 8 11 3 6 9 12
(4,3)
De-interleaver
represents an error
1 2 3 4 5 6 7 8 9 10 11 12

(b)

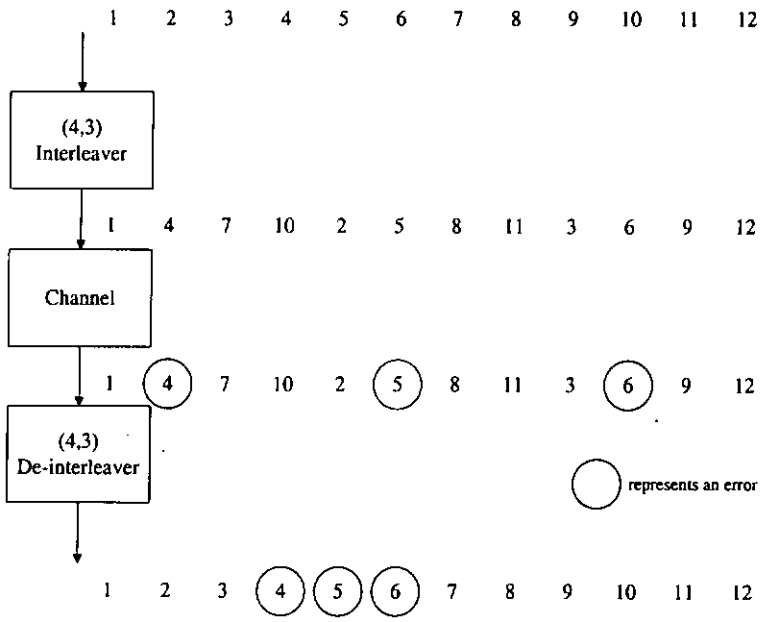

(c)

Figure 4.4 Interleaver example ($M = 4$, $N = 3$) (a) 3 symbol error burst (b) 7 symbol error burst (c) periodic sequence of single errors spaced by 4 symbols

Interleaving depth is one of the parametric values used in this thesis to investigate the performance impacts under different scenarios. For example, under low vehicle speed (i.e., low Doppler frequency), short interleaving depth is expected to give poor performance while long interleaving depth gives better performance in high vehicle speed than in low vehicle speed situation. More discussions on that are found in Chapter 5.

4.5 Modulation

The modulation method used in this thesis is quaternary phase shift keying (QPSK). QPSK modulator is basically two binary phase shift keying (BPSK)

modulators connected in parallel as shown in Figure 4.5 (a). Symbols are split serial-to-parallel and fed into the binary phase shift keying (BPSK) modulators in the two branches, which are termed as I-branch and Q-branch. In BPSK modulation, an input binary bit 1 will have an output -1; and an input binary bit 0 will have an output 1. Finally, the two bits are combined as shown in the figure. Figure 4.5 (b) shows the signal space of a QPSK modulator. Since QPSK modulator processes two bits at a time, the modulated output data have a rate half of that of the input data. At the receiving end, data are QPSK demodulated.

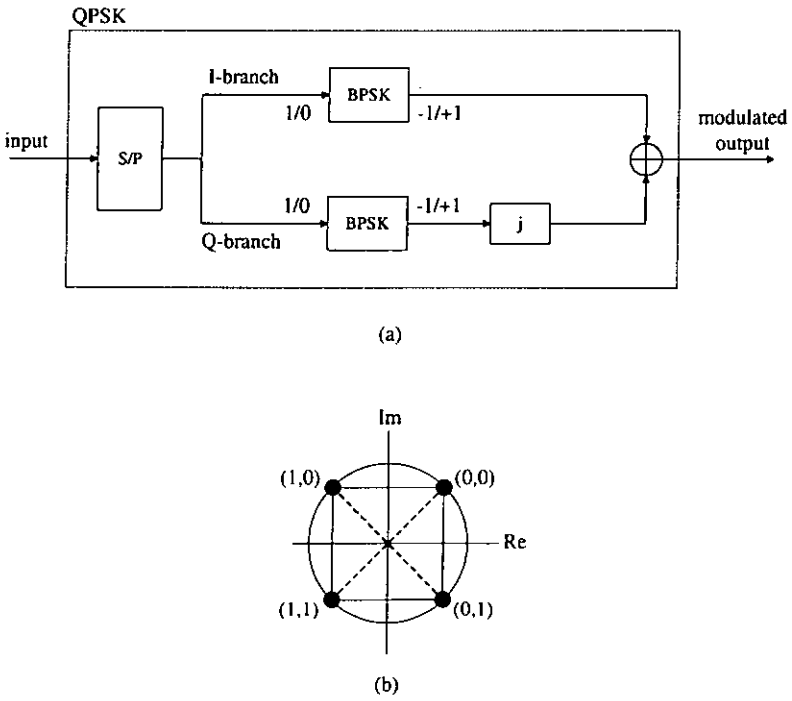

Figure 4.5 QPSK modulator (a) structure (b) signal space

4.6 Spreading Codes

In UTRA, there are two levels of spreading. In the first level of spreading, modulated data is spread with short codes, which are Walsh-Hadamard codes. Different codes are assigned to different users in the same cell for channelization and the same set of codes are used in different cells. Cell specific long codes are assigned to different cells to minimize the inter-cell interference. Virtually there are unlimited number of long codes available for use. In this thesis, *m*-sequences and Walsh-Hadamard codes are used as long spreading sequences and short spreading sequences, respectively. These two types of codes are discussed in more detail in the following sections.

4.6.1 Long Spreading Codes

As mentioned earlier, spreading a signal before transmitting through a channel gives many advantages. However, the choice of a spreading sequence can decide the performance of a system [74]. First of all, the autocorrelation function of the sequence is desired to be one at zero shift and zero elsewhere. That is, low correlation sidelobes. Secondly, optimal crosscorrelation is preferred. In addition, the family size of the sequence should be large and ease of generation of the same sequence at different locations (e.g., at base stations and on mobile units) is required. The *m*-sequence is one of the most suitable codes for use as spreading codes although it does not have ideal autocorrelation and crosscorrelation functions. But these properties improve with increasing sequence length. In addition, generation of the same sequence

at both the base station and mobile unit is easy. The properties of *m*-sequences are discussed in more detail in [78]-[80]. But in general, a shift register generator (SFG) of *M* stages is required to construct an *m*-sequence. The form of the linear feedback logic is important in order to have a maximal length sequence and the maximal length of an *m*-sequence is $2^M - 1$, where *M* is the number of stages in the SFG. We will take the example of 4 stages SFG to illustrate the construction of the sequence as shown in Figure 4.6.

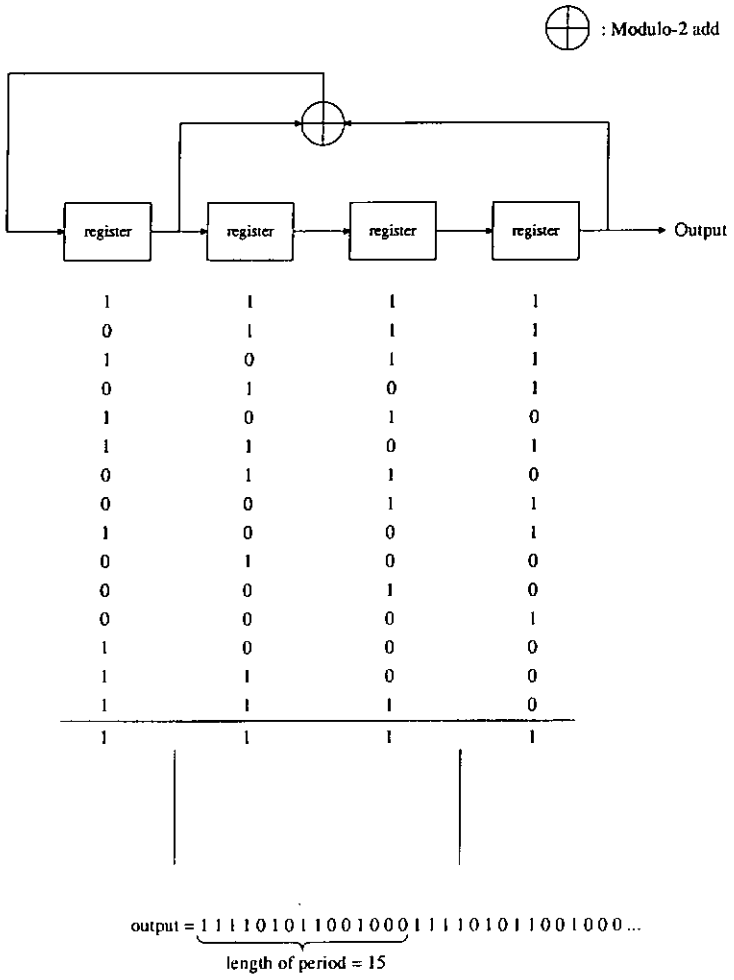

Figure 4.6 Construction of an *m*-sequence

It should be noted that the initial states of the registers should not be all zeroes in order to generate the sequence. And different initial conditions in the shift registers create shifts of *m*-sequence. As shown in Figure 4.6, the maximal length of the sequence is $2^4 - 1 = 15$. And in spread spectrum communications, these are called chips. The selection of the linear feedback logic in order to generate an *m*-sequence is given in [81, pp. 341-342]. As shown in Figure 4.7, the *m*-sequence has near ideal autocorrelation, $R_c(t)$. That is, the peak value $R_c(0) = N$ and off peak values $R_c(j) = -1$, where N is the length of the sequence and $1 \leq j \leq N-1$. The off peak values relative to the peak value is $R_c(j)/R_c(0) = -1/N$ and this ratio is small for large N. Therefore the longer the sequence, the better the *m*-sequence in terms of its autocorrelation function.

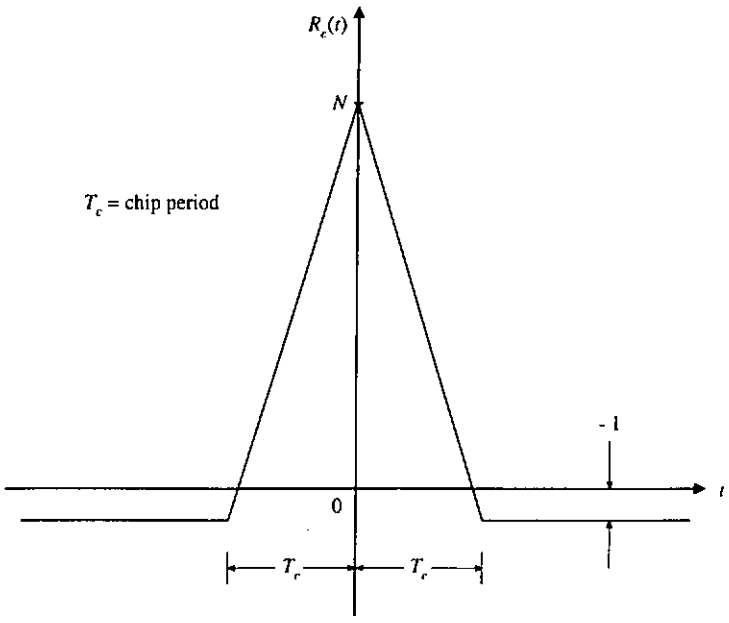

Figure 4.7 Autocorrelation of an *m*-sequence

In practice, the near ideal case of autocorrelation of an *m*-sequence is not feasible since only non-periodic correlation of the *m*-sequence is available. That is, only part of the *m*-sequence, which is usually very long, is used for correlation. For example, in Interim Standard-95 (IS-95), an *m*-sequence with length 2^{42}-1 is used. For the proposed UTRA system, the long code used is a length of 2^{18}-1 Kasami sequences. The non-ideal case of autocorrelation creates interference between different paths in multipath propagation and this interference is dominant when the processing gain of the system is low. Interpath interference is described in more detail in Section 5.2 of Chapter 5.

Different families of spreading codes are proposed to achieve better system performance. For example, in [75], binary Gold, binary Kasami, and polyphase generalized chirp-like (GCL) sequences are discussed and compared. Binary Gold sequences, which are derived from *m*-sequences, have large family size and good correlation properties provided that the sequence length is long. But the performance is poor for short sequence length (e.g., $N = 63$) especially in a multi-user environment and this can be improved by increasing N. Kasami sequences are similar to Gold sequences and can be considered as a subset of Gold sequences since they both have three-valued autocorrelation and crosscorrelation functions. The correlation sidelobes of Kasami sequences are lower than that of the Gold sequences, which is preferable. However, the small family size of Kasami sequences is a disadvantage. Different from binary sequences, where values are real, the complex valued feature of polyphase sequences is advantageous for systems

employing quadrature modulation schemes such as QPSK. Another distinction can be made between binary sequences and polyphase sequences is while binary sequences are two-valued, polyphase sequences can have any value. It can be shown that specific GCL sequences can have ideal autocorrelation and optimum crosscorrelation [76]. These advantages make them very attractive for CDMA systems. However, the system complexity as a result increases. Table 4.2 summarizes the different properties of the above three mentioned sequences, where M is the number of shift registers used to generate the sequence and $\phi(n)$ is the Euler phi-function. The system complexity can be represented in terms of n and M; the larger the values of n and M, the more complex the system is.

Table 4.2 Properties of different kinds of spreading sequences

	Gold sequences	Kasami sequences	GCL sequences (optimum)
sequence length, N	2^M-1	2^M-1, M even	n^2, n odd prime
family size	2^M+1	$2^{M/2}$	$\phi(n)$
correlation properties	good for large N	good	best
complexity	acceptable	acceptable	high

A set of spreading codes called extended structured codes (ESC) is proposed in [77] that is for use in a CDMA system with Rake receiver. This

family of codes can optimize the performance of a Rake receiver in a multi-user environment.

Although only a small subset of *m*-sequences have small crosscorrelation peak values, a 2^{33}-1 long *m*-sequence is used for spreading because only a single cell is considered in this thesis.

4.6.2 Tree-Structured Code Generation [71]

As mentioned above, the long spreading codes that are used to distinguish between different cells is a long *m*-sequence PN code. To separate between different users in the same cell, short codes called Walsh-Hadamard codes are used. Since one of the requirements for 3G systems is the support of multirate data transmission, it is necessary to use some special form of short codes so that the spread data have the same bandwidth even for different data bit rates. OVSF scheme is one of the solutions for that [52].

In OVSF scheme, the spreading factor (SF) is chosen by the relationship:

$$SF = R_c / R_b , \tag{4.4}$$

where R_c and R_b are the chip rate and symbol rate, respectively. The orthogonal codes with spreading factor of 2^m can be constructed by starting with $C_0 = 1$:

$$C_m = \begin{bmatrix} C_{m-1} & C_{m-1} \\ C_{m-1} & \overline{C}_{m-1} \end{bmatrix}, \tag{4.5}$$

where $\overline{C}_{m-1}$ is the complement of C_{m-1}. All codes of C_m are orthogonal to each other and so are the C_{m-1} codes. According to (4.5), two codes of C_m are generated from each code of C_{m-1} and these two codes are not orthogonal to the code from which they are generated. For example, $C_4(1)$ (mother code) is not orthogonal to $C_5(1)$, $C_5(2)$, $C_6(1)$, $C_6(2)$, $C_6(3)$, and $C_6(4)$. Therefore these codes cannot be used simultaneously in order to maintain orthogonality. (4.5) can be written as

$$C_m = \begin{bmatrix} C_m(1) \\ C_m(2) \\ C_m(3) \\ C_m(4) \\ \vdots \\ C_m(2^m-1) \\ C_m(2^m) \end{bmatrix} = \begin{bmatrix} C_{m-1}(1) & C_{m-1}(1) \\ C_{m-1}(1) & \overline{C}_{m-1}(1) \\ C_{m-1}(2) & C_{m-1}(2) \\ C_{m-1}(2) & \overline{C}_{m-1}(2) \\ & \vdots \\ C_{m-1}(2^{m-1}) & C_{m-1}(2^{m-1}) \\ C_{m-1}(2^{m-1}) & \overline{C}_{m-1}(2^{m-1}) \end{bmatrix} \tag{4.6}$$

and Figure 4.8 shows the tree-structured code constructed in this manner and the codes in each row (i.e., for a specific m value) are orthogonal to each other.

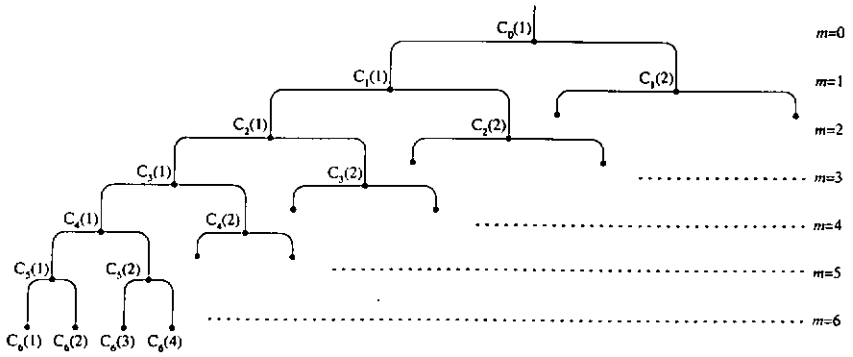

Figure 4.8 Tree-structured code

For example, for a data bit rate 64 kbits/sec, after it is channel encoded with a 1/3 rate convolutional encoder followed by QPSK modulation, the resultant symbol rate is 96 ksymbols/sec. Therefore from (4.4), $SF = (3.072 \times 10^6) / (96 \times 10^3) = 32 = 2^5$. And one of the spreading codes $C_5(1)$, $C_5(2)$, $C_5(3)$, ..., $C_5(32)$ can be used for spreading. It can also be seen from (4.4) that the spreading factor is inversely proportional to the symbol rate. That is, higher data rate users have lower processing gains while lower data rate users have higher processing gains.

4.7 Multipath Channel Model

The simulation channel model is a wide sense stationary uncorrelated scattering (WSSUS) Rayleigh channel with a maximum of six independently frequency selective fading paths. Each Rayleigh fading path is simulated by using the Jakes' model [82] and it is shown in Figure 4.9.

For more than one path in the channel, correlations between different paths are minimized according to the methods as described in [82]. Uniform delay profile is used in all simulation experiments although exponential delay profile is commonly used as the multipath power delay profile (MPDP). By using uniform delay profile as the MPDP, the analysis becomes simpler and it provides the worst case scenario. Figure 4.10 shows the multipath channel model.

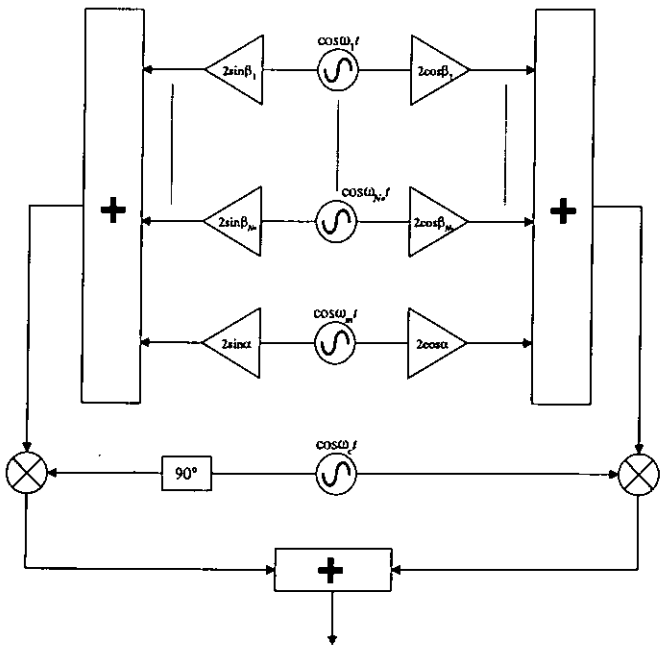

Figure 4.9 Jakes' Rayleigh fading model

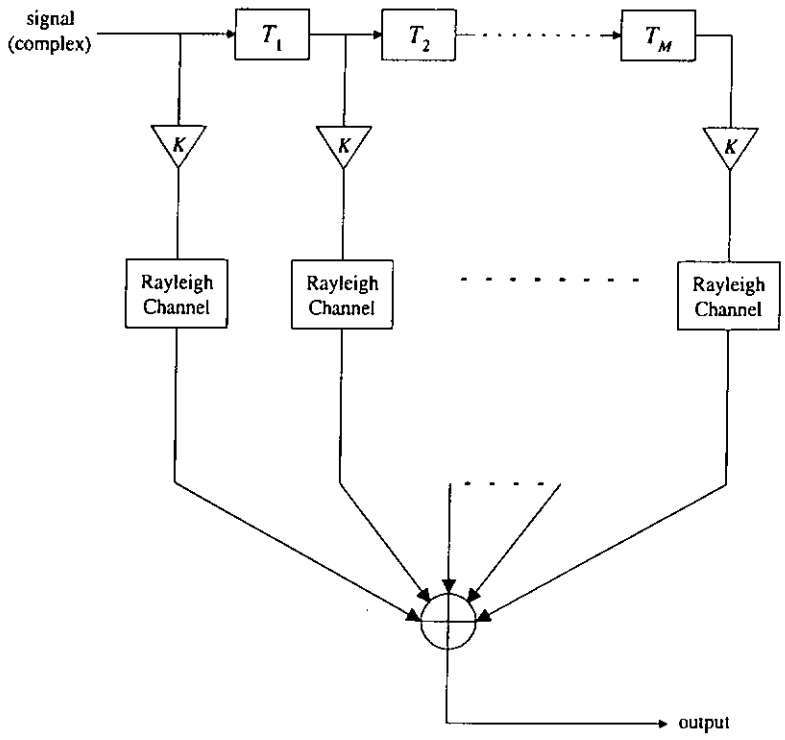

Figure 4.10 Multipath fading channel

In the figure, $K = E_b/(MN_0)$ is the channel gain, where M is the total number of signal paths and E_b/N_0 is the average signal energy per information bit-to-background noise power spectrum density ratio. T_n $(1 \leq n \leq 6)$, in terms of integer multiples of chip period, are the delays between two successive paths. Although n is varied in different simulation experiments, the maximum delay spread is always a lot smaller than the symbol duration of the desired user in all simulation cases. In other words, we can treat intersymbol interference (ISI) as negligible in this thesis.

4.8 Miscellaneous Issue

It is worthwhile to point out that a fair amount of time was spent on the system design process, especially on adjusting the time delays at different locations in the system. In the software packages MATLAB and SIMULINK, the sample times for different blocks should be adjusted accordingly. For example, the sample time for a convolutional decoder should be set correctly or errors will be obtained. Since a rate 1/3 convolutional decoder decodes three bits at a time, these three bits should be the three bits (possibly with errors) coming out from the convolutional encoder. This is shown more clearly with Figure 4.11. If the sample time is wrong, decoded bits are wrong no matter the incoming bits are with errors or not as depicted in Figure 4.11 (a). With an appropriate delay adjustment, the convolutional decoder samples at the right time and thus the decoded bits are correct as depicted in Figure 4.11 (b).

Another example is the delays in the Rake receiver's fingers should be properly time-aligned before combining.

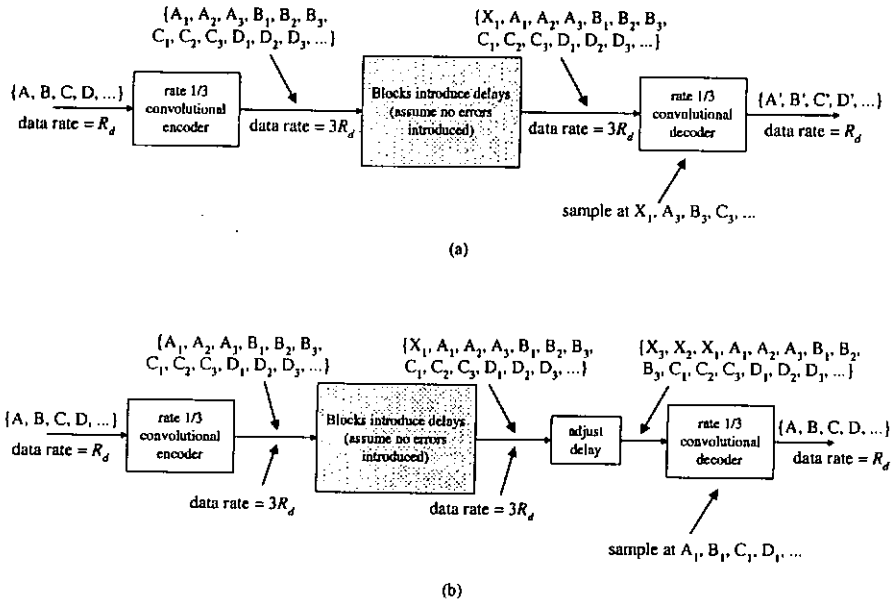

Figure 4.11 Convolutional encoding and decoding processes

(a) without delay adjustment (b) with delay adjustment

4.9 Rake Receiver

The Rake receiver first proposed by Price and Green [8] is used in the simulation experiments to achieve diversity gain. A Rake receiver consists of a bank of correlators and the received multipath signal is correlated with each of the correlator, which is termed as finger. Because of the autocorrelation properties of the long spreading sequence, only one path is filtered out. Paths from the fingers are then combined for bit decisions. Different combining methods are simulated that include selection diversity (SD), and maximal ratio

combining (MRC). Only the strongest path is selected for bit decisions in SD. On the other hand, the outputs of fingers are weighted accordingly to their relative strengths and summed together in MRC. In terms of the system performance, MRC gives the best results than SD does and these are discussed in detail in Chapter 5.

Coherent reception requires knowledge of the time-varying channel characteristics. The use of pilot signal is one of the techniques to acquire the required information but this increases the interference to other users since extra transmission power is needed. As a result, the system capacity will decrease. It is well-known that coherent reception outperforms non-coherent reception by 3 dB. In this thesis, perfect channel estimates are assumed and this avoids the need of channel estimations.

Rake combining is one of the techniques used to resolve and combine different paths [11] by virtue of path diversity. In W-CDMA, where the chip rate is high, more resolvable paths are available for path combining [83]. In general, for the case that no ISI is occurred, the maximum number of resolvable paths is (PG+1), where PG is the processing gain of the signal. By adjusting the delays in the path arrival times and combining the time-aligned replicas of the bit or symbol sequence, the signal-to-noise ratio (SNR) at the receiver is improved. The effectiveness of the Rake receiver depends on the signal bandwidth, the channel coherence bandwidth, and also the number of fingers in it. On the other hand, the number of fingers required is increased for a channel with higher delay spread in order to capture a given percentage of

the total signal power. In theory, all power from the paths should be collected for a good performance. However, it is impractical to implement a Rake receiver with as many fingers as the number of signal paths in order to collect all energy because of hardware complexity and high power consumption on the mobile unit. In addition, out of these paths some are non-significant to the receiver since power for those paths are too low for combining and detection and thus act as noisy components. Therefore the Rake receiver shown in Figure 4.12 is implemented with the path searching function. The number of fingers in the Rake receiver is another parametric value investigated in this thesis. The number of fingers in the Rake receiver is matched to the number of paths in the mobile channel for a matched receiver scenario. For an unmatched receiver scenario, the number of fingers can be set accordingly. And the implementation of path searching can further improve the system performance on an unmatched Rake receiver. With the path searching algorithm implemented, the fingers are locked onto the strongest signal paths. As will be shown later in Chapter 5, an unmatched Rake receiver with searching algorithm implemented performs as good as a matched Rake receiver.

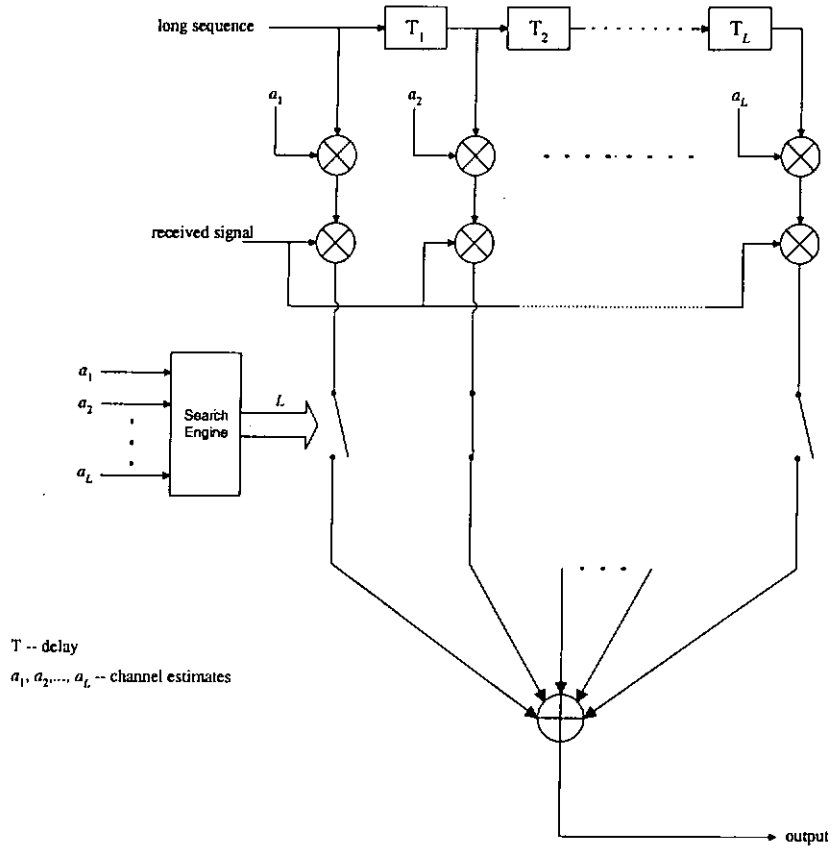

Figure 4.12 Rake receiver with path searching

4.10 Diversity Techniques

Many diversity techniques are available to achieve a more reliable communication system. Rake diversity as described in the previous section is a common and powerful technique used in CDMA systems to mitigate the impairments caused by the multipath fading environments. Antenna diversity is another technique to improve the system performance. This is a space diversity method since two antennas are spaced apart so that the signals received by these antennas are uncorrelated with each other. Before the small microstrip antenna is invented, antenna diversity is only feasible in the reverse

link because it was impossible to place the antennas on the mobile unit. The two antennas provide two independently fading signals and thus diversity is exploited. More than two antennas can be implemented but it is limited by the hardware complexity. There is tradeoff between hardware complexity and system improvement. Two different kinds of antenna diversity are investigated in this thesis, which are antenna diversity based on BER detection and post-detection antenna diversity.

4.10.1 Antenna Diversity (BER based)

In this type of diversity, the selection of antenna is based on the BER. If an error is detected at the output of the receiver, the connection of the current antenna is switched to another one as shown in Figure 4.13 (a). There are many ways to monitor the occurrence of an error in the system and one way is to use Hamming code to achieve this goal. The way it is done in this thesis, however, is different. We generated two sets of data, one for each antenna branch, and computed the BER off-line. When an error is found by comparing the received data (from one antenna) with the transmitted data, we switched to use the received data from another antenna and continued the computation of BER. Again, switching occurs whenever an error is detected. This can be described more clearly by the flowchart shown in Figure 4.14. This off-line processing is not practical in real systems but it makes the design process more straightforward in this project. The use of only one Rake receiver in this BER

based antenna diversity simplifies the hardware structure. Simulation results are shown in Chapter 5.

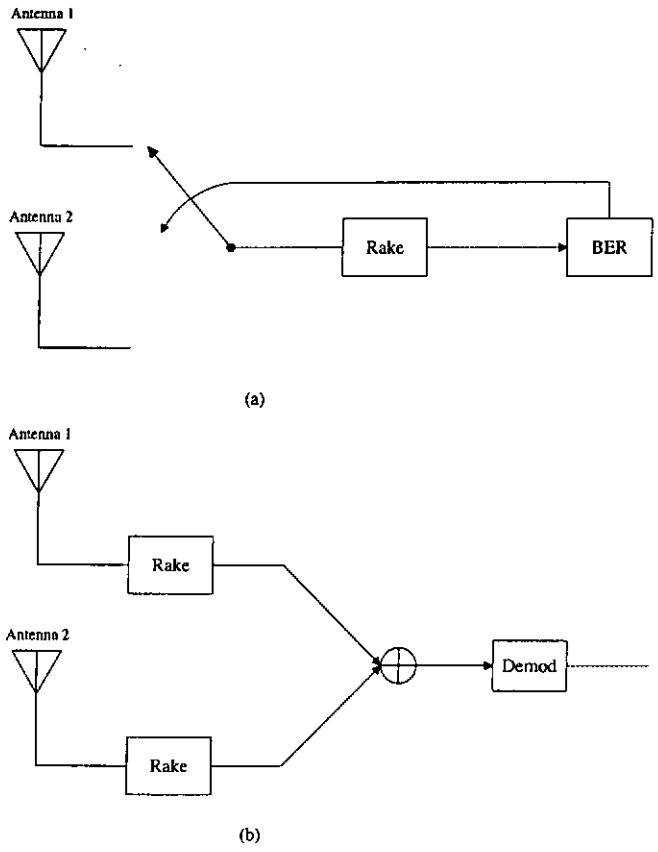

Figure 4.13 Antenna diversity (a) BER based (b) Post-detection method

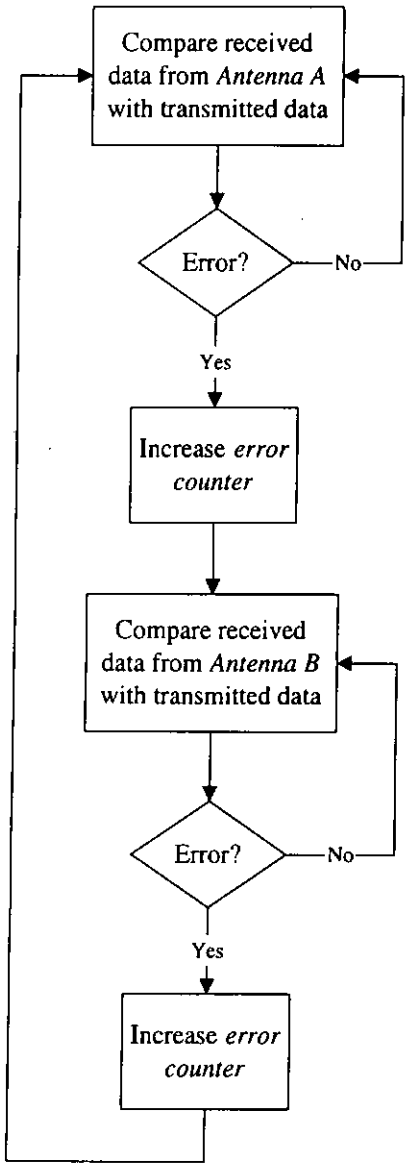

Figure 4.14 Flowchart of BER based antenna diversity

4.10.2 Antenna Diversity (Post-Detection)

As shown in Figure 4.13 (b), the implementation of post detection antenna diversity needs two Rake receivers in the receiving end and this complicates the hardware structure. The multipath signals from the two antennas are

resolved and combined in the two Rake receivers. Finally, the outputs of the Rake receivers are combined to form a composite signal. Again, more than two antennas can be used but this complicates the hardware structure. There is a tradeoff between system performance and hardware complexity. Simulation results for the antenna diversity with post-detection method are shown in Chapter 5.

4.11 Summary

In this chapter, the system model and different aspects of the system are described. In particular, channel coding, interleaving, spreading codes, and multipath channel model are discussed in detail. Methods to improve the performance of a system are suggested. For example, diversity gain obtained from Rake combining and antenna diversity. The sensitivities of UTRA system performance to the parameter number of fingers in the Rake receiver are first introduced in this chapter. In addition, the diversity gain provided by collecting two uncorrelated signals using two antennas are explained.

Chapter 5

SIMULATION RESULTS

5.1 Introduction

Preliminary study on the sensitivity of Universal Terrestrial Radio Access (UTRA) performance to system parameters is given in [84]. In this chapter, results of the investigation into the parametric sensitivities of UTRA system are reported. The parameters selected include the number of fingers in Rake receiver, path searching algorithm, interleaving depth, and antenna diversity. The sensitivity analysis is deemed necessary because under different scenarios (e.g., different number of signal paths, and different Doppler frequencies), varying of the parameters will have different impacts on the system performance. For example, the performance improvement by increasing the number of fingers in an unmatched Rake receiver is more sensitive for a system without path searching algorithm implemented than a system with the algorithm implemented. System performance is expressed in terms of average bit error rate (BER) probability versus average signal energy per information bit-to-background noise power spectrum density ratio (E_b/N_0) for several values of the selected parameters. It should be noted that in all the simulation

results shown in the following, unless otherwise stated, the interleaving depth is 10 msec, Doppler frequency is 80 Hz ($f_m T_s = 8.33\times10^{-4}$), and the maximum delay spread is always a lot smaller than the symbol duration of the desired user (i.e., $\tau_{max} \ll T_s$) so that intersymbol interference (ISI) is negligible. Before the simulation results are presented, interpath interference (IPI) is explained in Section 5.2. Simulation results for matched Rake receiver and unmatched Rake receiver are presented in Section 5.3. The performance improvement provided by the path searching algorithm is also presented and analyzed in that section. In Section 5.4, the system performance under different interleaving depths and Doppler frequencies are given. In Section 5.5, the performances of two types of antenna diversity are discussed. The power control aspects and how the system performs under imperfect power control are discussed in Section 5.6. Finally, this chapter is summarized in Section 5.7.

5.2 Interpath Interference

Before going into the discussion of Rake receiver, we have to first understand the effect of IPI that many literature have ignored or treated as negligible [9][11][26]. The way a Rake receiver separates multipath signal is utilizing the autocorrelation properties of the PN codes. Because of the autocorrelation of a PN sequence is one at zero time delay and approximate zero elsewhere, paths can be separated with little interference between them. However, this is only true for ideal case as shown in Figure 5.1. Figure 5.1 shows the case of ideal periodic autocorrelation properties of PN sequence with length N of 15. When

the time delay is zero, the normalized peak value is one; otherwise, the sidelobes are -1/N (= -1/15). The longer the sequence, the lower the sidelobes are. For the non-ideal case (i.e., partial-periodic correlation), sidelobes are high especially for low processing gain [50]. And this is shown in Figure 5.2 where the PN sequence used is with length N of 2^{33}-1. The sidelobes of the partial-periodic autocorrelation of the PN sequence [85] introduces IPI in Rake combining. It should be noted that the IPI is not depending on the number of fingers in the Rake receiver but on the number of signal paths in the channel. In the following sections, some of the simulation results show that IPI has dominant effects on the system performance.

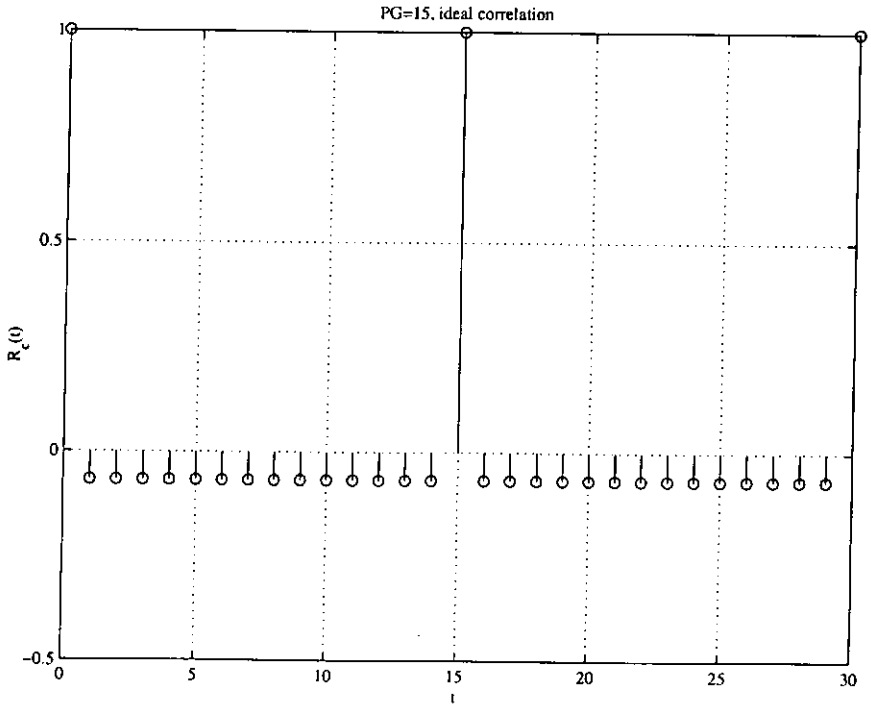

Figure 5.1 Ideal periodic autocorrelation of a PN sequence

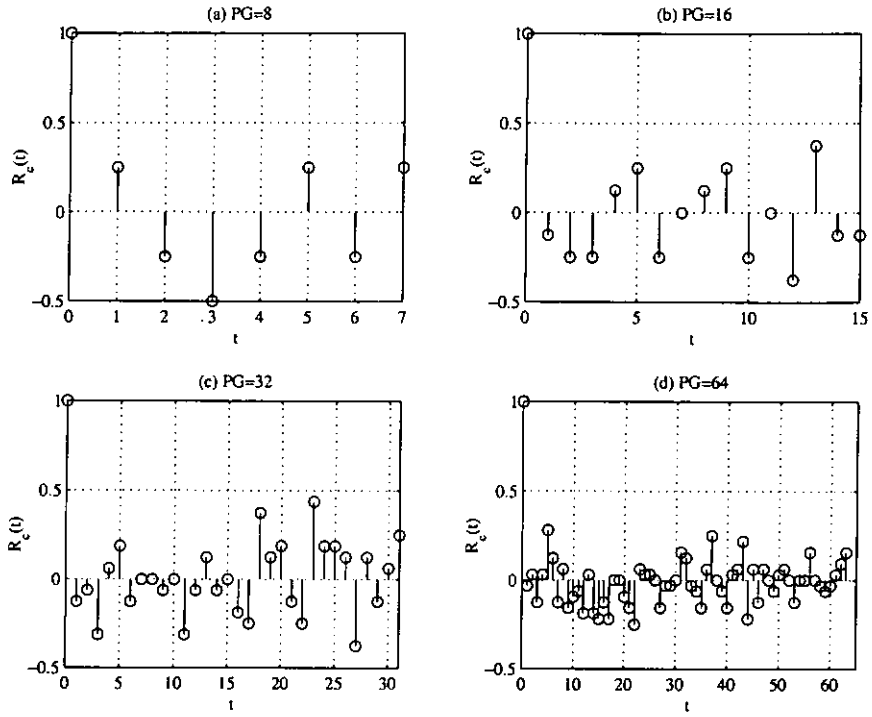

Figure 5.2 Non-ideal partial-periodic autocorrelation of

a PN sequence with different processing gains

5.3 Rake Diversity

In a multipath fading environment, the use of Rake receiver significantly improves the system performance [8]. Therefore the performance comparison for a system with conventional and Rake receiver, the impact on the system performance with the selection of number of fingers in relation to the number of paths, and the performance improvement obtained when a path searching algorithm is implemented are discussed. In particular, the sensitivities of UTRA system performance to the parameters are investigated.

In the results provided in the past, many of them investigated the scenarios where the number of fingers equals the number of signal paths [13]-[15][18][20]. However, this matched receiver case is only feasible when the chip rate is low and the number of resolvable paths is small. In the third generation (3G) systems, where the chip rate is high and thus the number of resolvable paths is usually high, a Rake receiver with number of fingers not matched to number of signal paths seems more practical in the hardware point of view. Therefore two different types of Rake receiver are investigated. The first type is called matched Rake receiver, where the number L of fingers is matched to the number M of signal paths ($L = M$). And the second type is called unmatched Rake receiver, where the number of fingers is not matched to number of signal paths ($L < M$).

Before going into the discussion of matched Rake receiver, we first investigate the performance of a conventional receiver to emphasize the importance of a Rake receiver.

5.3.1 Conventional Receiver

The BER performance of a conventional receiver (i.e., a Rake receiver with only one finger) in a fading channel is depicted in Figure 5.3. It can be observed from the figure that the performance degrades as the number of signal paths, M, increases. This is intuitively correct since more power is lost when the number of signal paths increases but the receiver is able to use only one path. The loss of signal power depends on the multipath power delay

profile (MPDP). It can also be noted from the figure that even at high E_b/N_0, the performance is still poor. And for $M = 2$ to 6, the curves saturate at high E_b/N_0. It is because there is only one finger in the Rake receiver and therefore diversity is not used.

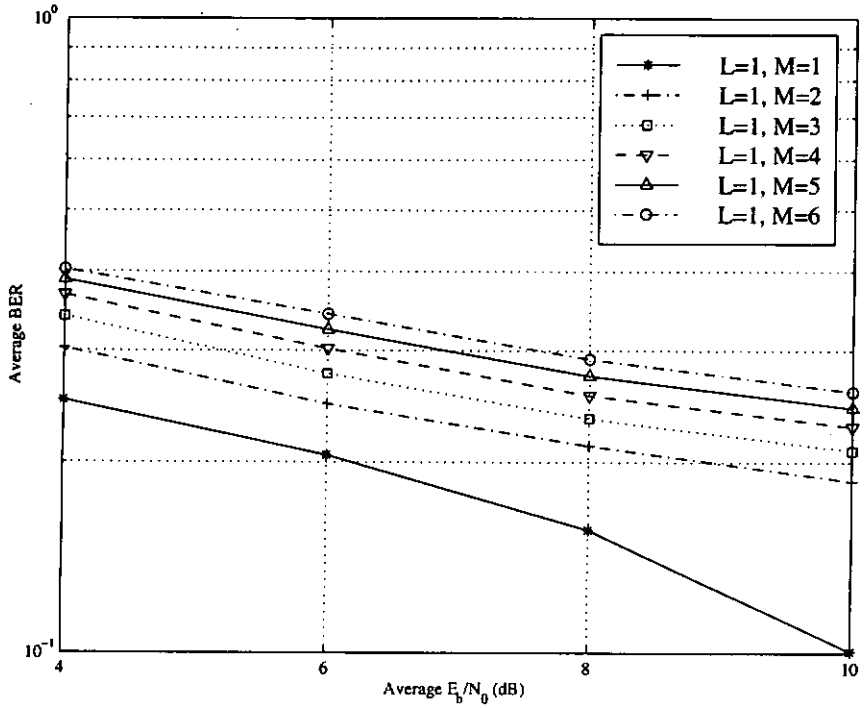

Figure 5.3 BER performance of a conventional receiver

The theoretical BER performance of a receiver with number L of fingers under uniform MPDP environment is [11]

$$\overline{P_e} = \left[\frac{1}{2}(1-\mu)\right]^L \sum_{k=0}^{L-1} \binom{L-1+k}{k} \left[\frac{1}{2}(1+\mu)\right]^k, \qquad (5.1)$$

where

$$\mu = \sqrt{\frac{\overline{\gamma_c}}{1+\overline{\gamma_c}}} \tag{5.2}$$

and

$$\overline{\gamma_c} = \frac{E_b/N_0}{M} \tag{5.3}$$

is the average signal-to-noise ratio (SNR) per signal path.

It is assumed that $E(a_k^2) = 1$ in the whole context of this thesis where a_k is the Rayleigh distributed amplitudes of the multipath signal. Therefore $\overline{\gamma} = \frac{E_b}{N_0} E(a_k^2) = \frac{E_b}{N_0}$. That is, the average received SNR is not affected by fading.

For the case of a conventional receiver, where the number of fingers equals one, (5.1) can be modified with $L = 1$ as

$$\overline{P_e} = \left[\frac{1}{2}(1-\mu)\right]. \tag{5.4}$$

A graph plotted according to (5.4) is given in Figure 5.4. It should be noted that the BER performance is plotted against average E_b/N_0 and the conversion between average E_b/N_0 and $\overline{\gamma_c}$ is given in (5.3). As shown in the diagram, the theoretical results have better performance compared to that of the simulation results. It is because in the theoretical analysis, no IPI and no inter-user interference are assumed. However, the trends of the curves for both the theoretical and simulation cases are similar.

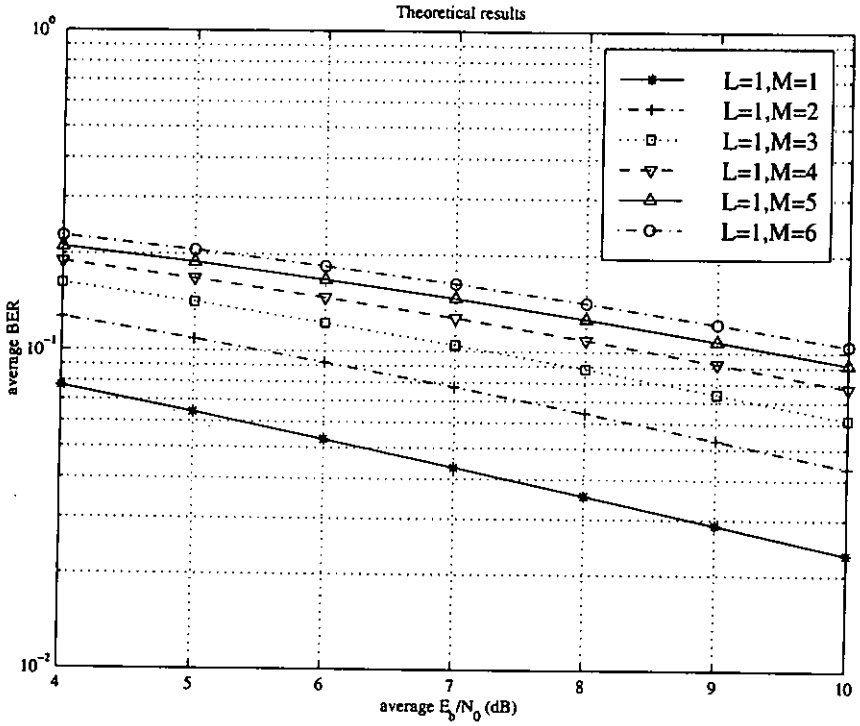

Figure 5.4 Theoretical results of the performance of a conventional receiver

From these results, we can conclude that a conventional receiver gives poor system performance in a multipath fading environment. It is expected that the use of a Rake receiver with more than one finger will provide significant improvement in the system performance and this is discussed next.

5.3.2 Matched Rake Receiver

Figure 5.5 shows the structure of a matched Rake receiver where the number L of fingers is equal to the number M of signal paths. As shown in the figure, the received multipath components are resolved and each path has equal SNR γ_c

$(\gamma_{c1} = \gamma_{c2} = \ldots = \gamma_{cM} = \gamma_c)$ since uniform MPDP is used. For the case of a matched receiver, the number L of fingers is matched to the number M of signal paths and therefore the total SNR γ_b at the input of the combiner is $(\gamma_1 + \gamma_2 + \ldots + \gamma_L) = (\gamma_1 + \gamma_2 + \ldots + \gamma_M) = E_b/N_0$. In other words, there is no power loss in the matched Rake receiver case.

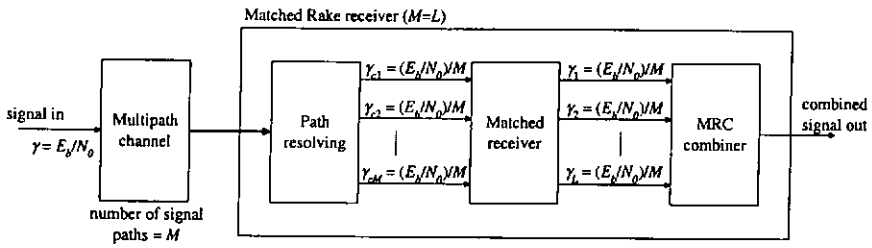

Figure 5.5 Structure of a matched Rake receiver

The performance improvement with increasing number L of fingers in a Rake receiver is shown in Figure 5.6. It should be noted that in this case the number M of signal paths is fixed as 6. As shown in the figure, the performance improves with increasing L. This can easily be explained by the fact that increasing the number of fingers used in the Rake receiver means achieving higher order of diversity gain. For $L = 1$, the BER performance stays about the same for all E_b/N_0's. It is because of no diversity gain and strong IPI presented, especially in high E_b/N_0's, in this case. It should be noted that this case is in contrast with the single finger and single path case ($L = 1$, $M = 1$), where BER reduces with increasing E_b/N_0's. As the number of fingers increases, the BER shows bigger improvement for higher E_b/N_0. This is

because of the higher order of diversity gain. In particular, there is a 2 dB improvement when the number of fingers is increased from 4 to 5 at BER of 10^{-2}. And there is a 1 dB improvement when the number of fingers is increased from 5 to 6 at BER of 10^{-2}. And the case of $L = 6$ gives the best performance since the receiver is matched to the channel. That is, the number of fingers is matched to the number of signal paths ($L = M$). It can be concluded from this figure that for an environment with fixed number of signal paths, the more number of fingers in the Rake receiver, the better the system performance is.

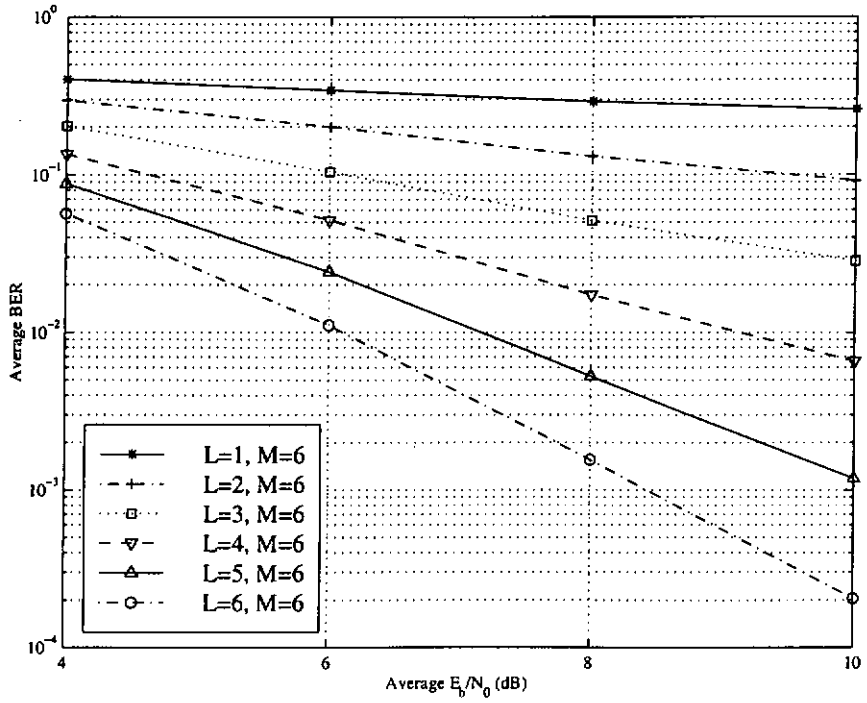

Figure 5.6 BER performance of a system with $M = 6$ as a function of L

The BER performance of a matched Rake receiver is shown in Figure 5.7. As depicted in the figure, the BER performance is improved significantly

when compared to the conventional receiver case. The performance improves with increasing L. This makes sense because the order of diversity increases with increasing number of fingers. It should be noted for the case where $L = 5$ and 6, their performances are similar for $E_b/N_0 = 4$ to 8 dB. For $E_b/N_0 > 8$ dB, the performance for $L = 5$ outperforms $L = 6$, and for $E_b/N_0 > 10$ dB, the performance for $L = 4$ outperforms $L = 6$. It is because in this case IPI dominates over the diversity gain [86]. From Figure 5.3 and Figure 5.7, we can conclude that a matched Rake receiver has better performance over a conventional receiver. However, as the number of signal paths and fingers increases, IPI is more dominant in high E_b/N_0 [3] and as a result gives poorer performance.

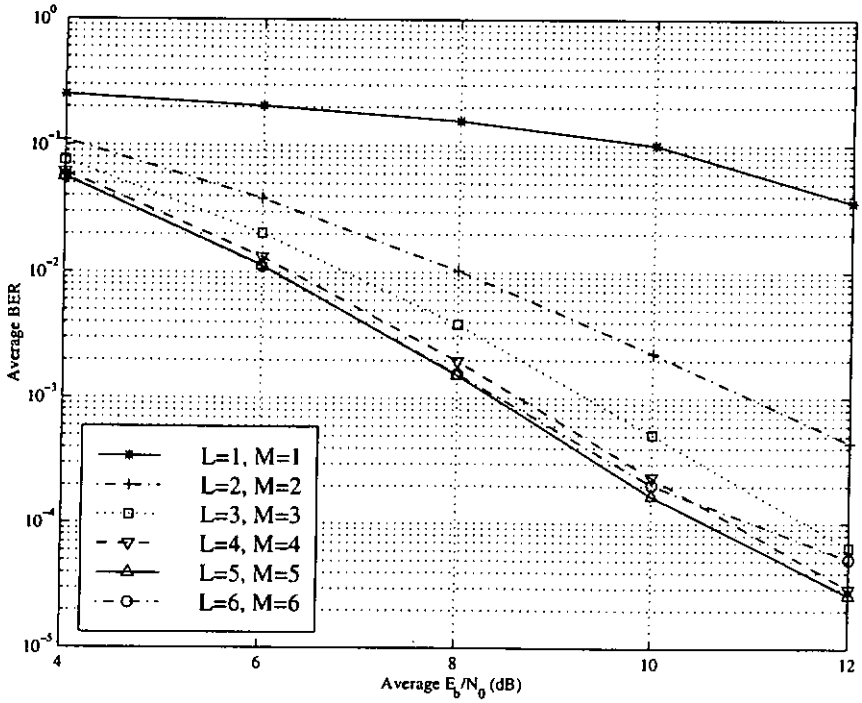

Figure 5.7 BER performance of a matched Rake receiver

5.3.3 Unmatched Rake Receiver

In hardware complexity point of view, it is sometimes not practical to implement a Rake receiver with number of fingers matched to the number of signal paths in the channel. This is because in wideband systems, where the number of resolvable paths is usually high, the implementation of a matched Rake receiver increases the hardware complexity and consumes more power. More importantly is that the movement of the mobile unit results in significant changes in the number of paths and the shape of the MPDP. Thus, the number of paths will dynamically change. An unmatched Rake receiver can be implemented regardless of the number of signal paths and this is investigated in the next section.

5.3.3.1 Without Path Searching Algorithm

The structure of an unmatched Rake receiver is shown in Figure 5.8 where the number L of fingers is smaller than the number M of signal paths. Since uniform MPDP is used, the received multipath components from the channel are resolved and each path has equal SNR γ_c ($\gamma_{c1} = \gamma_{c2} = \ldots = \gamma_{cM} = \gamma_c$). For the case of an unmatched receiver, the number L of fingers is smaller than the number M of signal paths and therefore the total SNR γ_b at the input of the combiner is $(\gamma_1 + \gamma_2 + \ldots + \gamma_L) < (\gamma_{c1} + \gamma_{c2} + \ldots + \gamma_{cM}) = E_b/N_0$. In fact, γ_b in this case is equal to $\frac{L}{M}\left(E_b/N_0\right)$. In other words, there is power loss in the

unmatched Rake receiver case and the amount of power loss decreases with increasing number L of fingers in the unmatched Rake receiver.

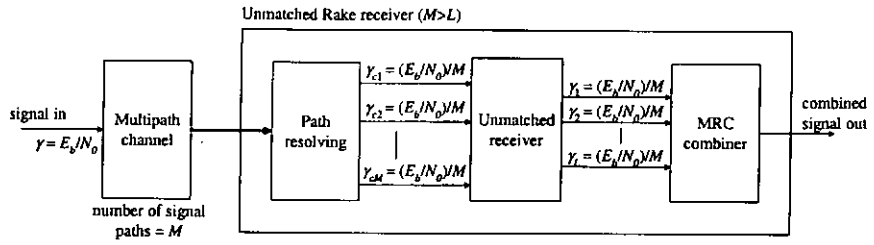

Figure 5.8 Structure of an unmatched Rake receiver

The performance of a 3-finger Rake receiver ($L = 3$) without path searching algorithm as a function of number of signal paths in the channel is shown in Figure 5.9. As we can observe from the figure, the best performance is achieved at $M = 3$ and degrades at $M = 4$ to 6. This makes sense because for $M = 3$, this is a matched Rake receiver case. However, for $M = 4$ to 6, because more power is lost in greater number of signal paths, the performance of course degrades. A path searching algorithm can be implemented to improve the performance of an unmatched Rake receiver and this is shown in the next section.

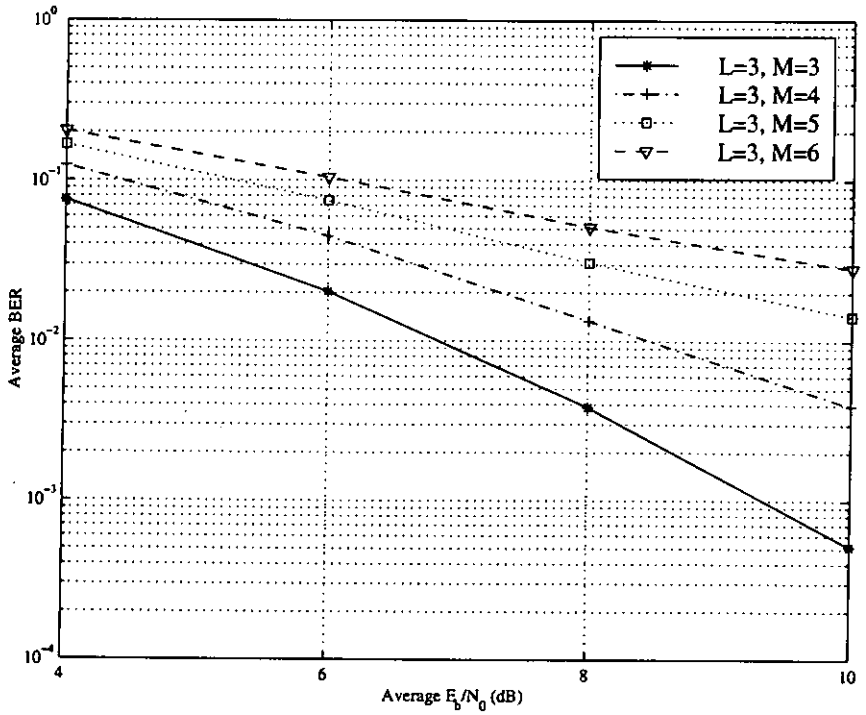

Figure 5.9 BER performance of an unmatched Rake receiver

5.3.3.2 With Path Searching Algorithm

With path searching algorithm implemented, the instantaneously received power of each multipath component is compared every symbol period and the Rake receiver fingers are locked onto the paths with strongest powers. That is, out of the M signal paths, L strongest paths are chosen for combining. Another method of assigning fingers in the Rake receiver is using the average power based scheme, where powers over several symbol periods are averaged. And the fingers pick the ones with strongest average powers. Since the Doppler frequency of the system is significantly smaller than the symbol rate, the instantaneous received power based finger assignment scheme is used and it has a superior performance [87]. The finger assignment technique can be

further explained by Figure 5.10 where the structure of an unmatched Rake receiver with path searching algorithm implemented is shown. The received multipath components are resolved followed by path searching. Each resolved path has equal average SNR $(E_b/N_0)/M$ since uniform MPDP is used. In the unmatched receiver with path searching algorithm implemented, out of the M signal paths, L paths with strongest power are selected for every symbol period cycle for combining. That is, SNR's $\gamma_1 \geq \gamma_2 \geq \ldots \geq \gamma_L$ where $\gamma_1 = max\{\gamma_{c1}, \gamma_{c2}, \ldots, \gamma_{cM}\}$. Therefore the input SNR for the combiner is improved when compared to an unmatched receiver without path searching algorithm implemented, where the first L paths are chosen for combining.

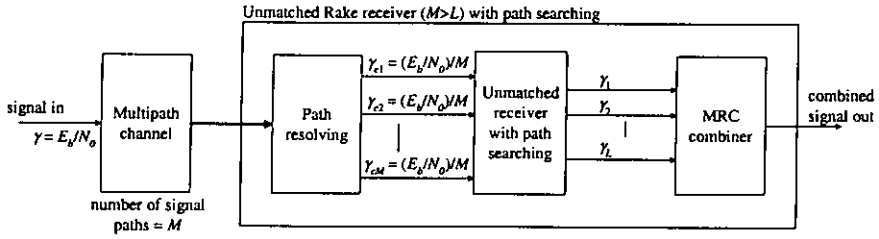

Figure 5.10 Structure of an unmatched Rake receiver with path searching algorithm

The improved input SNR for the combiner gives better system performance as shown in Figure 5.11 to Figure 5.15. Figure 5.11 to Figure 5.15 show the performance of a system without and with path searching algorithm implemented as a function of L. In Figure 5.11, the performance improvement for the implementation of path searching for $L = 1$ is shown. This case can be

considered analogous to SC. As shown in the figure, at $E_b/N_0 = 10$ dB, BER of 3×10^{-1} is achieved without the use of path searching and of 2×10^{-2} with path searching algorithm implemented. The case of $L = 2$ is shown in Figure 5.12. At $E_b/N_0 = 10$ dB, BER of 1×10^{-1} is achieved without the use of path searching and of 2×10^{-3} with path searching algorithm implemented. Similarly as shown in Figure 5.13 for the case of $L = 3$, BER of 3×10^{-2} is achieved without the use of path searching and of 5×10^{-4} with path searching algorithm implemented at $E_b/N_0 = 10$ dB. And as shown in Figure 5.14 for the case of $L = 4$, BER of 7×10^{-3} is achieved without the use of path searching and of 3×10^{-4} with path searching algorithm implemented at $E_b/N_0 = 10$ dB. For the case of $L = 5$, BER of 1×10^{-3} is achieved without the use of path searching and of 2×10^{-4} with path searching algorithm implemented at $E_b/N_0 = 10$ dB as shown in Figure 5.15. Table 5.1 summarizes the BER performance improvement when path searching algorithm is implemented under different number L of fingers in the Rake receiver. As shown in Figure 5.16, the performance improvement obtained from path searching gets smaller as the number L of fingers in the Rake receiver increases. This is reasonable because when $L = 1$, the probability that the signal goes into deep fade is high and the use of path searching improves the performance significantly. On the other hand, signal variation in the output of the receiver is small for $L = 5$, and the implementation of path searching does not have a significant improvement on the system performance. Therefore the performance improvement obtained by the use of path searching is more sensitive when the number of fingers in the Rake receiver is small.

Table 5.1 BER performance (at E_b/N_0 = 10 dB) improvement achieved from the implementation of path searching algorithm

L	without path searching	with path searching	improvement
1	3×10^{-1}	2×10^{-2}	1 order of magnitude
2	1×10^{-1}	2×10^{-3}	2 order of magnitude
3	3×10^{-2}	5×10^{-4}	2 order of magnitude
4	7×10^{-3}	3×10^{-4}	> 1 order of magnitude
5	1×10^{-3}	2×10^{-4}	1 order of magnitude

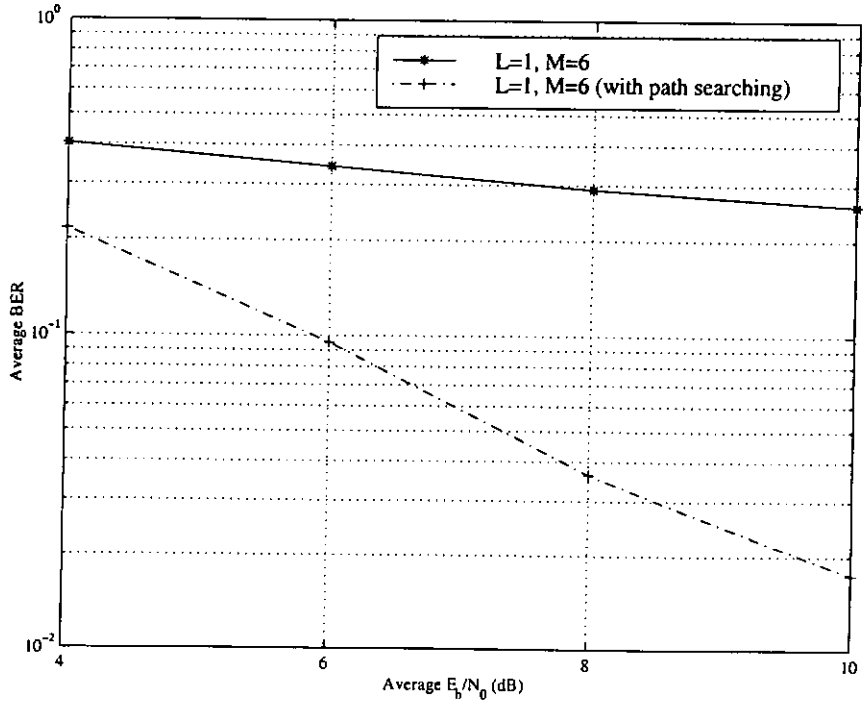

Figure 5.11 BER performance of an unmatched Rake receiver with and without path searching (L = 1)

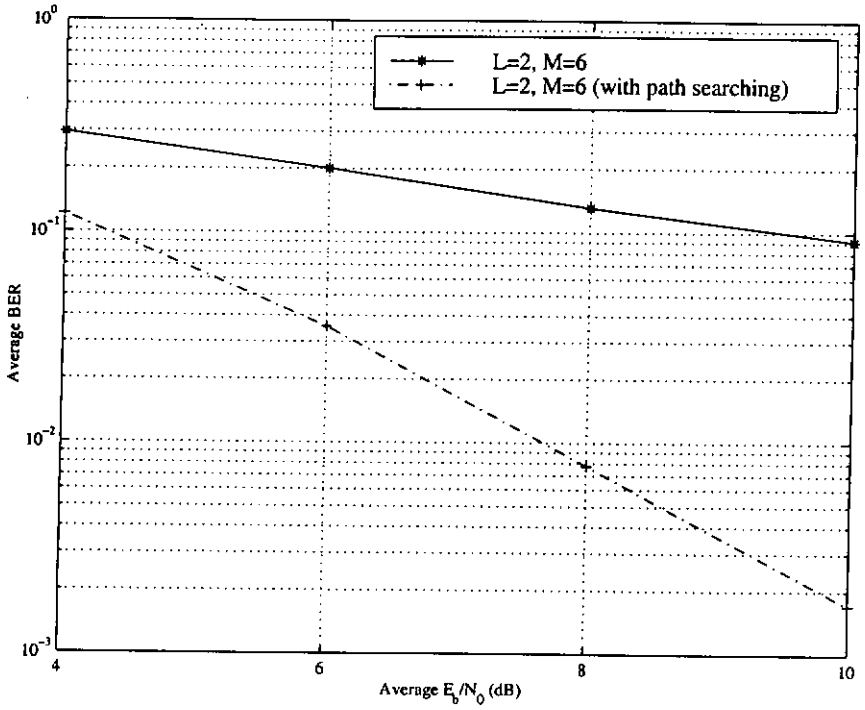

Figure 5.12 BER performance of an unmatched Rake receiver with and without path searching ($L = 2$)

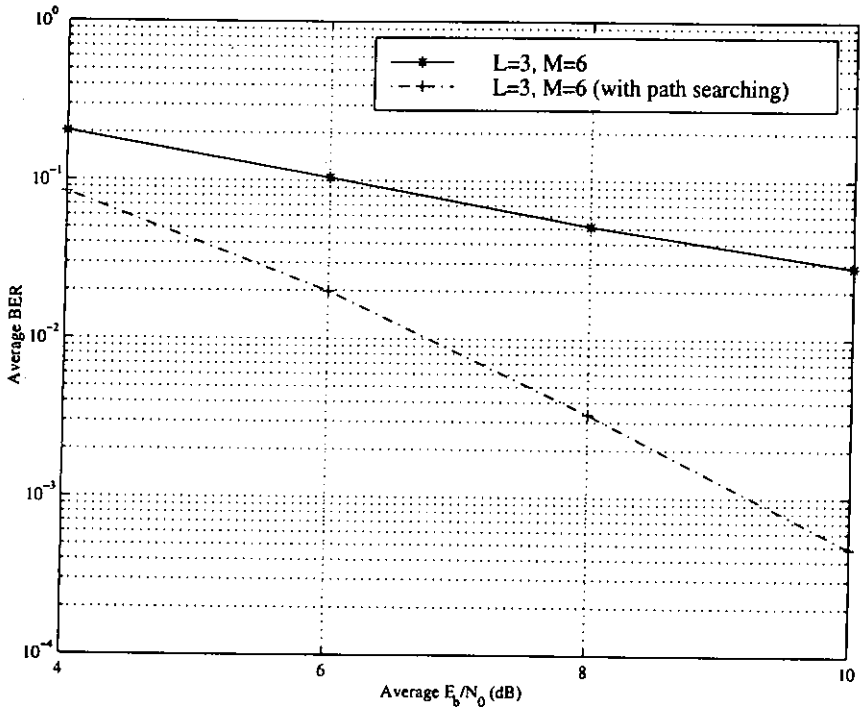

Figure 5.13 BER performance of an unmatched Rake receiver with and without path searching ($L = 3$)

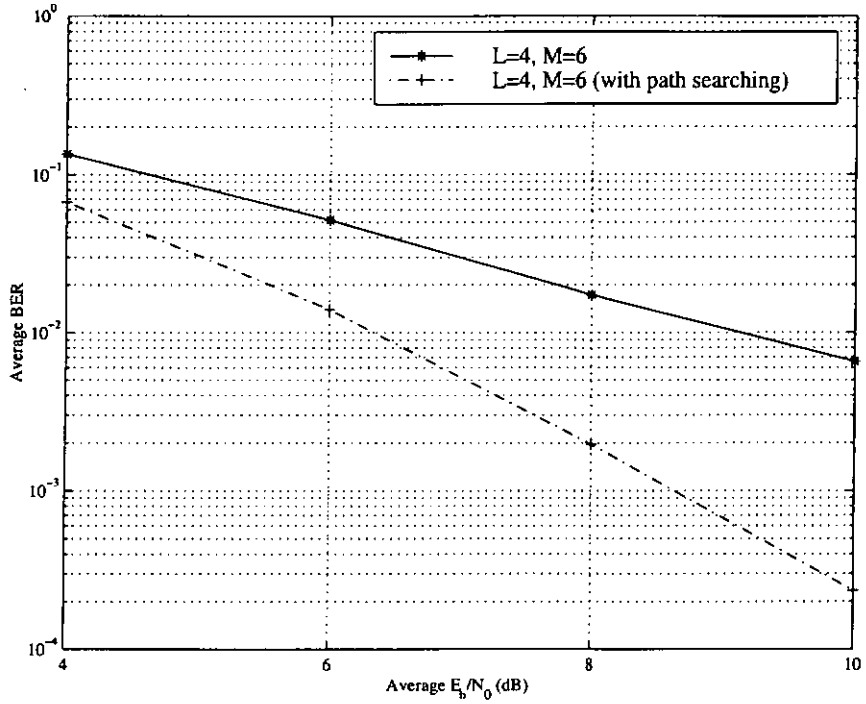

Figure 5.14 BER performance of an unmatched Rake receiver with and without path searching ($L = 4$)

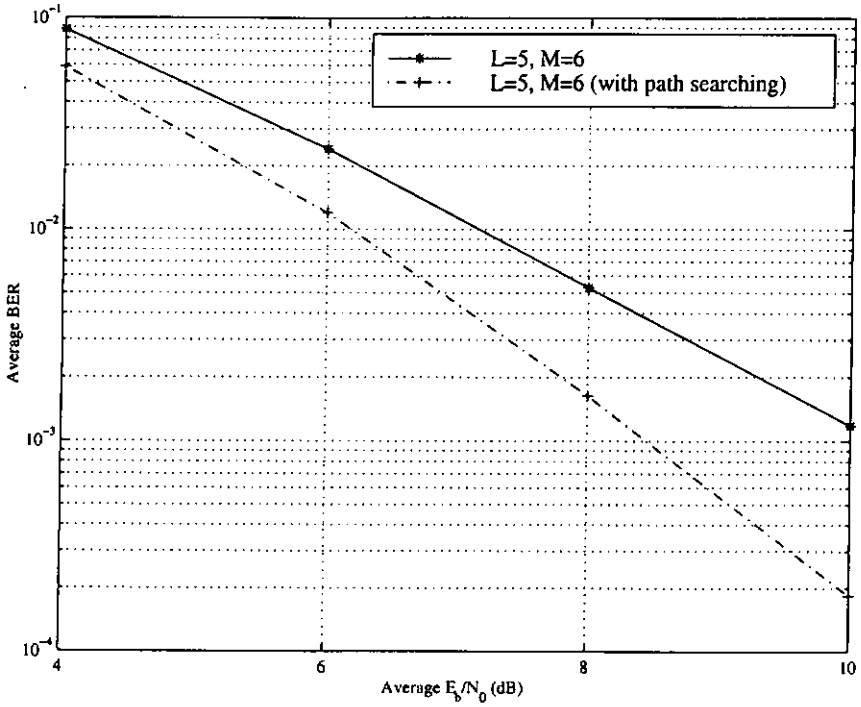

Figure 5.15 BER performance of an unmatched Rake receiver with and without path searching ($L = 5$)

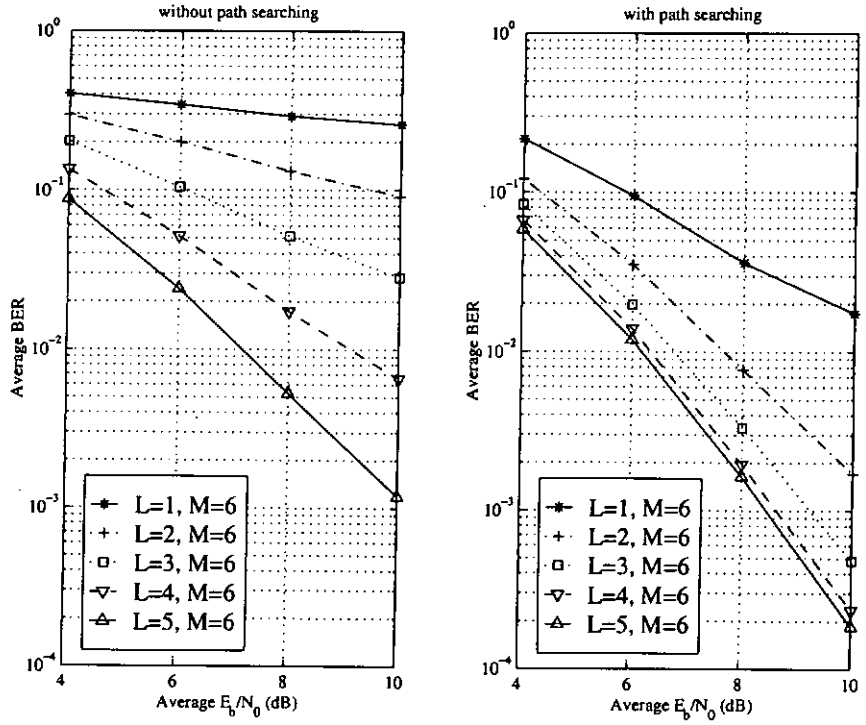

Figure 5.16 Summary of BER performance of an unmatched Rake receiver with and without path searching (L = 1 to 5)

Shown in Figure 5.17 is the BER performance of a 3-finger Rake receiver with path searching algorithm implemented under different channel conditions. It can be observed from the figure that the case of M = 4 has the best performance. It is because the power loss in this case is least among the three cases. The performance improvement with the use of path searching algorithm can be observed by comparing Figure 5.9 with Figure 5.17, which is given as a summary in Figure 5.18.

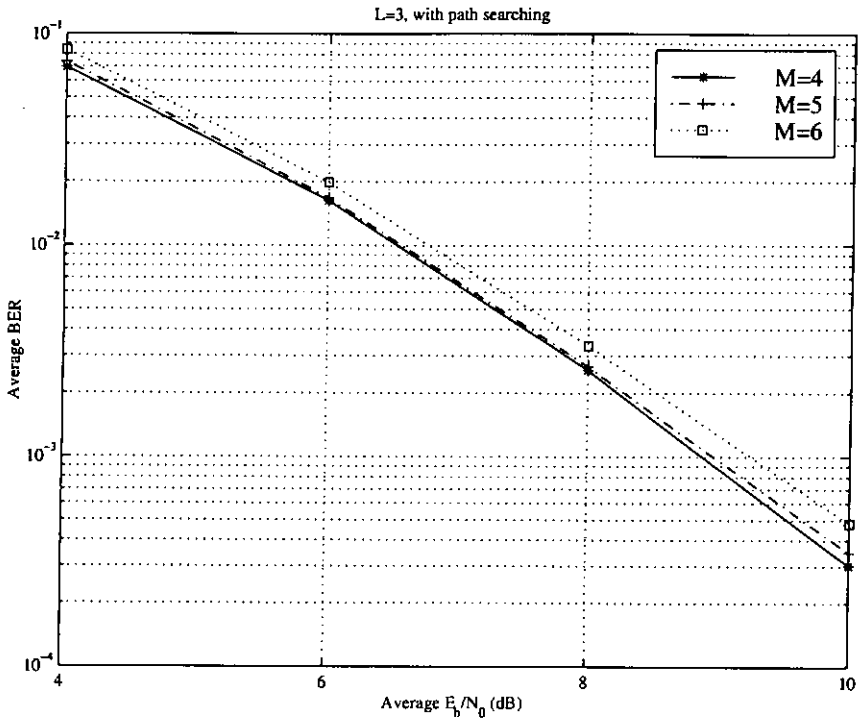

Figure 5.17 BER performance of a 3-finger Rake receiver with path searching under different channel environments

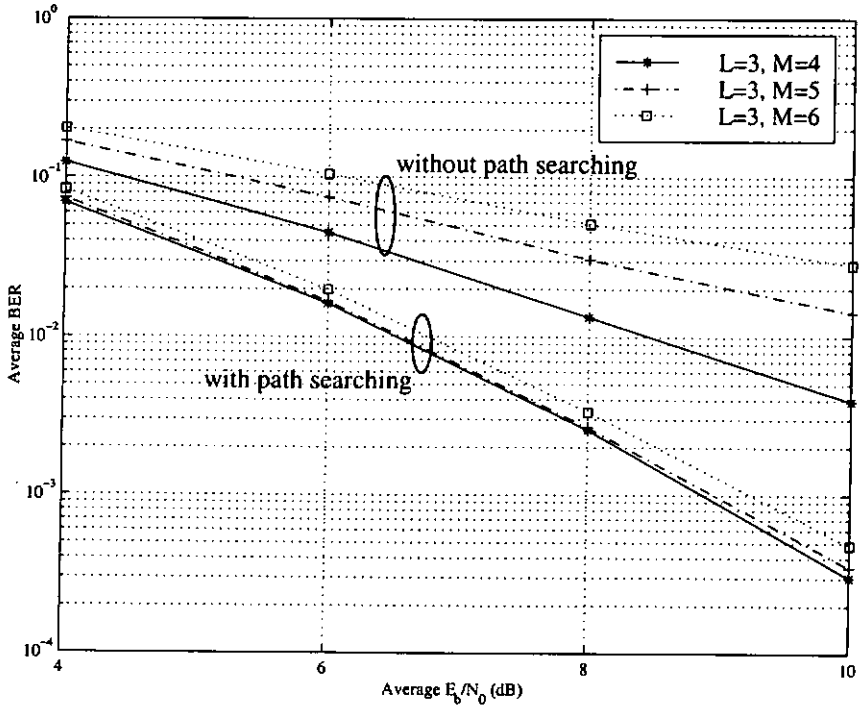

Figure 5.18 Comparison of BER performance of a 3-finger Rake receiver with and without path searching under different channel environments

Yang [21] derived an equation of the captured energy for an L-finger Rake receiver with path searching algorithm as

$$\rho_{path\ searching} = \sum_{k=1}^{L}\left\{\binom{M}{k}\frac{k}{M}\sum_{j=0}^{M-k}\left[(-1)^j\binom{M-k}{j}\frac{1}{(j+k)^2}\right]\right\}. \tag{5.5}$$

Since the captured energy for an L-finger Rake receiver without path searching technique is

$$\rho_{no\ path\ searching} = \frac{L}{M}, \tag{5.6}$$

the gain in dB provided by the use of path searching is

$$gain = 20\log_{10}\left(\frac{\rho_{path\ searching}}{\rho_{no\ path\ searching}}\right)$$

$$= 20\log_{10}\left(\sum_{k=1}^{L}\left\{\binom{M}{k}\frac{k}{L}\sum_{j=0}^{M-k}\left[(-1)^j\binom{M-k}{j}\frac{1}{(j+k)^2}\right]\right\}\right). \qquad (5.7)$$

For $L = 3$, $M = 4$, by (5.7), this gain is 1.94 dB. For $L = 3$, $M = 5$, by (5.7), this gain is 3.23 dB. For $L = 3$, $M = 6$, by (5.7), this gain is 4.17 dB. The simulation results shown in Figure 5.18 closely agree with these theoretical values.

The performance of an unmatched Rake receiver with path searching algorithm implemented is analyzed. The theoretical results are compared with the results obtained from the simulation experiments to confirm the correctness in the following.

Refer back to Figure 5.10, the selected path with index K ($1 \le K \le L$) has the maximal SNR of M-K+1 paths under the condition that K-1 paths have already been selected with the maximal SNR from the M paths. In other words, $\gamma_1 \ge \gamma_2 \ge \ldots \ge \gamma_L$. Although the probability density function (pdf) for the path with index M is Rayleigh distributed, the selected path with index K is no longer Rayleigh distributed and can be expressed as [88]

$$p_{\gamma_K}(\gamma) = \frac{M!\gamma_c^{-1}}{(M-K)!(K-1)!}\left[1-e^{-\frac{\gamma}{\gamma_c}}\right]^{M-K} e^{\frac{-K\gamma}{\gamma_c}}, \qquad (5.8)$$

where γ_c is the SNR per signal path.

To compute the BER performance of a system with path searching algorithm implemented, it is necessary to obtain the pdf of the input signal to the maximal ratio combining (MRC) combiner. That is, the pdf of the signal with SNR $\gamma_b = \gamma_1 + \gamma_2 + \ldots + \gamma_L$. There are several ways to obtain this pdf such as using the characteristic function, the Fourier transformation, or the Laplace transformation. However, the pdf given in (5.8) does not give practical calculations for this. Therefore (5.8) is approximated by a Gamma pdf as [88]

$$p_{\gamma_K}(\gamma) = \left(\frac{m_K}{\overline{\gamma_K}}\right)^{m_K} \frac{\gamma^{m_K-1}}{\Gamma(m_K)} e^{-\frac{m_K}{\overline{\gamma_K}}\gamma} \tag{5.9}$$

with mean $\overline{\gamma_K}$ and m_K given as

$$m_K = \frac{\overline{\gamma_K}^2}{\overline{\gamma_K^2} - \overline{\gamma_K}^2}, \tag{5.10}$$

where

$$\overline{\gamma_K} = \int \gamma \, p_{\gamma_K}(\gamma) d\gamma$$

$$= \frac{M!}{(K-1)!} \gamma_c \sum_{i=K}^{M} \frac{1}{(M-i)!(i-K)!} \frac{(-1)^{i-K}}{i^2}, \tag{5.11}$$

and

$$\overline{\gamma_K^2} = \int \gamma^2 p_{\gamma_K}(\gamma) d\gamma$$

$$= \frac{M!}{(K-1)!} 2\gamma_c^2 \sum_{i=K}^{M} \frac{1}{(M-i)!(i-K)!} \frac{(-1)^{i-K}}{i^3}. \tag{5.12}$$

From [88], the Gamma pdf for the MRC SNR γ_b can be approximated by

$$p_{\gamma_b}(\gamma) = \left(\frac{m_b}{\overline{\gamma_b}}\right)^{m_b} \frac{\gamma^{m_b-1}}{\Gamma(m_b)} e^{-\frac{m_b}{\overline{\gamma_b}}\gamma}, \tag{5.13}$$

where $\gamma_b = \sum_{K=1}^{L} \gamma_K$, $\overline{\gamma_b} = \sum_{K=1}^{L} \overline{\gamma_K}$, and

$$m_b = \left(\sum_{K=1}^{L} \overline{\gamma_K}\right)^2 \left(\sum_{K=1}^{L} \frac{\overline{\gamma_K}^2}{m_K}\right)^{-1}. \tag{5.14}$$

The conditional BER probability for coherent quaternary phase shift keying (QPSK) reception is given by [11]

$$P_e(\gamma_b) = Q(\sqrt{2\gamma_b}), \tag{5.15}$$

where $Q(x)$ is the Q-function defined as

$$Q(x) = \frac{1}{\sqrt{2\pi}} \int_x^{\infty} e^{-t^2/2} dt. \tag{5.16}$$

And the Q-function is bounded by

$$\left(1 - \frac{1}{x^2}\right) \frac{1}{x \cdot \sqrt{2} \cdot \pi} e^{-x^2/2} \le Q(x) \le \frac{1}{x \cdot \sqrt{2} \cdot \pi} e^{-x^2/2}. \tag{5.17}$$

The average BER probability is

$$\overline{P_e} = \int_0^{\infty} P_e(\gamma_b) p_{\gamma_b}(\gamma_b) d\gamma_b. \tag{5.18}$$

Therefore the upper bound of average BER probability is given by [90]

$$\overline{P}_{e,upperbound} = \int_0^{\infty} \frac{1}{\sqrt{2\gamma_b}\cdot\sqrt{2}\cdot\pi} e^{-2\gamma_b/2} \cdot \left(\frac{m_b}{\overline{\gamma_b}}\right)^{m_b} \frac{\gamma_b^{m_b-1}}{\Gamma(m_b)} e^{-\frac{m_b}{\overline{\gamma_b}}\gamma_b} d\gamma_b$$

$$= \frac{1}{2\pi}\left(\frac{m_b}{\overline{\gamma_b}}\right)^{m_b} \frac{1}{\Gamma(m_b)} \int_0^{\infty} \gamma_b^{m_b-1-\frac{1}{2}} e^{-\gamma_b\left(\frac{m_b}{\overline{\gamma_b}}+1\right)} d\gamma_b$$

$$= \frac{1}{2\pi}\left(\frac{m_b}{\overline{\gamma_b}}\right)^{m_b} \frac{1}{\Gamma(m_b)} \frac{1}{\left(\frac{m_b}{\overline{\gamma_b}}+1\right)^{m_b-\frac{1}{2}}} \Gamma\left(m_b-\tfrac{1}{2}\right)$$

$$= \frac{1}{2\pi}\left(\frac{m_b}{\overline{\gamma_b}}\right)^{m_b} \frac{\Gamma\left(m_b-\frac{1}{2}\right)}{\Gamma(m_b)} \left(\frac{m_b}{\overline{\gamma_b}}+1\right)^{\frac{1}{2}-m_b}. \tag{5.19}$$

Similarly, the lower bound of average BER probability is given by [90]

$$\overline{P}_{e,lowerbound} = \frac{1}{2\pi}\left(\frac{m_b}{\overline{\gamma_b}}\right)^{m_b} \frac{\Gamma\left(m_b-\frac{1}{2}\right)}{\Gamma(m_b)} \left(\frac{m_b}{\overline{\gamma_b}}+1\right)^{\frac{1}{2}-m_b} - \frac{1}{4\pi}\left(\frac{m_b}{\overline{\gamma_b}}\right)^{m_b} \frac{\Gamma\left(m_b-\frac{3}{2}\right)}{\Gamma(m_b)} \left(\frac{m_b}{\overline{\gamma_b}}+1\right)^{\frac{3}{2}-m_b} \tag{5.20}$$

The theoretical BER performance (upper bound case) of an unmatched Rake receiver is shown in Figure 5.19. The curve for theoretical result has slight improvement over the computer simulation results as shown in Figure 5.20. This can be explained by the fact that in the theoretical analysis, inter-user interference is assumed to be negligible. If the inter-user interference is considered as noise, the effective E_b/N_0 for the theoretical analysis will be degraded by a certain amount. In addition, nearly ideal correlation properties of the spreading code function is assumed [88] and therefore IPI is ignored, which is a phenomenon happens in the simulation results as shown in Figure 5.7. It should be noted that in Figure 5.19 and Figure 5.20, the BER performance is

plotted against $\overline{\gamma_b}$ but not average E_b/N_0. The conversation between E_b/N_0 and γ_b is given in Appendix A.

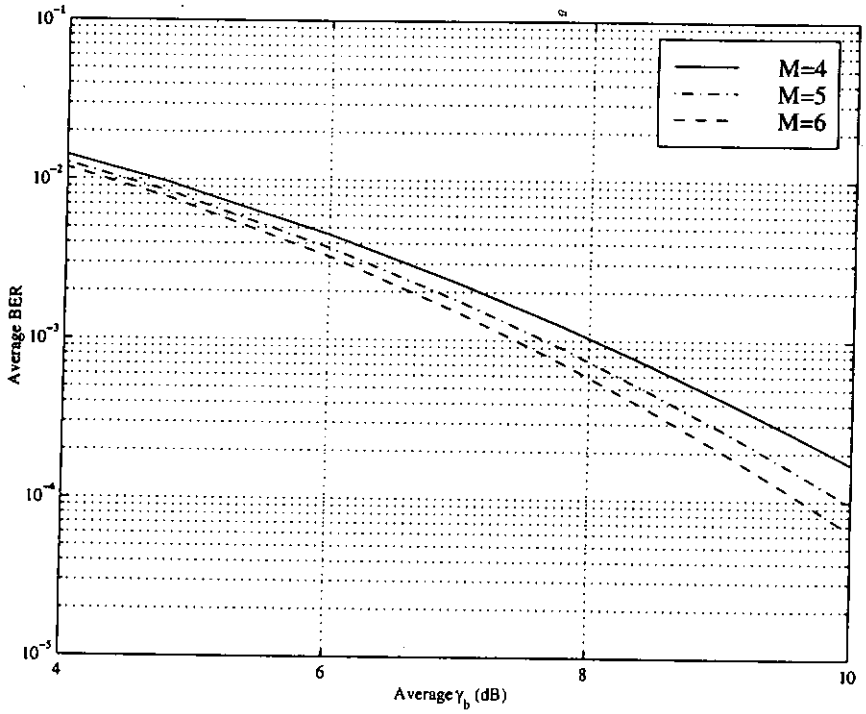

Figure 5.19 Theoretical BER performance of an unmatched Rake receiver with path searching ($L = 3$)

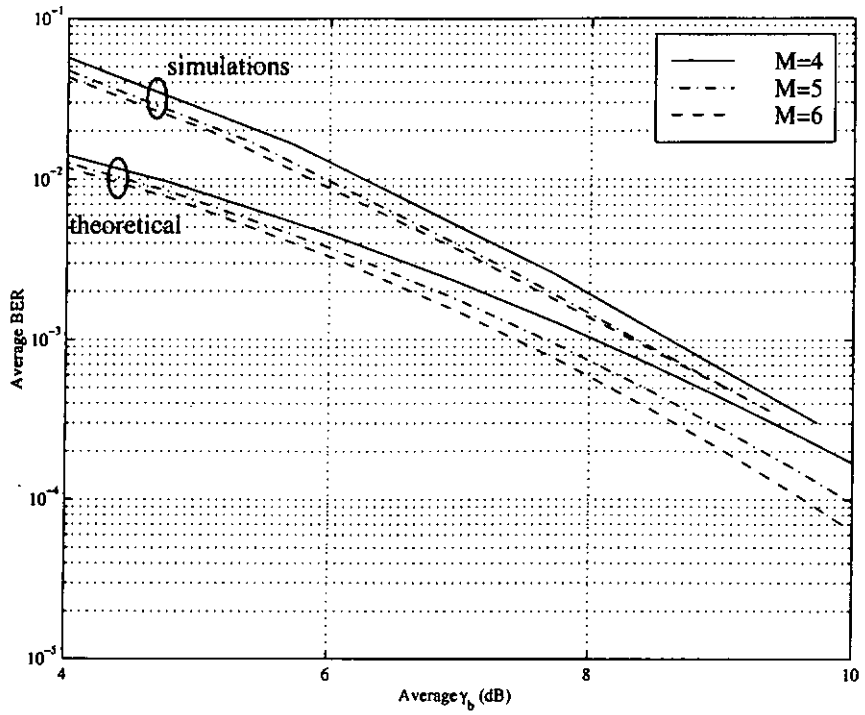

Figure 5.20 Comparison of theoretical and simulated BER performance of an unmatched Rake receiver with path searching ($L = 3$)

5.4 Interleaving Depth and Doppler Frequency

Rake diversity can give significant improvement to the system performance as shown in the previous sections. Another diversity technique is interleaving, which is one kind of time diversity. In fading environments, the combination of convolutional code and interleaving enhances the system performance significantly [89]. It should be noted that a system only implemented with interleaving but without channel coding still has poor performance. These are depicted in Figure 5.21 and Figure 5.22. In fact, as shown in the figures, the performance for this case (the line with "+" marks) is almost the same as a

system without both interleaving and channel coding (the line with "□" marks). The reason is when interleaving is used, a channel that exhibits bursty error characteristics can be looked as if it were a memoryless channel. However, if no channel coding is used with interleaving, the errors still cannot be corrected even though interleaving has dispersed the bursty errors. In words, the interleaver turns a bursty errors channel into a memoryless channel and channel coding, which is designed optimally for memoryless channels, corrects the independently occurring errors.

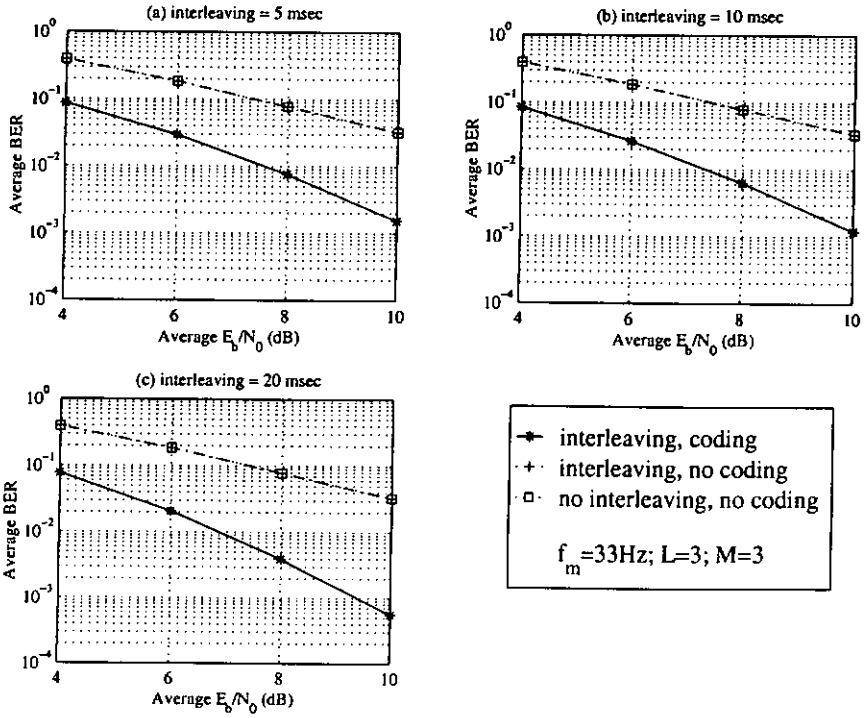

Figure 5.21 The effects of interleaving and channel coding on BER performance (f_m = 33Hz) (a) 5 msec (b) 10 msec, and (c) 20 msec

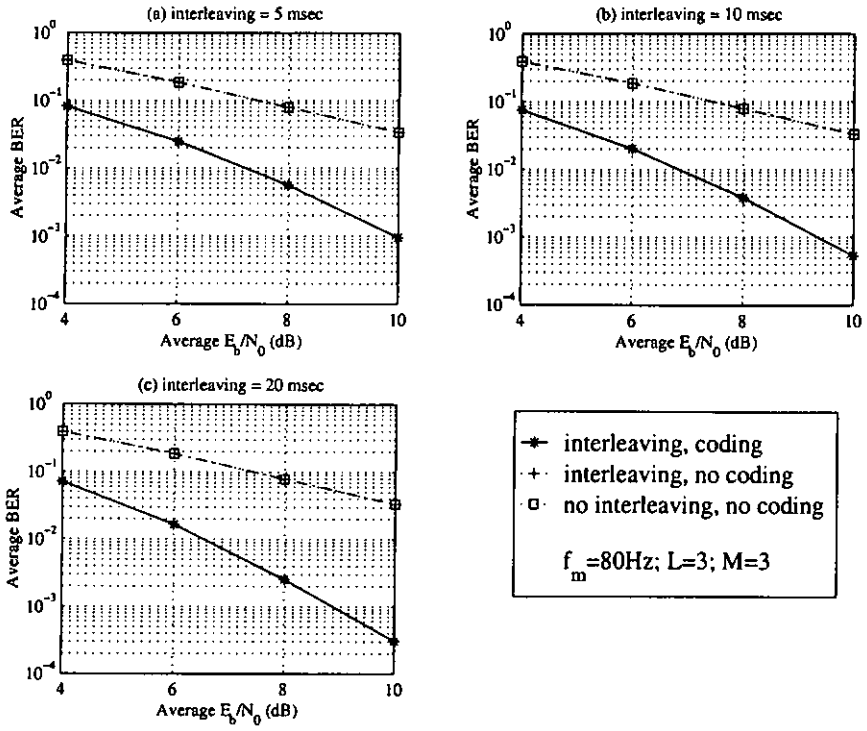

Figure 5.22 The effects of interleaving and channel coding on BER performance (f_m = 80Hz) (a) 5 msec (b) 10 msec, and (c) 20 msec

System performances as a function of the parameters interleaving depth and Doppler frequency are shown in Figure 5.23 to Figure 5.25. For all cases, performance improves with longer interleaving depth at high E_b/N_0. It is because bursty errors that are caused by the fading channel are more separated by longer interleaving depth. On the other hand, performances for different interleaving depths at low E_b/N_0 are similar because in this case, error bursts occur so often that even interleaving depth as long as 20 msec cannot correct the errors. In general, higher Doppler frequency gives better system performance because in higher Doppler frequency, the fade duration is shorter.

However, the performance with higher Doppler frequency is expected to degrade in real systems because the channel is fading so fast that it is difficult to mitigate the power variations with power control process. Moreover, channel estimation becomes more difficult in fast fading channels.

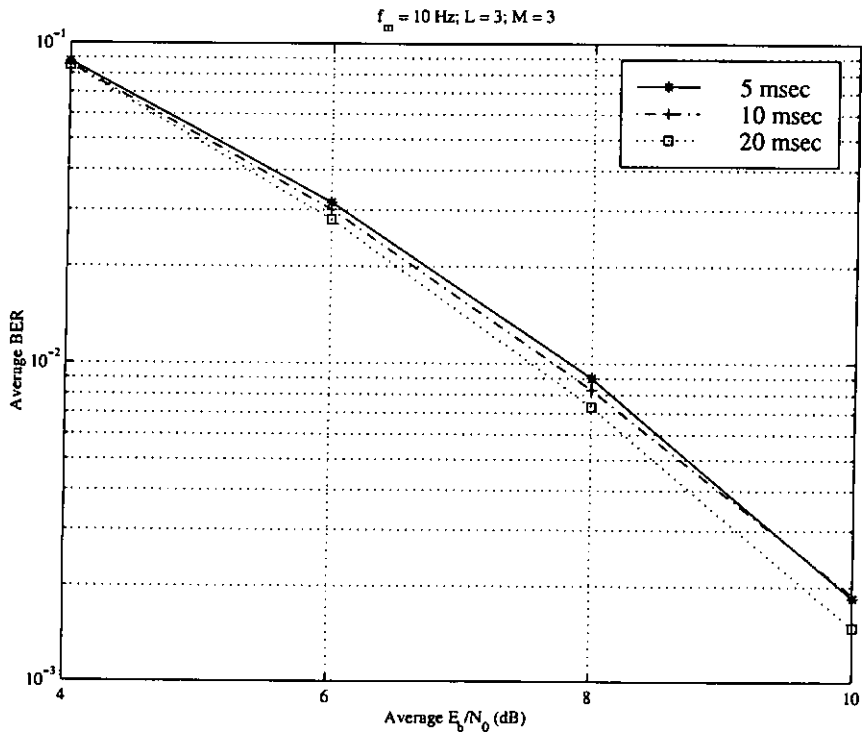

Figure 5.23 BER performance as a function of interleaving depth ($f_m T_s = 1.04\times10^{-4}$)

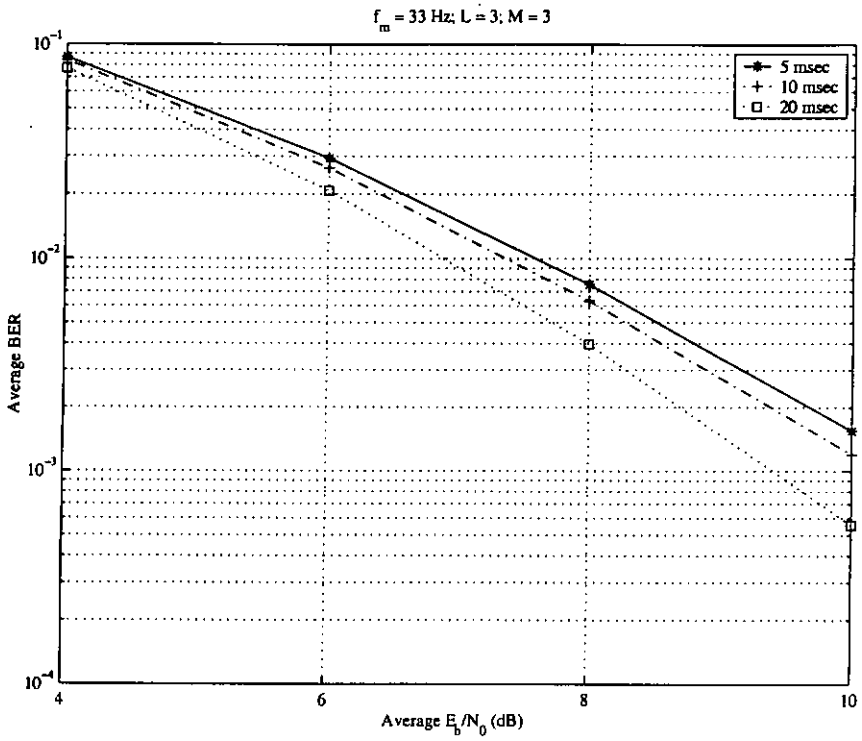

Figure 5.24 BER performance as a function of

interleaving depth ($f_m T_s = 3.44\times10^{-4}$)

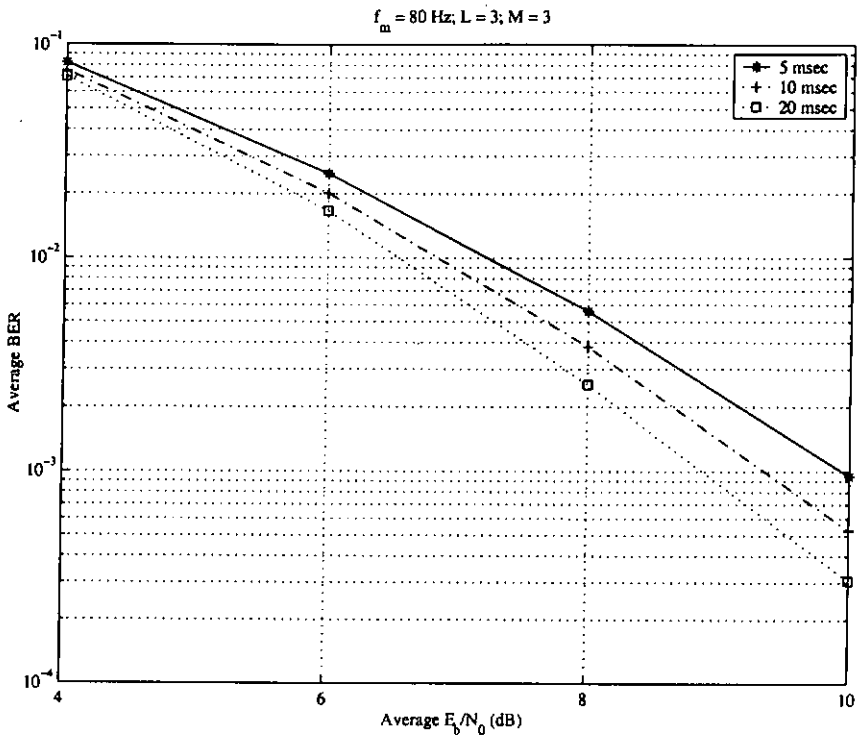

Figure 5.25 BER performance as a function of

interleaving depth ($f_m T_s = 8.33 \times 10^{-4}$)

The BER performance of a matched Rake receiver ($L = 3$, $M = 3$) with different maximum Doppler frequencies, f_m, for the three signal paths is shown in Figure 5.26. The cases with $f_m = 40$ Hz, 60 Hz, and 80 Hz are included as references.

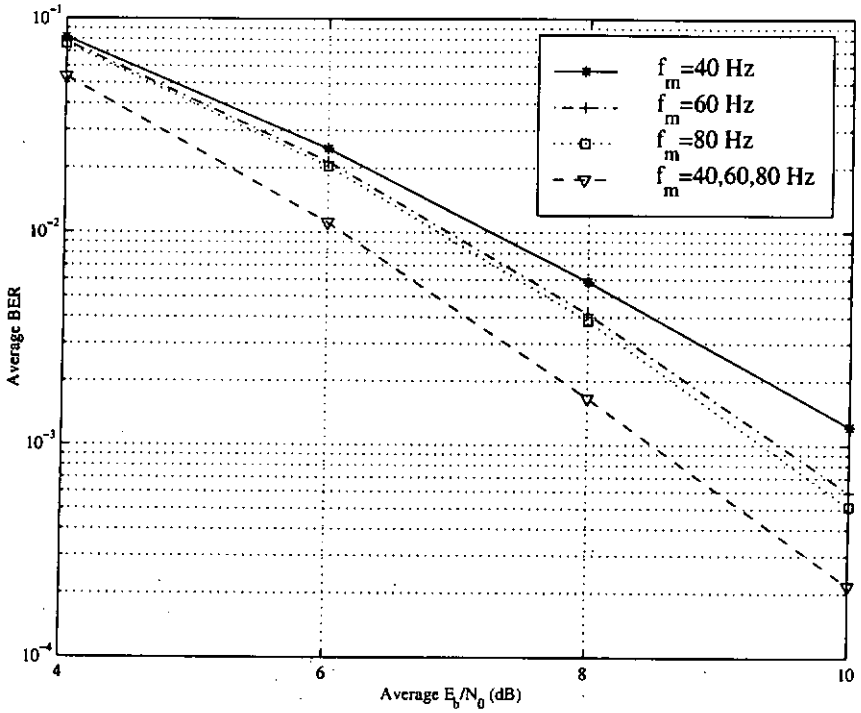

Figure 5.26 BER performance with different f_m for individual signal paths

5.5 Antenna Diversity

Antenna diversity is one kind of space diversity that is achieved by two or more antennas separated with sufficient distance. When two antennas are spaced apart with a distance far enough so that the two signals received are uncorrelated, antenna diversity gain can improve system performance in this case. After the invention of microstrip antenna, it is feasible to employ antenna

diversity in the forward link where the mobile unit is small. There are two types of antenna diversity investigated in this thesis. The first type is BER based, where the current antenna is switched to a new one when an error is detected. Another type is post-detection method, where two Rake receivers are required. More detailed descriptions of these two types of antenna diversity are given in latter sections.

5.5.1 BER based Antenna Diversity

In this type of antenna diversity, the selection of antenna is based on the BER. When an error is detected, the current antenna is switched to another one. The BER performances with different number L of fingers in the Rake receiver and number M of signal paths in the channel are shown in Figure 5.27 to Figure 5.29. Shown in Figure 5.27 is the BER performance of a system employed with BER based antenna diversity with $L = 1$ and $M = 1$. As we can see from the figure, the diversity gain obtained is not significant. For BER of 10^{-1}, about 1 dB gain is obtained. The BER performance for $L = 2$ and $M = 2$ is shown in Figure 5.28. Again, as shown in the figure, only 1 dB gain is obtained for BER of 10^{-2}. For $L = 3$ and $M = 3$, the improvement is about 1 dB for both BER of 10^{-2} and 10^{-3} as shown in Figure 5.29.

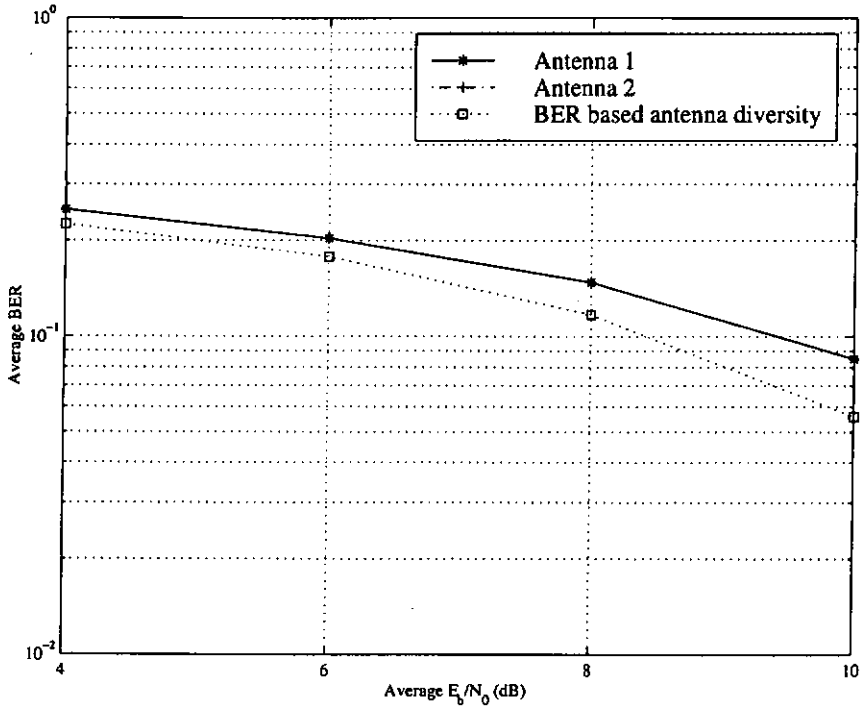

Figure 5.27 BER based antenna diversity ($L = 1$, $M = 1$)

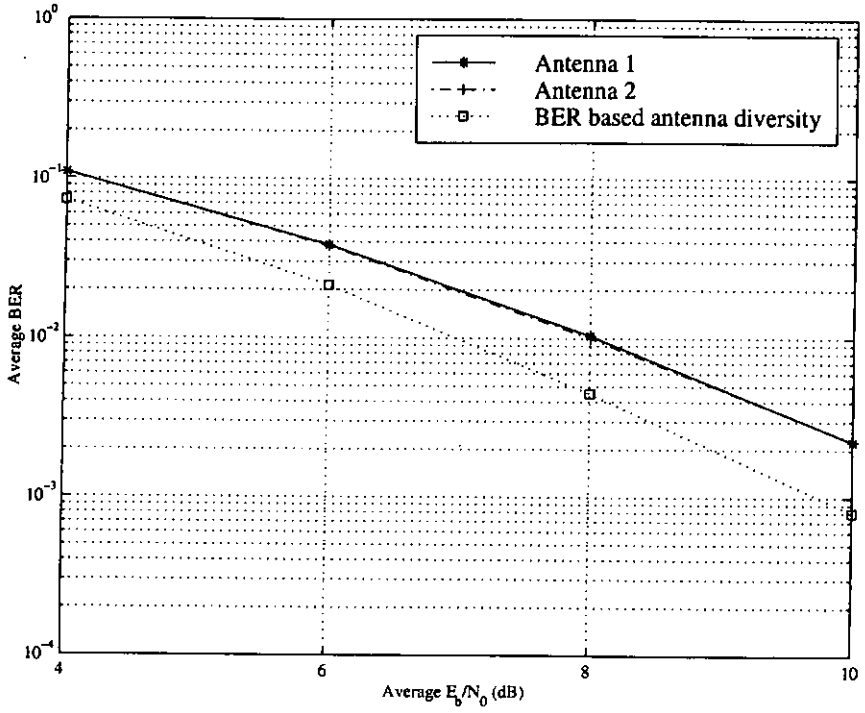

Figure 5.28 BER based antenna diversity ($L = 2$, $M = 2$)

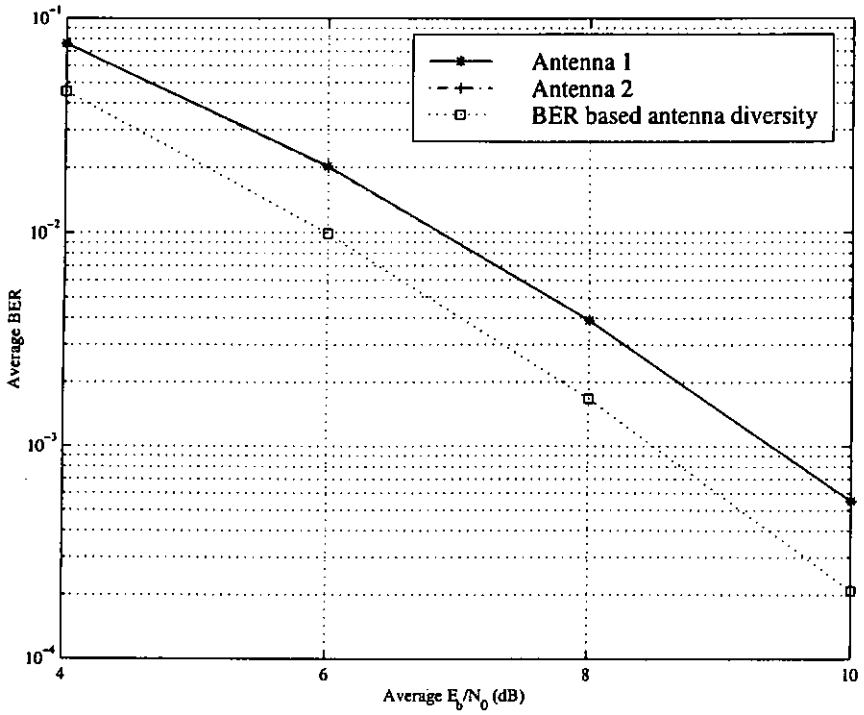

Figure 5.29 BER based antenna diversity ($L = 3$, $M = 3$)

The BER based type antenna diversity is one kind of switch diversity because there are switching between antennas. Table 5.2 and Table 5.3 show the number of switching and switching frequency, respectively, under different scenarios. As shown in Table 5.3, the switching frequency is very high at low E_b/N_0 for $L = 1$ and $M = 1$. The increased demand of power consumption for the high frequency of switching makes this BER based antenna diversity not feasible especially in the forward link.

Table 5.2 Number of switching under different channel environments

E_b/N_0	Number of switching (in 50 seconds)		
	$L = 1, M = 1$	$L = 2, M = 2$	$L = 3, M = 3$
4 dB	720,412	233,617	145,349
6 dB	570,006	68,164	31,598
8 dB	374,617	14,438	5,356
10 dB	178,988	2,565	670

Table 5.3 Switching frequency under different channel environments

E_b/N_0	Switching frequency (Hz)		
	$L = 1, M = 1$	$L = 2, M = 2$	$L = 3, M = 3$
4 dB	14,408	4,672	2,907
6 dB	11,400	1,363	632
8 dB	7,492	289	107
10 dB	3,580	51	13

As a summary, the performance gain of the BER based antenna diversity is not sensitive to the number of fingers in the Rake receiver and signal paths in the channel. In addition, the high frequency of switching makes this BER based antenna diversity not feasible especially in the forward link. However, the implementation of only one Rake receiver in the receiving end is the advantage of using it.

5.5.2 Post-Detection Antenna Diversity

Different from the BER based antenna diversity, post-detection antenna diversity needs the implementation of two Rake receivers and thus increases hardware complexity. However, this gives better system performance. The BER performance of a system employed with post-detection antenna diversity is shown in Figure 5.30 with different number L of fingers in the Rake receiver and different number M signal paths in the channel. As shown in the figure, the performance does not have an error floor with increasing E_b/N_0 even only one finger is used in the Rake receiver. It is because antenna diversity is applied in this case. In fact, a 1-finger matched Rake receiver system with antenna diversity can be looked as if it were a 2-finger matched Rake receiver system without antenna diversity. However, as shown in Figure 5.31, there is an inferiority when compared with Figure 5.7 ($L = 2$, $M = 2$). It is because the signal in the 1-finger Rake receiver experiences deep fades and results in a wrong decision at the output of the receiver with a higher probability.

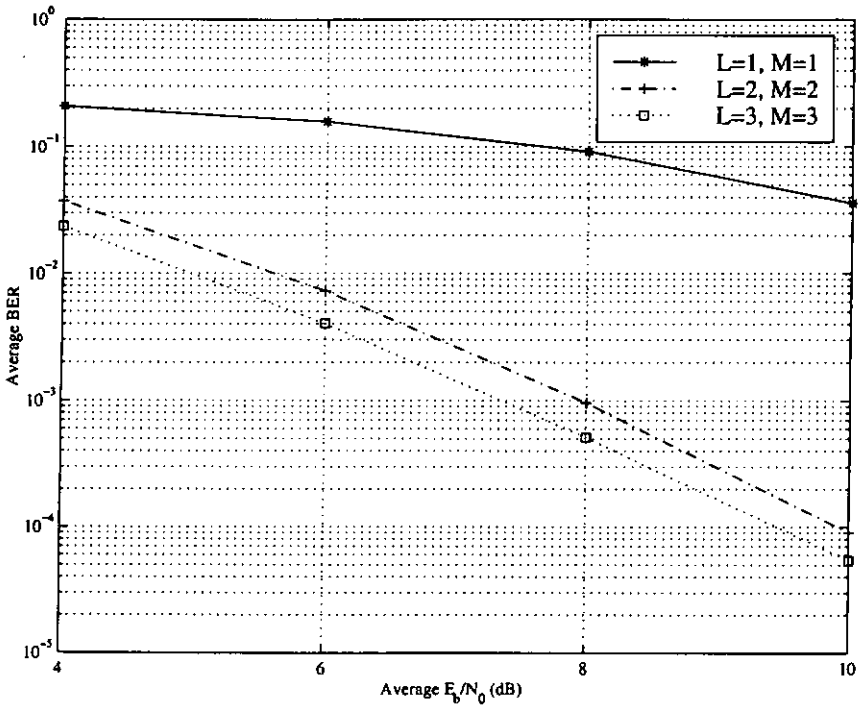

Figure 5.30 BER performance of post-detection antenna diversity

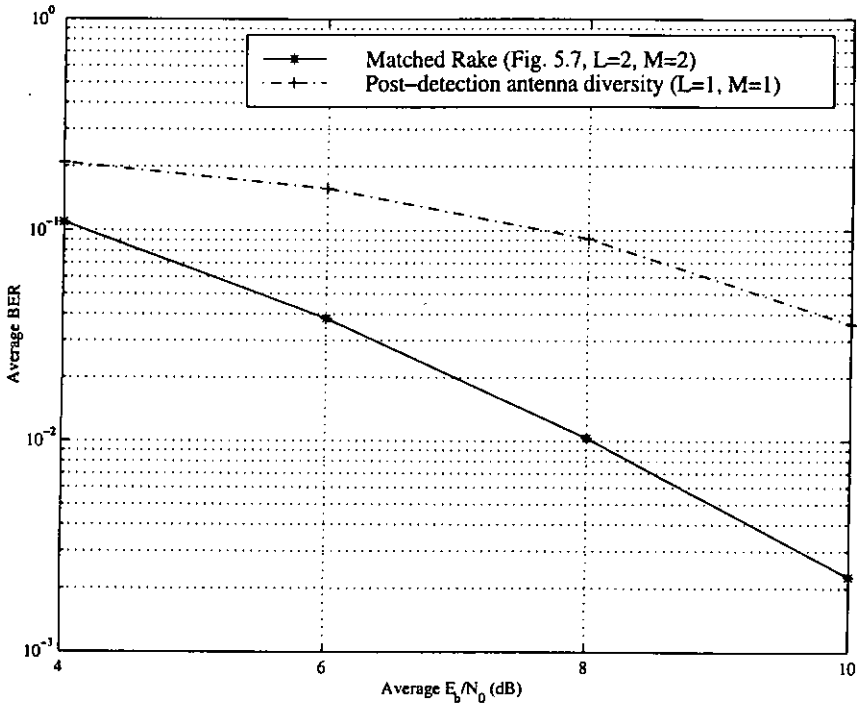

Figure 5.31 BER performance comparison of matched Rake receiver (Figure 5.7, $L = 2$, $M = 2$) and post-detection antenna diversity ($L = 1$, $M = 1$)

Similarly, the case of $L = 2$ and $M = 2$ can be looked as if it were a 4-finger matched Rake receiver system without antenna diversity. And the performance comparison for the case where $L = 4$ and $M = 4$ as shown in Figure 5.7 is given in Figure 5.32. It can be seen from the figure that antenna diversity gives better system performance because IPI is more dominant for large M.

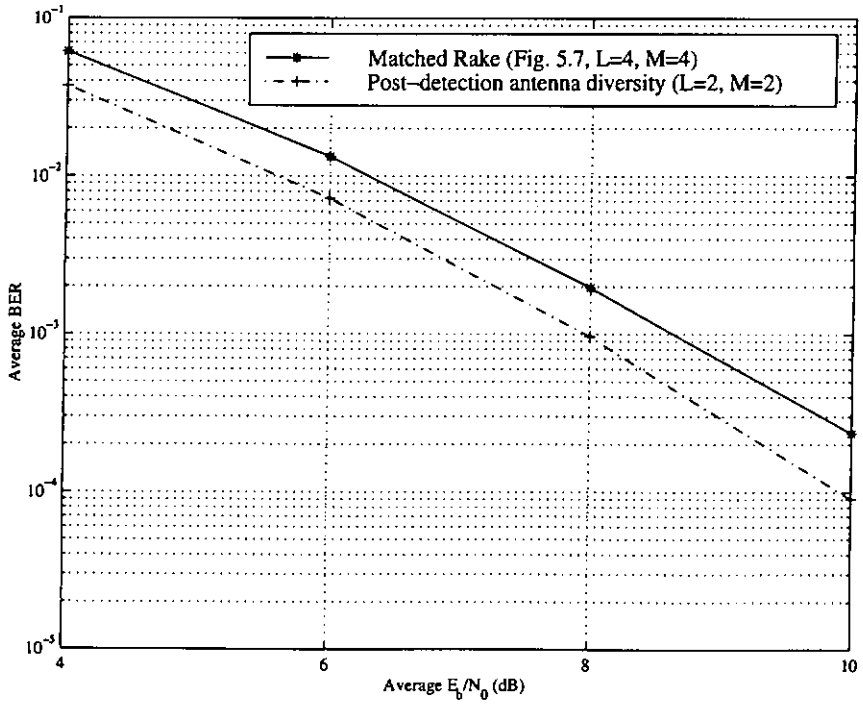

Figure 5.32 BER performance comparison of matched Rake receiver (Figure 5.7, $L = 4$, $M = 4$) and post-detection antenna diversity ($L = 2$, $M = 2$)

For the case of $L = 3$ and $M = 3$, the performance has a greater improvement over the case where $L = 6$ and $M = 6$ as shown in Figure 5.7. This performance improvement as depicted in Figure 5.33 can be explained by the fact that M is larger in this case and therefore IPI is more dominant.

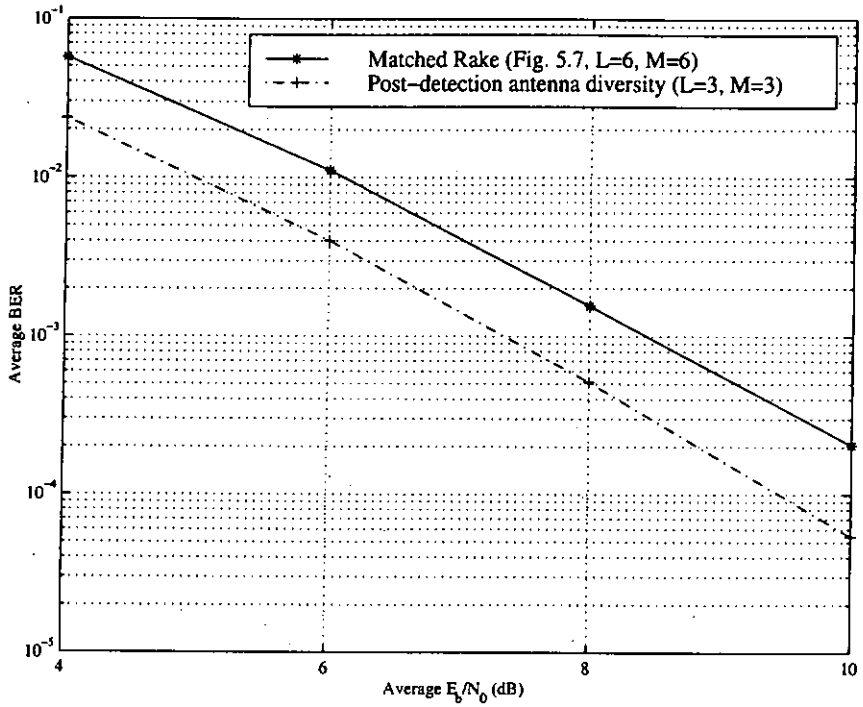

Figure 5.33 BER performance comparison of matched Rake receiver (Figure 5.7, $L = 6$, $M = 6$) and post-detection antenna diversity ($L = 3$, $M = 3$)

Therefore it can be concluded that the performance of post-detection antenna diversity with n antennas (only $n = 2$ is investigated in this thesis), each with L fingers employed in the Rake receiver, is similar to a nL-finger matched Rake receiver without antenna diversity. In particular, when the

number of fingers (and signal paths) is large, post-detection antenna diversity gives better performance because of IPI phenomenon.

5.6 Power Control Aspects

Because of the synchronous data transmission, forward link power control is not an issue as important as in the reverse link for single cell operating environment [47]. Therefore perfect power control is assumed in the simulations of forward link performance. The effects of imperfect power control on the system performance are investigated in this section. It should be noted that this imperfect power control investigation is applicable on both the forward and reverse links.

Same as the previous simulations, the desired user is the one with 64 kbits/sec data transmission rate ($R2$ user). For perfect power control, the transmit power of the desired user should be twice of the power of the users with 32 kbits/sec data transmission rate ($R1$ users) as explained in Section 4.2 of Chapter 4. However, in the case of imperfect power control, the power is unbalanced. Figure 5.34 shows the system performance with different cases as depicted in Table 5.4. For example, Case I represents the situation where $P_{R2} = P_{R2\ balanced}$, $P_{R1} = 1.5\ P_{R1\ balanced}$, $P_{R1} = 1.6\ P_{R1\ balanced}$, and $P_{R1} = 1.7\ P_{R1\ balanced}$.

Table 5.4 Different cases of imperfect power control

	P_{R2}	P_{R1}	P_{R1}	P_{R1}
Case I	1	1.5	1.6	1.7
Case II	1	0.6	0.7	0.8
Case III	1	0.4	0.5	0.6
Case IV	1	0.1	0.2	0.3
Case V	0.5	1	1	1
Case VI	1	1	1	1

As shown in the figure, Case IV has the best performance. It is because in this case, the other users ($R1$ users) are transmitting with the lowest powers. On the other hand, the performances for Cases II, III, and IV only have marginal improvements when compared to perfect power control Case VI. That means imperfect power control where the $R1$ users are transmitting with lower powers does not have significant effects (i.e., improvement) on the desired $R2$ user. In Case I, the $R1$ users are transmitting with higher powers. And results show that the performance of the desired $R2$ user is degraded when compared to perfect power control Case VI. However, the degradation is not significant. The imperfect power control on the other users has no significant effect on the performance of the desired user because the interference between different users is minor. On the other hand, the imperfect power control on the

desired $R2$ user gives significant degradation on its performance as shown with Case V in Figure 5.34.

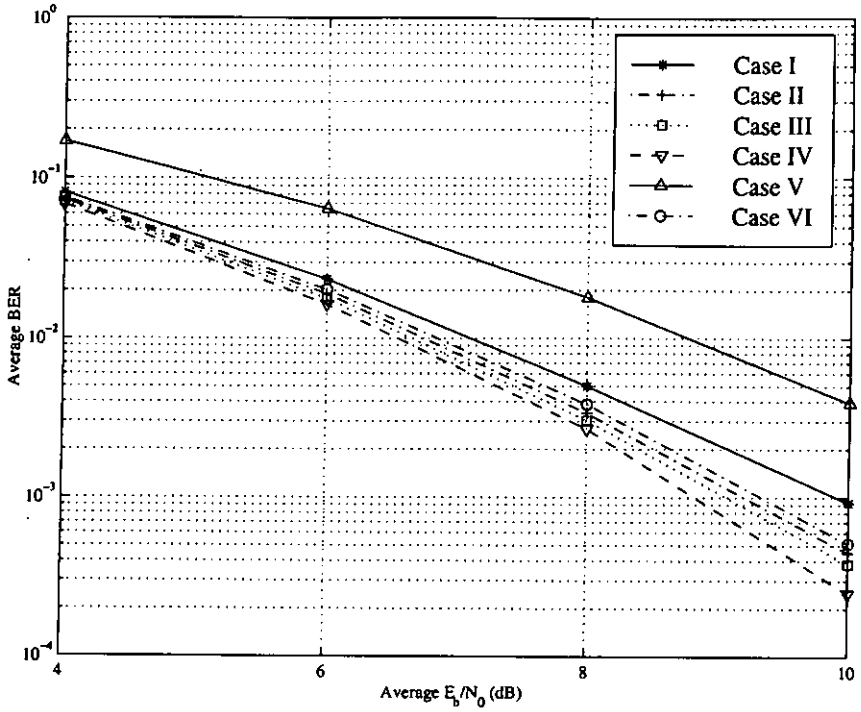

Figure 5.34 BER performance of imperfect power control

Therefore we can conclude that the BER performance mainly depends on the power control on the desired user. Even if there is imperfect power control on the other users, there is no significant effect as observed on the desired user. However, this may not be true when the number of users in the system increases to tens or hundreds.

5.7 Summary

In this chapter, sensitivities of UTRA system performance to the parameters– number of fingers in the Rake receiver, implementation of path searching algorithm, interleaving depth and antenna diversity– are presented. In all cases, matched Rake receiver provides the best performance but hardware complexity is high. The implementation of path searching algorithm gives significant improvement on a system with unmatched Rake receiver. The performance is comparable to the matched Rake receiver case. In general, longer interleaving depth provides better system performance but the delay introduced in it is the main concern of choosing the interleaving depth. The BER based antenna diversity requires high number of switching when the E_b/N_0 is low. This high frequency of switching consumes more power and thus not feasible especially in the forward link. In general, the gain provided by the BER based antenna diversity is only 1 dB in most of the cases and it is not sensitive to the number of fingers in the Rake receiver and signal paths in the channel. A system employed with post-detection antenna diversity with L fingers in each antenna (a total of 2 antennas) is analogous to a $2L$-finger matched Rake receiver system without antenna diversity. In particular, for more number of signal paths, the post-detection antenna diversity method is superior. Power control is important in CDMA systems. However, imperfect power control on other users does not give significant performance improvement for the advantage user (i.e., the one with perfect power control) in a 4-user system.

Chapter 6

CONCLUSIONS AND FURTHER RESEARCH

6.1 Conclusions

The sensitivities of UTRA system performance to the parameters including the number of fingers in the Rake receiver, the implementation of path searching algorithm, interleaving depths, Doppler frequencies, antenna diversity, and power control are investigated in this thesis. It can be concluded that best system performance is obtained from using a matched Rake receiver. That is, the number of fingers in the Rake receiver is matched to the number of signal paths in the channel. However, because of the number of resolvable paths in a wideband system is usually large and the number of signal paths changes dynamically as the mobile unit moves, the implementation of a matched Rake receiver seems not practical in a 3G system. It is more feasible to implement an unmatched Rake receiver where the number of fingers in the Rake receiver is not matched to the number of signal paths in the channel. Simulation results show that the performance of an unmatched Rake receiver is, as expected, inferior to that of a matched Rake receiver. In fact, the performance

degradation is significant. However, the implementation of path searching algorithm in an unmatched Rake receiver gives significant improvement on the system performance. And the performance is comparable to the matched Rake receiver case. Theoretical results show the close agreement with the results obtained from simulation experiments.

System performance improves with increasing interleaving depths but the delay introduced is a prime consideration for the system designers in choosing this parameter. The interleaving depth should be chosen carefully or the delay introduced in it becomes intolerable for services such as speech or real-time video conferencing. Simulation results show that system with higher Doppler frequencies gives better performance. The reason is that the duration of deep fades is shorter for higher Doppler frequencies and therefore the interleaver can disperse the bursty errors more efficiently into random errors. However, this may not be the case in real systems since the channel changes rapidly in high Doppler frequencies. And it is difficult to achieve optimal measurements for channel estimation and power control in a rapidly changing environment.

Besides Rake diversity, antenna diversity is used as another means to combat fast fading in order to provide further system improvement. Two types of antenna diversity are investigated. The performance improvement of the BER based antenna diversity is not sensitive to the parameter number of fingers used in the Rake receiver. That is, no significant improvement is observed when the number of fingers in the Rake receiver is increased. In

addition, the high frequency of switching between antennas makes this method not feasible especially in the forward link since it consumes large amount of power. The performance of post-detection antenna diversity with n antennas (only $n = 2$ is investigated in this thesis), each with L fingers employed in the Rake receiver, is similar to a system with nL-finger matched Rake receiver without antenna diversity. In particular, when the number of fingers (and signal paths) is large, the post-detection antenna diversity gives better performance because of the IPI phenomenon.

The BER performance mainly depends on the power control on the desired user. In other words, imperfect power control on the other users does not result in significant improvement on the desired user in a 4-user system.

The matched Rake receiver is the most unattractive structure in terms of hardware complexity. However, it gives the best system performance. An unmatched Rake receiver gives the simplest structure. However, the performance of it is unacceptable. An unmatched Rake receiver with path searching is less complex than a matched Rake receiver. In addition, the performance of unmatched Rake receiver with path searching is comparable to that of a matched Rake receiver. Therefore to realize good performance with reasonably complexity, it is suggested to use an unmatched Rake receiver with path searching algorithm. Accurate channel estimates are necessity for an unmatched Rake receiver with path searching. When a channel is fading rapidly and as a result, channel estimations become inaccurate, the performance gain obtained by path searching may be reduced. Therefore it is

important to have accurate channel estimates for an unmatched Rake receiver with path searching algorithm.

Wireless communications are getting popular nowadays. The feasibility of multimedia applications over mobile radio channels can be realized by the 3G cellular systems in the 21st century. The analysis of parametric sensitivities of 3G UTRA cellular system given in this thesis are helpful to cellular system designers in developing reliable 3G systems with considerations of the tradeoff between system performance and complexity.

6.2 Further Research

Further investigation can be done on different kinds of channel. That is, channels with different kinds of distributions such as Nakagami-*m* and Rician. And performance comparisons can be made with the results obtained in this thesis.

Investigations can be further extended to the situations when the signal paths are correlated. These results can be compared with the ones available in this thesis. Degradation because of the correlated paths can be obtained and compared.

REFERENCES

[1] E. Dahlman, B. Gudmundson, M. Nilsson, and J. Sköld, "UMTS/IMT-2000 based on wideband CDMA," *IEEE Communications Magazine*, pp. 70-80, September 1998.

[2] W. C. Y. Lee, "Overview of cellular CDMA," *IEEE Transactions on Vehicular Technology*, Vol. 40, No. 2, pp. 291-302, May 1991.

[3] A. Baier, U. Fiebig, W. Granzow, W. Koch, P. Teder, and J. Thielecke, "Design study for a CDMA-based third-generation mobile radio system," *IEEE Journal on Selected Areas in Communications*, Vol. 12, No. 4, pp. 733-743, May 1994.

[4] R. H. Rækken, H. Langaas, G. Løvnes, and S. E. Paulsen, "Wideband impulse response measurements at 900 MHz and 1.7 GHz," *GLOBECOM'91*, pp. 1303-1307, December 1991.

[5] E. S. Sousa, V. M. Jovanović, and C. Daigneault, "Delay spread measurements for the digital cellular channel in Toronto," *IEEE Transactions on Vehicular Technology*, Vol. 43, No. 4, pp. 837-847, November 1994.

[6] D. C. Cox, and R. P. Leck, "Correlation bandwidth and delay spread multipath propagation statistics for 910-MHz urban mobile radio channels," *IEEE Transactions on Communications*, Vol. COM-23, No. 11, pp. 1271-1280, November 1975.

[7] G. Wu, A. Jalali, and P. Mermelstein, "On channel models for microcellular CDMA systems," *IEEE Transactions on Vehicular Technology*, Vol. 44, No. 3, pp. 706-711, August 1995.

[8] R. Price, and P. E. Green, Jr., "A Communication technique for multipath channels," *Proceedings of the IRE*, pp. 555-570, March 1958.

[9] N. L. B. Chan, "Multipath propagation effects on a CDMA cellular system," *IEEE Transactions on Vehicular Technology*, Vol. 43, No. 4, pp. 848-855, November 1994.

[10] G. L. Turin, "Introduction to spread-spectrum antimultipath techniques and their application to urban digital radio," *Proceedings of the IEEE*, Vol. 68, No. 3, pp. 328-353, March 1980.

[11] J. G. Proakis, *Digital Communications, Third Edition*. New York: McGraw-Hill, 1995.

[12] M. K. Simon, and M. Alouini, "A unified performance analysis of digital communication with dual selective combining diversity over correlated Rayleigh and Nakagami-*m* fading channels," *IEEE Transactions on Communications*, Vol. 47, No. 1, pp. 33-43, January 1999.

[13] J. N. Pierce, and S. Stein, "Multiple diversity with nonindependent fading," *Proceedings of the IRE*, pp. 89-104, January 1960.

[14] V. A. Aalo, "Performance of maximal-ratio diversity systems in a correlated Nakagami-fading environment," *IEEE Transactions on Communications*, Vol. 43, No. 8, pp. 2360-2369, August 1995.

[15] C. Kchao, and G. L. Stüber, "Analysis of a direct-sequence spread-spectrum cellular radio system," *IEEE Transactions on Communications*, Vol. 41, No. 10, pp. 1507-1516, October 1993.

[16] A. Annamalai, C. Tellambura, and V. K. Bhargava, "Unified analysis of equal-gain diversity on Rician and Nakagami fading channels," *WCNC'99*, pp. 10-14, September 1999.

[17] V. Aalo, and S. Pattaramalai, "Average error rate for coherent MPSK signals in Nakagami fading channels," *Electronics Letters*, Vol. 32, No. 17, pp. 1538-1539, 15th August 1996.

[18] V. Kaasila, and A. Mämmelä, "Bit error probability of a matched filter in a Rayleigh fading multipath channel in the presence of interpath and intersymbol interference," *IEEE Transactions on Communications*, Vol. 47, No. 6, pp. 809-812, June 1999.

[19] T. Eng, N. Kong, and L. B. Milstein, "Comparison of diversity combining techniques for Rayleigh-fading channels," *IEEE Transactions on Communications*, Vol. 44, No. 9, pp. 1117-1129, September 1996.

[20] S. Chennakeshu, and J. B. Anderson, "Error rates for Rayleigh fading multichannel reception of MPSK signals," *IEEE Transactions on Communications*, Vol. 43, No. 2/3/4, pp. 338-346, February/March/April 1995.

[21] J. Yang, "Diversity receiver scheme and system performance evaluation for a CDMA system," *IEEE Transactions on Communications*, Vol. 47, No. 2, pp. 272-280, February 1999.

[22] N. Kong, T. Eng, and L. B. Milstein, "A selection combining scheme for Rake receivers," *ICUPC'95*, pp. 426-430, November 1995.

[23] N. Kong, and L. B. Milstein, "Average SNR of a generalized diversity selection combining scheme," *IEEE Communications Letters*, Vol. 3, No. 3, pp.57-59, March 1999.

[24] M. Alouini, and M. K. Simon, "Performance of coherent receiver with hybrid SC/MRC over Nakagami-*m* fading channels," *IEEE Transactions on Vehicular Technology*, Vol. 48, No. 4, pp. 1155-1164, July 1999.

[25] M. Z. Win, R. K. Mallik, G. Chrisikos, and J. H. Winters, "Canonical expressions for the error probability performance of M-ary modulation with hybrid selection/maximal-ratio combining in Rayleigh fading," *WCNC'99*, pp. 266-270, September 1999.

[26] M. Z. Win, and Z. A. Kostić, "Impact of spreading bandwidth on Rake reception in dense multipath channels," *IEEE Journal on Selected Areas in Communications*, Vol. 17, No. 10, pp. 1794-1806, October 1999.

[27] G. L. Turin et al., "A statistical model of urban multipath propagation," *IEEE Transactions on Vehicular Technology*, Vol. VT 21, pp. 1-9, 1972.

[28] K. Pahlavan, and A. H. Levesque, *Wireless Information Networks*. New York: John Wiley & Sons, Inc., 1995.

[29] Y. Akaiwa, *Introduction to Digital Mobile Communication*. New York: John Wiley & Sons, Inc., 1997.

[30] W. C. Y. Lee, *Mobile Communications Engineering: Theory and Applications, Second Edition*. New York: McGraw-Hill, 1998.

[31] R. W. Hamming, "Error detecting and error correcting codes," *Bell System Technical Journal*, April 1990.

[32] Association of Radio Industries and Businesses (ARIB) IMT-2000 Study Committee, "Japan's proposal for candidate radio transmission technology on IMT-2000: W-CDMA," June 1998.

[33] R. M. Fano, "A heuristic discussion of probabilistic coding," *IEEE Transactions on Information Theory*, Vol. IT-9, pp. 64-74, April 1963.

[34] A. J. Viterbi, "Error bounds for convolutional codes and asymptotically optimum decoding algorithm," *IEEE Transactions on Information Theory*, Vol. IT-13, pp. 260-269, 1967.

[35] G. D. Forney, Jr., "The Viterbi algorithm," *Proceedings of the IEEE*, Vol. 61, pp. 268-278, 1973.

[36] T. S. Rappaport, *Wireless Communications: Principles and Practice.* Upper Saddle River, N.J.: Prentice-Hall, 1996.

[37] T. Ojanperä, and R. Prasad, "An overview of third-generation wireless personal communications: A European perspective," *IEEE Personal Communications*, pp. 59-65, December 1998.

[38] N. Yang, "The third generation wireless network using CDMA air interface," *WCNC'99*, pp. 649-653, September 1999.

[39] W. Mohr, "UTRA FDD and TDD, a harmonized proposal for IMT-2000," *ICCT'98*, pp. 495-499, October 1998.

[40] G. L. Turin, "The effects of multipath and fading on the performance of direct-sequence CDMA systems," *IEEE Journal on Selected Areas in Communications*, Vol. SAC-2, No. 4, pp. 597-603, July 1984.

[41] M. S. Alencar, and F. M. Assis, "Use of the Rake receiver to counterbalance the effect of fading on the capacity of a CDMA channel," *VTC'96*, pp. 652-655, May 1996.

[42] A. Higashi, T. Taguchi, and K. Ohno, "Performance of coherent detection and Rake for DS-CDMA uplink channels," *PIMRC'95*, pp. 436-440, September 1995.

[43] R. L. Pickholtz, L. B. Milstein, and D. L. Schilling, "Spread spectrum for mobile communications," *IEEE Transactions on Vehicular Technology*, Vol. 40, No. 2, pp. 313-322, May 1991.

[44] P. Bergholm, M. Honkanen, and S. Häggman, "Simulation of a microcellular DS-CDMA radio network," *ICUPC'95*, pp. 838-842, November 1995.

[45] T. Ojanperä, K. Rikkinen, H. Häkkinen, K. Pehkonen, A. Hottinen, and J. Lilleberg, "Design of a 3rd generation multirate CDMA system with multiuser detection, MUD-CDMA," *ISSSTA'95*, pp. 334-338, September 1996.

[46] A. Jalali, and P. Mermelstein, "Effects of diversity, power control, and bandwidth on the capacity of microcellular CDMA systems," *IEEE Journal on Selected Areas in Communications*, Vol. 12, No. 5, pp. 952-961, June 1994.

[47] F. Simpson, and J. M. Holtzman, "Direct sequence CDMA power control, interleaving, and coding," *IEEE Journal on Selected Areas in Communications*, Vol. 11, No. 7, pp. 1085-1095, September 1993.

[48] K. S. Gilhousen, I. M. Jacobs, R. Padovani, A. J. Viterbi, L. A. Weaver, Jr., and C. E. Wheatley III, "On the capacity of a cellular CDMA system," *IEEE Transactions on Vehicular Technology*, Vol. 40, No. 2, pp. 303-311, May 1991.

[49] T. Hu, and M. M. K. Liu, "Power control for wireless multimedia CDMA systems," *Electronics Letters*, Vol. 33, No. 8, pp. 660-662, 10th April 1997.

[50] Chih-Lin I., and R. D. Gitlin, "Multi-code CDMA wireless personal communications networks," *ICC'95*, pp. 1060-1064, June 1995.

[51] E. Dahlman, and K. Jamal, "Wide-band services in a DS-CDMA based FPLMTS system," *VTC'96*, pp. 1655-1660, May 1996.

[52] K. Okawa, and F. Adachi, "Orthogonal multi-spreading factor forward link for coherent DS-CDMA mobile radio," *ICUPC'97*, Vol. 2, pp. 618-622, October 1997.

[53] S. Sasaki, H. Kikuchi, J. Zhu, and G. Marubayashi, "Performance of differential parallel combinatorial CDMA systems in Rayleigh fading channels," *ISSSTA'96*, pp. 697-701, September 1996.

[54] S. Ramakrishna, and J. M. Holtzman, "A comparison between single code and multiple code transmission schemes in a CDMA system," *VTC'98*, pp. 791-795, May 1998.

[55] M. O. Sunay, and J. Kähtävä, "Provision of variable data rates in third generation wideband DS CDMA systems," *WCNC'99*, pp. 505-509, September 1999.

[56] K. C. Hwang, and K. B. Lee, "Performance analysis of low processing gain DS/CDMA systems with random spreading sequences," *IEEE Communications Letters*, Vol. 2, No. 12, pp. 315-317, December 1998.

[57] S. Onoe, K. Ohno, K. Yamagata, and T. Nakamura, "Wideband-CDMA radio control techniques for third-generation mobile communications systems," *VTC'97*, pp. 835-839, May 1997.

[58] S. J. Lee, H. W. Lee, and D. K. Sung, "Capacities of single-code and multicode DS-CDMA systems accommodating multiclass services," *IEEE Transactions on Vehicular Technology*, Vol. 48, No. 2, pp. 376-384, March 1999.

[59] K. S. Jin, Y. Shin, and S. Im, "A predistorter for nonlinear distortion in multi-code CDMA systems," *PIMRC'98*, pp. 1481-1485, September 1998.

[60] G. J. R. Povey, and M. Nakagawa, "A review of time division duplex – CDMA techniques," *ISSSTA'98*, pp. 630-633, September 1998.

[61] G. J. R. Povey, "Capacity of a cellular time division duplex CDMA system," *IEE Proceedings on Communications*, Vol. 141, No. 5, pp. 351-356, October 1994.

[62] G. J. R. Povey, H. Holma, and A. Toskala, "TDD-CDMA extension to FDD-CDMA based third generation cellular system," *ICUPC'97*, pp. 813-817, October 1997.

[63] S. E. El-Khamy, E. E. Sourour, and T. A. Kadous, "Wireless portable communications using pre-Rake CDMA/TDD/QPSK systems with different combining techniques and imperfect channel estimation," *PIMRC'97*, pp. 529-533, September 1997.

[64] R. Esmailzadeh, E. Sourour, and M. Nakagawa, "Prerake diversity combining in time-division duplex CDMA mobile communications," *IEEE Transactions on Vehicular Technology*, Vol. 48, No. 3, pp. 795-801, May 1999.

[65] C. Berrou, A. Glavieux, and P. Thitimajshima, "Near Shannon limit error-correcting coding and decoding: Turbo-codes," *ICC'93*, pp. 1064-1070, May 1993.

[66] S. R. Kim, J. G. Lee, H. Lee, B. S. Kang, and J. W. Jeong, "A coherent dual-channel QPSK modulation for CDMA systems," *VTC'96*, pp. 1848-1852, April 1996.

[67] A. Hottinen, H. Holma, and A. Toskala, "Multiuser detection for multirate CDMA communications," *ICC'96*, pp. 1819-1823, June 1996.

[68] T. Ottosson, and A. Svensson, "Multi-rate schemes in DS/CDMA systems," *VTC'95*, pp. 1006-1010, July 1995.

[69] S. Yao, and E. Geraniotis, "Optimal power control law for multi-media multi-rate CDMA systems," *VTC'96*, pp. 392-396, April 1996.

[70] J. T. H. Wu, and E. Geraniotis, "Power control in multi-media CDMA networks," *VTC'95*, pp. 789-793, July 1995.

[71] F. Adachi, M. Sawahashi, K. Okawa, "Tree-structured generation of orthogonal spreading codes with different lengths for forward link of

DS-CDMA mobile system," *Electronics Letters*, Vol. 33, No. 1, pp. 27-28, 2nd January 1997.

[72] R. Steele, *Mobile Radio Communications*. London: Pentech Press, 1992.

[73] G. D. Forney, "Burst-correcting codes for the classic bursty channel," *IEEE Transactions on Communication Technology*, Vol. COM19, pp. 772-781, October 1971.

[74] D. L. Noneaker, and M. B. Pursley, "The effects of sequence selection on DS spread spectrum with selective fading and Rake reception," *IEEE Transactions on Communications*, Vol. 44, No. 2, pp.229-237, February 1996.

[75] M. P. Lötter, and L. P. Linde, "A comparison of three families of spreading sequences for CDMA applications," *COMSIG'94*, pp. 68-75, October 1994.

[76] B. M. Popović, "Generalized chirp-like polyphase sequences with optimum correlation properties," *IEEE Transactions on Information Theory*, Vol. 38, No. 4, pp. 1406-1409, July 1992.

[77] E. L. Strat, "New spreading codes for a DS-CDMA mobile radio system using a Rake receiver in a multi-user interference environment," *ISSSTA'94*, pp. 401-405, July 1994.

[78] J. H. Lindholm, "An analysis of the pseudo-randomness properties of subsequences of long m-sequences," *IEEE Transactions on Information Theory*, Vol. IT-14, pp. 509-576, July 1968.

[79] D. V. Sarwate, and M. B. Pursley, "Cross-correlation properties of pseudorandom and related sequences," *Proceedings of the IEEE*, Vol. 68, pp. 593-619, May 1980.

[80] D. V. Sarwate, M. B. Pursley, and T. U. Basar, "Partial correlation effects in direct sequence spread-spectrum multiple-access communication systems," *IEEE Transactions on Communications*, Vol. COM-32, pp. 567-573, May 1984.

[81] J. K. Holmes, *Coherent Spread Spectrum Systems*. Malabar, Florida: R. E. Krieger Publishing Co., 1982.

[82] W. C. Jakes, *Microwave Mobile Communications*. New York: Wiley, 1974.

[83] Y. Hara, H. Morikawa, and M. Mizumachi, "Multipath fading effects on the performance of wideband CDMA systems," *ICUPC'95*, pp. 620-624, November 1995.

[84] R. H. M. Yuen, and A. U. H. Sheikh, "Parametric sensitivities of Universal Terrestrial Radio Access system (UTRA)," *WCNC'99*, pp. 923-927, September 1999.

[85] G. Mazzini, and V. Tralli, "Effects of spreading code on the performance of CDMA picocellular systems with Rake receivers," *ICUPC'95*, pp. 436-441, November 1995.

[86] K. Okawa, Y. Okumura, M. Sawahashi, and F. Adachi, "1.92 Mbps data transmission experiments over a coherent W-CDMA mobile radio link," *VTC'98*, pp. 1300-1304, May 1998.

[87] K. Cheun, "Performance of direct-sequence spread-spectrum Rake receivers with random spreading sequences," *IEEE Transactions on Communications*, Vol. 45, No. 9, pp. 1130-1143, September 1997.

[88] H. Erben, S. Zeisberg, H. Nuszkowski, and A. Finger, "BER performance of Rake receivers with synchronisation in realistic mobile radio environments," *ISSSTA'94*, pp. 460-464, July 1994.

[89] G. Xue, and S. Cheng, "Simulation of uplink CDMA Rake receiver with selective diversity and coding," *ICCT'96*, pp. 362-365, May 1996.

[90] I. S. Gradshteyn, and I. M. Ryzhik, *Table of Integrals, Series, and Products*. New York: Academic Press, 1980.

Appendix A

RELATIONSHIP BETWEEN E_b/N_0 AND γ_b

To convert from γ_b to E_b/N_0 (or vice versa), we need to first know the mean value of γ_K. And this can be computed using the following equation:

$$E(\gamma_K) = \int_{-\infty}^{\infty} \gamma_K p_{\gamma_K}(\gamma_K) d\gamma_K \,, \tag{A.1}$$

where $p_{\gamma_K}(\gamma_K)$ is given in (5.8).

Then, γ_b can be represented in terms of γ_c, which is

$$\gamma_b = \sum_{K=1}^{L} E(\gamma_K) \,. \tag{A.2}$$

Since

$$\gamma_c = \frac{(E_b/N_0)}{M} \,, \tag{A.3}$$

the relationship between γ_b and E_b/N_0 for specific values of L and M can be found.

In this analysis, $L = 3$ and $M = 4$ to 6. And the case of $L = 3$ and $M = 4$ is shown as an example as follows.

For $K = 1$, using (A.1) and (5.8),

$$E(\gamma_1) = \int_{-\infty}^{\infty} \gamma_1 \frac{4!\,\gamma_c^{-1}}{(4-1)!\,(1-1)!}\left[1 - e^{-\frac{\gamma_1}{\gamma_c}}\right]^{4-1} e^{-\frac{(1)(\gamma_1)}{\gamma_c}} d\gamma_1 . \qquad \text{(A.4)}$$

Using Binomial Theorem, it can be easily shown that (A.4) becomes

$$E(\gamma_1) = \frac{25}{12}\gamma_c . \qquad \text{(A.5)}$$

Similarly,

$$E(\gamma_2) = \frac{13}{12}\gamma_c , \qquad \text{(A.6)}$$

and

$$E(\gamma_3) = \frac{7}{12}\gamma_c . \qquad \text{(A.7)}$$

Therefore using (A.2), γ_b can be computed as

$$\gamma_b = \sum_{K=1}^{3} E(\gamma_K)$$

$$= \frac{15}{4}\gamma_c . \qquad \text{(A.8)}$$

And using (A.3), (A.8) can be expressed as

$$\gamma_b = \frac{15}{16}(E_b/N_0). \qquad \text{(A.9)}$$

The relationships between γ_b and E_b/N_0 for cases with $M = 5$ and 6 can be computed in a similar way and they are summarized in Figure A.1.

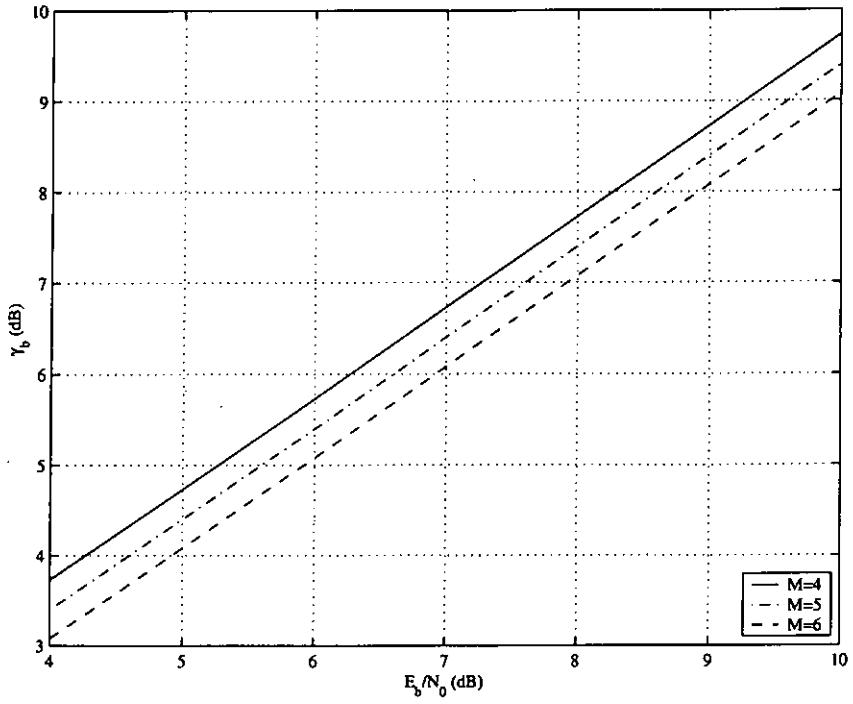

Figure A.1 Relationship between E_b/N_0 and γ_b